UC Berkeley
UC Berkeley Electronic Theses and Dissertations

Title

A Hitchhiker's Guide to the Pleistocene Sea: Using Isotopic Analysis of Fossil Coronulid Barnacles to Reconstruct Prehistoric Whale Migration

Permalink

https://escholarship.org/uc/item/2nv1k41f

Author

Taylor, Larry Dale

Publication Date

2020

Peer reviewed|Thesis/dissertation

eScholarship.org Powered by the California Digital Library
University of California

A Hitchhiker's Guide to the Pleistocene Sea: Using Isotopic Analysis of Fossil Coronulid Barnacles to Reconstruct Prehistoric Whale Migration

By

Larry Dale Taylor

A dissertation submitted in partial satisfaction of the

requirements for the degree of

Doctor of Philosophy

in

Integrative Biology

in the

Graduate Division

of the

University of California, Berkeley

Committee in charge:

Professor Seth Finnegan, Chair
Professor John Chiang
Professor Mary Power
Professor Emeritus David Lindberg

Fall 2020

Abstract

A Hitchhiker's Guide to the Pleistocene Sea: Using Isotopic Analysis of Fossil Coronulid Barnacles to Reconstruct Prehistoric Whale Migration

by

Larry D. Taylor

Doctor of Philosophy in Integrative Biology

University of California, Berkeley

Professor Seth Finnegan, Chair

Migration is an integral feature of modern mysticete whale ecology, and one that intricately links their behavior to the processes which shape the spatiotemporal distributions of oceanic productivity. Each year, mysticete whales travel thousands of miles to access seasonally productive, high-latitude waters where they feed in the summer before retreating to warm, low-latitude waters to breed and raise their calves in the winter. As the spatial and temporal distribution of oceanic productivity has shifted over geological timeframes, the changing demands of migration may have played key roles in shaping mysticete evolutionary history. And because mysticetes must rely on the most productive of waters to sustain their great mass, understanding how their migration routes have changed through time may also provide unique insight into productivity patterns in the ancient ocean.

Understanding what role migration may have played in mysticete evolution and using whale movements as a means of understanding prehistoric productivity patterns depends on having a reliable means of measuring migratory behavior in deep time, yet little is currently known of prehistoric whale migrations. My research seeks to address this knowledge gap via isotopic analysis of coronulids, the commensal barnacles which live attached to the skin of some mysticete lineages. As these barnacles grow, each new shell layer preserves an isotopic signature of the water in which it was formed, providing a mechanism by which to reconstruct the migration of the host whale. I first verify the reliability of the method by demonstrating that isotopic information from modern coronulids accurately reflects the known migratory paths of their host whales. Next, I show that migration was a widespread phenomenon by the Pleistocene, where every sampled population indicates evidence of migration. I then combine isotopic analysis with paleoceanographic modeling to constrain the migratory paths taken by several Pleistocene whales. Along the way, I discuss the implications of an unexpected and unique fossil discovery that could alter our understanding of one mysticete lineage's evolutionary history.

Dedication

Dedicated to my family.

Acknowledgements

First and foremost, I must thank my family, including my parents, Byron and Sherryl Taylor, my grandparents, Jesse and Nan Richeson and Vernon and Fannie Taylor, and my siblings, Amanda, Rachel, and Randy. I could not have been blessed with a better or more supportive family. I want to particularly recognize my father and grandparents, all of whom have passed before I was able to complete this dissertation. Without their love and support this would not be possible, and I deeply wish they could be here to celebrate with me. I also want to specifically thank my Mom, who has always been and remains my most consistent source of inspiration and support.

I must also recognize the many mentors who have helped me develop as a scientist. This begins with Jon Payne, Matt Knope, and Noel Heim, who gave me my first opportunity to dive into paleontological research, and to whom I am eternally grateful. I want to especially thank my Dissertation Committee members, Seth Finnegan, Dave Lindberg, John Chiang, and Mary Power, for all of their insight, support, and encouragement throughout this process. John, thank you for helping me to understand and appreciate the complexities of ocean currents and structure, which is critical for the research I've undertaken. Mary, thank you for your thought-provoking insights on ecology and ability to make me think of systems in new ways. Dave, thank you for teaching me much about barnacles and whales, but also for our enlightening chats about life. Seth, thank you for teaching me so much about how to be a good scientist, but also for teaching me much about how to be a good colleague, mentor, teacher, and person. It has been a privilege to have you as an advisor, and it is an even greater privilege to count you as a friend.

Many thanks as well to my Qualifying Exam Committee. This includes John Chiang and Dave Lindberg, as well as Todd Dawson, who is largely responsible for inspiring my current work and who taught me much of what I know regarding isotope systems, and Charles Marshall, who taught me about the nature of good questioning and planning my science accordingly.

Many thanks to Cindy Looy, Ivo Duijnstsee, Lisa White, and Kevin Padian for the constant support that all of them have offered me throughout my time at Berkeley, and for the roles they've each played in helping me refine my science. I want to particularly thank Lisa for all of her help, guidance, and energy in working on the ACCESS program; I've learned much from her that will be invaluable throughout the rest of my career. I also want to thank the entire UCMP community, particularly Chris Mejia, Mark Goodwin, Patricia Holroyd, Diane Erwin, and Ashley Dineen for the support of the ACCESS program, encouragement during my presentations to the group, and their general encouragement throughout the past five years.

Thank you to Wenbo Yang and Stefania Mambelli of the UC Berkeley Center for Stable Isotope Biogeochemistry. My research has been completely dependent on their expertise, mentoring, and dedicated work.

Much of my research has been enabled by generous funding from the Paleontological Society, the Geological Society of America, the Lerner-Gray Fund for Marine Research, Sigma Xi, the American Society of Naturalists, the Department of Integrative Biology, and the University of California Museum of Paleontology.

Acknowledgements, continued

Finally, I thank my wife, Anita, for her unending love and support, and for the incredible joy and purpose she has brought to my life. Anita, I love you more than you will ever know.

Table of Contents

Dedication……..……..…….....i

Acknowledgements……...……ii

Table of Contents……..…….....iv

List of Figures……..……..v

List of Tables……...vii

Introduction: An overview of mysticete migration and isotope systems……..... 1

Chapter I. Isotopes from fossil coronulid barnacle shells record evidence of migration in multiple Pleistocene whale populations……..…….....5

Chapter II. Fossils of *Cryptolepas rhachianecti*, a commensal barnacle of gray whales, from Pleistocene-aged deposits in Ecuador…...……..27

Chapter III. Using paleoceanographic models and isotopes from fossil coronulid barnacles to constrain the migrations of Pleistocene whales visiting the Canoa Basin, Ecuador..….....37

References……..……..……62

Appendix I. Bulk isotope data……..…….……...76

Appendix II. Clumped isotope data……..……...…….84

Appendix III. R code……...…….....90

List of Figures

1.1 A $\delta^{18}O$ profile from a modern-day *Coronula diadema* shell reflects the movements of its host, a humpback whale...……...……....13

1.2 A $\delta^{18}O$ profile from a modern-day *Coronula diadema* shell reflects the movements of its host, a humpback whale...……...14

1.3 A $\delta^{18}O$ profile from a modern-day *Cryptolepas rhachianecti* shell reflects the movements of its host, a California gray whale…….……..15

1.4 Congruent isotopic information recorded in multiple plates of the same barnacle and in multiple barnacles from the same whale.....16

1.5 Scanning electron micrographs of nannoplankton fossils of the Burica Formation……..17

1.6 $\delta^{18}O$ profiles from fossil whale barnacles indicate Pleistocene whales visiting the Burica Peninsula undertook migrations similar to their modern counterparts……..19

1.7 A comparison of $\delta^{18}O$ ranges from modern and Pleistocene-aged whale barnacles…....20

1.8 $\delta^{18}O$ profiles from fossil whale barnacles of the San Pedro and Bay Point Formations indicate migration in multiple prehistoric whale populations…..……..21

1.9 $\delta^{18}O$ profile and comparisons for a fossil whale barnacle suspected to have undergone diagenetic alteration…….……..22

1.10 Trace mineral concentrations for a fossil whale barnacle suspected to have undergone diagenetic alteration……...23

1.11 Scanning electron micrograph evidence of alteration in a fossil whale barnacle……....24

1.12 Creating maps of predicted barnacle calcite $\delta^{18}O$ using modern seawater temperature and $\delta^{18}O$ data…….……...…25

1.13 The structure of the common humpback whale barnacle, *Coronula diadema*…...…...…26

List of Figures, Continued

2.1 Location and glacial-interglacial dynamics of the Canoa Basin, Ecuador...……34

2.2 Two Pleistocene *Cryptolepas rhachianecti* fossils from the Canoa Basin compared to a modern *Cryptolepas rhachianecti* shell……..…….……..35

2.3 $\delta^{18}O$ profiles from two Pleistocene *Cryptolepas rhachianecti* shells……....36

3.1 Comparing $\delta^{18}O$ and $\delta^{13}C$ ranges from modern and fossil whale barnacles, grouped together by location…...…….……...47

3.2 Comparing individual $\delta^{18}O$ and $\delta^{13}C$ ranges from modern and fossil whale barnacles, grouped together by location.……...…….…….….48

3.3 Individual $\delta^{18}O$ profiles from fossil whale barnacles of the Canoa Basin.....49

3.4 Individual $\delta^{13}C$ profiles from fossil whale barnacles of the Canoa Basin.....51

3.5 A comparison of $\delta^{18}O$ ranges from Canoa Basin fossils against plausible migratory destinations based on modern seawater temperature and $\delta^{18}O$ data……..…..…..53

3.6 Mapping plausible migration destinations for the host whales of Canoa Basin fossils based on modern seawater temperature and $\delta^{18}O$ data….……...…...54

3.7 A comparison of $\delta^{18}O$ ranges from Canoa Basin fossils against plausible migratory destinations based on modeled paleoclimate seawater temperature and $\delta^{18}O$ data….....55

3.8 Mapping plausible migration destinations for the host whales of Canoa Basin fossils based on modeled paleoclimate seawater temperature and $\delta^{18}O$ data..……..…...……56

3.9 Mapping plausible migration destinations for the host whales of three Canoa Basin fossils based on modern temperature and $\delta^{18}O$ data……..……...…….57

3.10 Mapping plausible migration destinations for the host whales of three Canoa Basin fossils based on modeled paleoclimate seawater temperature and $\delta^{18}O$ data……...….58

3.11 $\delta^{18}O$ profiles for three Canoa Basin fossils selected for clumped isotope analysis, with notation of clumped sampling sites.…....……..…59

3.12 A mixing model used to help interpret Δ_{47} data for three Canoa Basin fossils.....61

List of Tables

1.1 Summary of $\delta^{18}O$ data from modern coronulids from Alaska and California compared against $\delta^{18}O$ data from fossil coronulids from Panama and California…….18

3.1 Summary of temperature and $\delta^{18}O$ assessed by clumped isotope analysis for three fossil coronulids of the Canoa Basin...……..……..60

Introduction: An overview of mysticete migration and isotope systems

The role of migration in mysticete evolutionary history

Like many animals, the ecology of modern mysticete whales revolves around annual cycles of change. Driven by the physiological necessity of accessing the ocean's most productive waters in order to sustain their great mass, mysticetes make the longest migrations of any mammal, often spanning thousands of miles and taking months to complete. In the Pacific Ocean, these migrations take whales from breeding areas in tropical waters along the coasts of Hawaii, Mexico, Central America, and the northern aspects of South America to seasonally productive feeding areas in the Southern Ocean, Gulf of Alaska, and Bering Sea, with smaller numbers also feeding exclusively in the California Current system (Calambokidis et al. 2001; Calambodikis et al 2009; Felix and Haase 2001). This is a lifestyle of extremes; despite the long migrations and the months that the whales will spend in the breeding areas, they will not eat from the time they leave their feeding waters until they return the following year, causing them to lose 25% of their body mass between feeding seasons (Nash et al. 2013).

The migratory lifestyle is one that mysticete whales are well adapted to, with enormous energy stores to sustain them through the months of fasting, powerful tail flukes to power their movements, and relatively efficient metabolic costs of travel enabled by their great size. Migration is so integral to their ecology, and their morphology so well-adapted to its demands, that migration has been hypothesized to have played key roles in mysticete evolutionary history (Marx and Fordyce 2015; Berger 2007). This idea has been bolstered by the observation that significant shifts in mysticete evolutionary trajectory occur during periods of Earth history that would have had profound impacts on migration (Marx and Fordyce 2015). Specifically, changes in climate, ocean productivity, and the spatial and temporal distribution of that productivity during the Pliocene and Pleistocene coincide with significant declines in mysticete diversity and morphological disparity (Marx and Fordyce 2015; Berger 2007; Slater et al 2017; Bartoli et al. 2005; Sancetta and Silvestri 1986; Marlow et al. 2000; Ravelo et al. 2004; Berger and Lange 1998; Martinez-Garcia et al. 2014; Kumar et al. 1995; Barron 1998; Jacobs et al. 2004).

In the Plio-Pleistocene, glacial-interglacial cycles had complex impacts on upwelling intensity, productivity, and delivery of nutrients to the tropics. Seasonal polar and subpolar productivity increased and remained relatively high while productivity in low and mid-latitude regions became increasingly seasonal, increasingly variable over glacial-interglacial shifts, and increasingly deprived of silicate and other nutrients during some intervals (Berger 2007; Ravelo et al. 2004; Berger and Lange 1998; Martinez-Garcia et al. 2014; Kumar et al. 1995; Barron 1998; Jacobs et al. 2004). During glacial periods, evidence points to a decrease in productivity along the western North American coast, along with a depression of productivity in general (and especially of silica-rich, diatom-based productivity) in the tropics and mid-latitude (Jacobs et al. 2004; Berger 2007; Berger and Lange 1998). At the same time, productivity increased in poleward waters, making polar feeding areas more attractive (Marinez-Garcia et al. 2014). A temporary decrease in diatom accumulation rate at 4.5 Ma in the mid-latitudes, coupled with an increase in diatom accumulation rate in the far north Pacific, may have been one of many initial

stimuli favoring migration (Barron 1998). These events coincide with a period in which mysticetes increasingly became a clade composed of giants, as all of the forms shorter than five meters went extinct while the clade's maximum size doubled (Marx and Fordyce 2015; Slater et al. 2017). It is during this same time that migration is suggested to have begun (Marx and Fordyce 2015; Berger 2007). As the Earth shifted towards modern productivity regimes characterized by wind-driven upwelling and seasonal, patchy accumulations of prey at high densities, migration may have become selectively favorable, which then contributed to a trend towards larger body size to enable more efficient feeding ecology, more efficient migration energetics, and a buffer of stored energy to sustain them between feeding seasons (Marx and Fordyce 2015; Berger 2007; Slater et al. 2017; Williams 1998).

Regardless of whether the increase in body size was driven by the need for migration, every modern mysticete lineage must, by necessity, find highly productive waters of great prey density on which to feed (Slater et al. 2017). Changes in the spatiotemporal distribution of ocean productivity over geological timescales would profoundly impact mysticete behavior, including shifts in migration as different feeding areas became more or less desirable. Accordingly, understanding prehistoric mysticete migrations is a means by which to gain insight into the magnitude, seasonality, and patchiness of productivity in the Plio-Pleistocene oceans, as well as how the spatial distribution of highly productive areas has shifted through different climate states.

Isotope systems and whale barnacles

Understanding how migration may have shaped mysticete evolution and how it may have shifted with the changing oceans depends on being able to reconstruct prehistoric whale migration. Prehistoric migratory behavior isn't discernable from the locations of mysticete fossils alone, however, as these fossils could simply be the remains of various resident populations. In the modern, isotopic studies can yield insight into the movements of marine animals, including odontocetes (McMahon et al. 2013; Matthews et al. 2016; Killingley 1980; Killingley and Lutcavage 1983; Detjen et al. 2015). Using isotopic analysis of fossils has also been used to gain information about the movements of extinct organisms (Fricke et al. 2011; Hoppe et al. 1999; Hoppe and Koch 2007; Price et al. 2002), but applying this technique requires a continuously-growing material that is not prone to diagenetic alteration. Enamel is one of the few mammalian tissues that can be useful in this regard, but edentulous mysticetes have none. However, mysticetes do carry one promising tissue: the shells of coronulid barnacles, which lived embedded in mysticete skin. The barnacles build shells of six plates of high-magnesium calcite that grow by continuously adding new material at the base, effectively growing downward into the skin faster than the whales might be able to shed them off (Monroe 1981; Seilacher 2005; Anderson 1993). The oxygen isotope ratio ($\delta^{18}O$) of each new growth increment is determined by the temperature and isotopic composition of the water it grew in (Killingley and Newman 1982). But carbonates reacted with an acid produce CO_2 gas, and the abundance of the "clumped" isotopologue of mass 47 (a molecule of CO_2 that includes one ^{13}C as well as one ^{18}O) is determined solely by the temperature of the carbonate's formation water (Eiler 2007; Kelson et al. 2017). Thus a barnacle attached to a migrating whale contains within its shell a continuous isotopic signature of the waters through which the whale is moving, with a year's worth of shell growth providing a record of the entire annual migration.

The idea of using coronulid isotopes to reconstruct whale migration was first put forward by J. S. Killingley. Killingley showed that the $\delta^{18}O$ signature retrieved from along the primary growth axis of a shell of *Cryptolepas rhachianecti* accurately recorded the migration of its host, a gray whale (*Eschrichtius robustus*) (Killingley 1980). Killingley himself wondered if this approach might be useful in the fossil record, but never carried out such a study. Killingley and others have since used the same approach to track the movements of sea turtles, who themselves carry barnacles (chelonibids) which are the sister group to the coronulids (Killingley and Lutcavage 1983; Detjen et al. 2015; Hayashi et al. 2013).

All of these studies have focused much less on the carbon isotopes retrieved from barnacle shells, either ignoring them entirely or interpreting them as being relatively uninformative on their own. When interpreted alongside oxygen isotopes, however, the carbon isotopes may help distinguish the types of environment an animal was in by providing insight into the varying influences of upwelling, freshwater input, and evaporation (Killingley and Lutcavage 1983, Sadler et al. 2012, Detjen et al. 2015). For example, periods of relatively high $\delta^{18}O$ and low $\delta^{13}C$ may be interpreted as a signal of upwelling, as upwelling would bring cold, ^{18}O-enriched and ^{13}C-depleted deep water to the surface. Freshwater input, which would include decaying organic matter, might be expected to manifest as a signal of coupled ^{18}O and ^{13}C depletion (Sadler et al. 2012). Applied to my research, it is clear that ^{13}C is less informative than $\delta^{18}O$ or Δ_{47}, but the $\delta^{13}C$ signal may provide additional clues of the whale's environment.

Applying isotope systems to the whale barnacle fossil record

The most common coronulid species in the fossil record is *Coronula diadema*, which inhabits the skin of humpback whales (*Megaptera novaeangliae*) and is known from deposits in California, Mexico, Ecuador, Panama, New Zealand, and Italy (Fleming 1959; Buckeridge 1983; Beau 1971; Dominici et al. 2011, Bianucci et al. 2006, Collareta et al. 2016; Bianucci et al. 2006a; Bianuci et al. 2006b). Humpback and gray whales are far more commonly infested by barnacles than other mysticete species, and individual whales often carry enormous numbers of barnacles on them. *Coronula diadema* builds a shell notably more robust than other coronulids, while the gray whale barnacle *Cryptolepas rhachianecti* has a much more fragile construction and readily breaks apart when removed from the skin. *C. diadema's* strong shell (which is well-suited to survive preservation) and the ubiquity of *C. diadema's* host (the humpback whale lineage) likely explain the fact that *C. diadema* accounts for the majority of the coronulid fossil record. Accordingly, the majority of my research focuses on *Coronula*, and it is therefore important to verify that *Coronula* shell isotopes accurately reflect the host whale's migration path, as Killingley's work only used *Cryptolepas*. The fossil record of *Cryptolepas* itself is in fact quite sparse, having been previously restricted to a few fossils from California and one sub-fossil from the Netherlands (Bosselaers and Collareta 2016; Zullo 1969).

Using fossil shell isotopic information to interpret prehistoric whale migration is much trickier than attempting to track migration in the present day because modern ocean conditions can be directly measured, whereas conditions in the prehistoric ocean must be reconstructed and modeled. The $\delta^{18}O$ profile retrieved from a barnacle shell will not directly reveal the temperature or isotopic composition of the ancient seawater, but are is useful when used in a comparative fashion. The total range of $\delta^{18}O$ measured within a shell is indicative of the range of conditions

the shell grew in, and may be compared against the range of $\delta^{18}O$ from modern-day coronulids as evidence for (or against) the presence of migration. This comparison is greatly aided, when possible, by comparing the fossil coronulid $\delta^{18}O$ to that retrieved from fossil mollusks collected from the same sediments. No matter what the barnacle and its whale are doing, the mollusk is not undertaking lengthy migrations, and as such the total range of $\delta^{18}O$ measured in its shell reflects the range of $\delta^{18}O$ expected from a shell growing entirely within the local region. This serves as a point of comparison for the barnacle $\delta^{18}O$ when determining if the whale was indeed migrating.

The actual temperature and isotopic composition of the seawater a barnacle experienced can be interpreted by combining $\delta^{18}O$ and Δ_{47} analyses. Shell Δ_{47} records only seawater temperature, and can then be used to disentangle temperature from seawater $\delta^{18}O$ in the shell's $\delta^{18}O$ profile. However, analyzing Δ_{47} requires much more shell material than does analyzing $\delta^{18}O$. Thus measuring $\delta^{18}O$ in Berkeley's Center for Stable Isotope Biogeochemistry requires perhaps 50μg of shell material per sample, whereas measuring Δ_{47} requires at least 24mg of material for the multiple sample runs necessary to reign in uncertainty. This means that only larger fossils are suitable for this type of analysis, as getting enough material from the shell of smaller barnacles would result in the interpreted temperature actually being an average taken over a wide range of the barnacle's growth layers. Nonetheless, when clumped isotope analysis is possible, it can be a powerful tool by which to constrain plausible prehistoric migration routes.

Finally, assessing preservation state and determining a fossil's age are both crucial for this research. Extensive diagenetic alteration will alter isotope profiles. Signs of diagenesis include unusual color or texture, isotope signatures that are difficult to explain in the absence of diagenesis, abnormal trace element abundances, or alteration to the fossil's microstructure (Land 1967). Determining the age of a fossil may be relatively easy, in a sense, if the fossil comes from a heavily-studied formation that has already been well-constrained. When this is not the case, biostratigraphy is a powerful tool that can be used to help establish the age of a sediment and the fossils it holds (Bralower et al. 1995; Triantaphyllou 2015).

The focus and structure of the primary chapters

Chapter I begins by analyzing modern coronulids, showing that shell isotope ratios align with expectations based on the known migration routes of the host whales. I then analyze fossil coronulids, where isotope data indicate the presence of similar long-range migrations among multiple prehistoric whale populations. In this chapter I also combine isotopic evidence, trace mineral abundance, and structural indicators to diagnose alteration in coronulid fossils.

Chapter II describes two Pleistocene-aged fossils my research team collected in Ecuador. Both fossils are of *Cryptolepas rhachianecti*, a coronulid known only to live on gray whales. These are the oldest known fossils of this species, and the first evidence of a population of gray whales within the southern hemisphere. This chapter interprets the significance of the find and discusses the isotope data collected from the shells.

Chapter III builds on Chapter I by asking whether isotope data from fossil coronulids can be used to reconstruct the migration routes of prehistoric whales. Here I use fossil coronulid $\delta^{18}O$ and Δ_{47} data in conjunction with models of Pleistocene seawater temperature and isotopic composition to constrain the migratory paths of prehistoric whales visiting the coast of Ecuador.

Chapter I

Isotopes from fossil coronulid barnacle shells record evidence of migration in multiple Pleistocene whale populations

Abstract

Migration is an integral feature of modern mysticete whale ecology, and the demands of migration may have played a key role in shaping mysticete evolutionary history. Constraining when migration became established and assessing how it has changed through time may yield valuable insight into the evolution of mysticete whales and the oceans in which they lived. However, there are currently few data which directly assess prehistoric mysticete migrations. Here we show that calcite $\delta^{18}O$ profiles of two species of modern whale barnacles (coronulids) accurately reflect the known migration routes of their host whales. We then analyze well-preserved fossil coronulids from three different locations along the eastern Pacific coast, finding that $\delta^{18}O$ profiles from these fossils exhibit trends and ranges similar to modern specimens. Our results demonstrate that migration is an ancient behavior within the humpback and gray whale lineages, and that multiple Pleistocene populations were undertaking migrations of similar extent to those of the present day.

Significance

Migration has long been hypothesized to have played a critical role in baleen whale evolution, but fossil constraints on the history of migration are sparse. Here we provide new evidence that the oxygen isotope composition of modern whale barnacle shells reliably records migration pathways. We also analyze fossil whale barnacle shells from three Pleistocene localities and show that they display isotope profiles similar to those of modern specimens. Our results indicate the presence of migration among all three ancient whale populations studied, and point to the possibility of reconstructing changes in migratory behaviors from the Pliocene to the present.

Introduction

Most modern mysticete whales undertake annual migrations that allow them to feed in cool, seasonally productive, high-latitude waters in summer before returning to warm, tropical waters where they breed in winter. In the northeast Pacific, migration routes span from breeding areas in Central America, Mexico, and Hawaii to feeding areas in the Gulf of Alaska, Bering Sea, and California Current system (Calambokidis et al. 2001; Calambokidis et al. 2009). These migrations link mysticete ecology to the processes which shape ocean productivity patterns, and short-term disruptions to these patterns induce corresponding changes in mysticete migratory behavior and distribution (Benson et al. 2002). During the Pliocene and Pleistocene the world's oceans became characterized by increasingly strong seasonal upwelling and patchy productivity distributions, and long-distance migrations are thought to have first become selectively favored at this time (Marlow et al. 2000; Ravelo et al. 2004; Slater et al. 2017; Marx and Fordyce 2015;

Berger 2007). The Plio-Pleistocene was also a pivotal time in mysticete evolution: taxonomic diversity and morphological disparity decreased, most small-bodied forms disappeared, and gigantism became established across the clade (Slater et al. 2017; Marx and Fordyce 2015). Whether these evolutionary trends were driven by changing patterns of ocean productivity and selection for migratory adaptations remains an open question.

Understanding when migration first became established, which ancient populations were migrating, and how stable the behavior has been through time may resolve questions of the significance of migration to mysticete evolution. However, we currently have little direct data regarding the migratory behaviors of prehistoric whale populations. Variation in stable isotopes across a continually-growing tissue can be useful in reconstructing animal movements (McMahon et al. 2013), but within the fossil record this requires a tissue that has a high preservation potential and is resistant to diagenetic alteration. Teeth are one such tissue, and variation in oxygen isotope ratios across layers of enamel or dentin has been used to constrain movements in both modern and extinct animals (Matthews et al. 2016; Britton et al. 2009; Evans et al. 2019; Fricke et al. 2011). While mysticetes don't have teeth, several lineages do play host to commensal barnacles, and $\delta^{18}O$ profiles collected from fossil whale barnacles may offer insight into the movements of ancient mysticetes (Collareta et al. 2018).

Coronulid barnacles belong to the superfamily Coronuloidea, which includes species adapted to live on turtles, manatees, crabs, and snakes (Hayashi et al. 2013). These barnacles live enclosed within a shell of six calcite plates and grow by depositing new material at the shell base, with the $\delta^{18}O$ values of each new growth increment determined primarily by the temperature and isotopic composition of the surrounding seawater (Killingley and Newman 1982). A continuously-growing barnacle can thus preserve an oxygen isotope signature of its host whale's movements, with a year's worth of shell growth recording an entire annual migration. This approach has been used to reconstruct the migration of modern day turtles and California gray whales (Killingley 1980; Killingley and Lutcavage 1983). While several fossil specimens of the gray whale barnacle (*Cryptolepas rhachianecti*) are known, a more promising system to investigate in the fossil record is that of the humpback whale lineage and their common barnacle, *Coronula diadema*, as this coronulid species is much more common in the fossil record, and is known from more than a dozen sites worldwide (Fleming 1959; Bianucci et al 2006a; Buckeridge 1983; Zullo 1969; Beu 1971; Dominici et al. 2011).

Here we investigate the potential of using fossil coronulid $\delta^{18}O$ values to gain insight into the migratory behaviors of prehistoric mysticete whales. Because the majority of the coronulid fossil record belongs to *Coronula diadema*, an important first step is to establish the reliability with which $\delta^{18}O$ profiles from this species accurately reflect a host whale's migration; we address this by analyzing modern *Coronula diadema* shells collected from whales with known migration routes. We then analyze Pleistocene-aged coronulids from three unlithified, shallow-sediment sites along the eastern Pacific coast.

Results

Modern coronulid $\delta^{18}O$ profiles show absolute values, ranges, and trajectories that are consistent with expectations given the known migratory pathways of their hosts. UCMP 221031

is a *Coronula diadema* shell collected from a humpback whale that washed ashore on the California coast and is believed to have belonged to the population which migrates between California and the southern Baja Peninsula. The $\delta^{18}O$ profile recovered from this specimen is consistent with the whale feeding in the waters off the California coast during the previous summer before migrating to the waters surrounding the southern Baja Peninsula (Fig. 1.1). CAS MAM 21691 is a *Coronula diadema* collected from a humpback whale that washed ashore near Sitka, Alaska. The $\delta^{18}O$ profile recovered is consistent with the host whale feeding in the waters near southeast Alaska the previous year before migrating to Hawaii, where the majority of Alaskan humpbacks spend their winters (Fig. 1.2; Calambokidis et al. 2001). Both of these barnacles are quite large (and therefore presumably old) and appear to record an entire migratory cycle. CAS MAM 21149 is a *Cryptolepas rhachianecti* shell collected from a gray whale that washed ashore in northern California. Its $\delta^{18}O$ profile is consistent with the whale having died while heading southward from the Bering Sea (California gray whales migrate from the Bering, Chukchi, and Beaufort Seas to breeding grounds along the Baja Peninsula; Fig. 1.3).

To test $\delta^{18}O$ variability across plates within individual barnacles we sampled two shell plates of UCMP 221031; both plates show very similar profiles (Fig. 1.4). To test $\delta^{18}O$ variability across barnacles from a single whale we sampled three small *Coronula* specimens (UCMP 221032, 221033, and 221034) that were collected from a single young whale with an unknown migration route. $\delta^{18}O$ profiles from these specimens do not record a full migratory cycle, but exhibit generally consistent trends (Fig. 1.4).

We examined fossil coronulids from Pleistocene-aged sediments of the San Pedro Formation and Bay Point Formation of California, and from sediments previously assigned to the Pliocene-aged Burica Formation of Panama, but which we herein assign a Middle to Late Pleistocene age based on the presence of *Emiliania huxleyi* (Fig. 1.5 ; Moore and Kennedy 1975; Wehmiller et al. 1977; Bryant 1987; Coates et al. 1992). $\delta^{18}O$ profiles from four large *Coronula diadema* specimens from the Burica Peninsula (UCMP 221022, 221028, 221029, and 221030) exhibit trends and ranges similar to modern specimens, but are more enriched, as would be expected if these barnacles grew during a glacial (Fig. 1.6, Fig. 1.7, Table 1.1). Stationary mollusks collected from the same beds yield notably smaller $\delta^{18}O$ ranges (Fig. 1.6 panel D, Fig. 1.7). Bay Point fossils (SDSNH 102564, 111656, 114317, all *Coronula*, and 134747, *Cryptolepas*) and San Pedro fossils (SDSNH 50195, *Coronula*, and 30462, *Cryptolepas*) are all small shell fragments, and thus yield truncated $\delta^{18}O$ profiles. Nevertheless $\delta^{18}O$ ranges and trajectories are comparable to those from modern specimens but are again more enriched on average (Bay Point fossils) and 1.64‰ (San Pedro fossils) (Fig. 1.7, Fig 1.8, Table 1.1). The exact shape of a $\delta^{18}O$ profile depends on the completeness of the specimen and the direction the host whale was moving in (California fossils, for example, may have come from whales feeding on the California coast, or possibly from those which were only passing by on northward or southward phases of a longer migration).

We examined all specimens for macroscopic indications of possible alteration. Textural and color abnormalities of CASG 78449, a *Coronula diadema* of poorly-constrained age from Mexico, suggest substantial alteration. The $\delta^{18}O$ profile from this specimen is notably depleted relative to all other specimens we analyzed (Fig. 1.9), which is consistent with open-system alteration in the presence of meteoric waters (Tucker and Wright 2008). We used ICP-OES to evaluate trace metal concentrations in four modern coronulids, CASG 78449, and the Burica

fossils. Fossil trace metal concentrations are generally not substantially different from the ranges seen in modern coronulids, but some fossils do show modest elevations in iron and manganese (Fig. 1.10). Scanning electron microscopy of modern coronulids, CASG 78449 and the Burica fossils revealed microscopic indications of alteration in CASG 78449, but not in the other fossils (Fig. 1.11).

Discussion

J.S. Killingley first recognized the potential of coronulid shell oxygen isotopes to track whale migration, showing that the $\delta^{18}O$ profile of a modern *Cryptolepas rhachianecti* shell was consistent with expectations based on the migration of its host, a California gray whale (*Eschrichtius robustus*). Here we extend this work by showing that modern $\delta^{18}O$ profiles from the barnacle *Coronula diadema* reliably reflect the migration paths of host humpback whales (*Megaptera novaeangliae*), and that fossils of both *Cryptolepas* and *Coronula* exhibit $\delta^{18}O$ profiles similar to those of modern individuals.

Interpreting coronulid shell $\delta^{18}O$ begins with understanding their life history. Coronulid growth rates, lifespan, and reproductive strategies are poorly understood due to their unusual habitat. Coronulids are thought to reproduce while their host whales are clustered together for their own breeding (Best 1991), and newly settled larvae will eventually grow shells that anchor into mysticete skin so securely that shells may remain attached for some time after the barnacle has died (Seilacher 2000). The shells erode at their apex during life (the barnacle retreats downwards in response) and thus a shell may not record the barnacle's entire lifespan (Seilacher 2005). The largest modern *Coronula diadema* shells we analyzed record less than two years of growth as inferred from progressions between the $\delta^{18}O$ profile's most enriched (corresponding to the whale's feeding season) and most depleted (whale's breeding season) values (Fig. 1.1, Fig. 1.2); this is in agreement with previous estimates that coronulids live between one and three years (Best 1991; Monroe 1981).

The largest fossils we analyzed are those from the Burica Peninsula, all of which are relatively complete shells or shell plates. Like modern coronulids, these fossils yield $\delta^{18}O$ profiles with clear signatures of the summer feeding season and winter breeding season (Fig. 1.6). $\delta^{18}O$ ranges recovered from these fossils equal or exceed those of modern specimens, and substantially exceed $\delta^{18}O$ ranges observed in stationary mollusks collected from the same beds (Fig. 1.6, Fig. 1.7). This suggests that the migrations of prehistoric whales was similar in extent to those of today, though a current lack of data on Pleistocene seawater isotopic composition prohibits us from specifying the exact migration paths of these whales. It is notable, however, that the range of $\delta^{18}O$ values seen in these fossils is quite variable (from 1.37‰ to 3.79‰). One possible explanation for this is that Pleistocene whales visiting the Burica Peninsula utilized a variety of different migratory routes. In the present day, whales that winter off the coast of Panama migrate north to feeding grounds which spread from southern California all the way to the northernmost Gulf of Alaska (Calambokidis et al. 2001; Calambokidis et al. 2009). During the southern hemisphere winter, some whales which feed off the coast of Antarctica also migrate to Panama (Acevdo-Guiterrez and Smultea 1995; Rasmussen et al. 2007). Our results therefore support the interpretation that Panamanian waters have served as a meeting point for whales from a variety of subpopulations for at least the last 270,000 years.

The Bay Point and San Pedro fossils are small shell fragments, with only one of these specimens appearing to capture a full migratory cycle (Fig. 1.8). The majority instead display a one-way trend in $\delta^{18}O$ values that is interpreted as capturing a portion of the host whale's migration. Even these one-way $\delta^{18}O$ profiles display $\delta^{18}O$ ranges that are too large to be accounted for by annual changes within the region, and are therefore taken as reflecting migratory movements of the host whales. While the incompleteness of these profiles make them more difficult to interpret, they nonetheless display a variety of $\delta^{18}O$ ranges and values. Whales off the California coast include individuals that spend the entire summer feeding in the regional upwelling zones as well as those which pass through on their way to the Pacific Northwest, Alaska, or (in the case of gray whales) even the Bering and Chukchi Seas. The specimen that seems to record a relatively complete migration, a *Coronula diadema* shell fragment (SDSNH 102564), yields a $\delta^{18}O$ range of 2.26‰, similar to the modern California *C. diadema* shell (UCMP 221031) which yielded a $\delta^{18}O$ range of 1.95‰ (Table 1.1). Taken together, our analysis of the Burica and California fossils confirm the presence of migratory behavior in multiple eastern Pacific mysticete populations belonging to both the humpback and gray whale lineages from three different Pleistocene time points.

Both the modern and fossil coronulids yield $\delta^{18}O$ profiles with a continuous progression between the most enriched and depleted values (noting that smaller fossils do not appear to record the full migratory cycle). These progressions sometimes display excursions from the primary $\delta^{18}O$ trend, which may be caused by the whale passing through waters that locally depart from the route's overall seawater temperature or $\delta^{18}O$ gradients. For example, positive $\delta^{18}O$ excursions against the $\delta^{18}O$ profile's primary trends can occur if the whale passes through either a region of temporarily lower temperature (such as a localized upwelling zone) or a region of high evaporation (preferential evaporation of ^{16}O leaves the water enriched in ^{18}O). Negative $\delta^{18}O$ excursions may occur if the whale's route passed through locally warmer regions or into coastal settings influenced by freshwater runoff, which can create localized depletions of 1-3‰ in seawater $\delta^{18}O$ values extending more than a dozen kilometers offshore (Khim et al. 2003).

Low-Mg calcite is less prone to diagenetic alteration than other biogenic carbonates, and our fossils come from shallow, unlithified sediments, but some fossils nonetheless show modest enrichments in Fe and Mn (Fig. 1.10), which can be indicators of diagenetic alteration (Land 1967, Brand and Veizer 1980). Although this suggests that they may have experienced some diagenetic alteration in the presence of reducing groundwaters, there is little indication that $\delta^{18}O$ profiles are pervasively altered (with the exception of CASG 78449). While recrystallization in the presence of meteoric waters typically causes depletions in bulk $\delta^{18}O$, the Burica, Bay Point and San Pedro fossils all have $\delta^{18}O$ values which are enriched relative to modern coronulid values, which is an unlikely outcome of independent diagenetic histories. These $\delta^{18}O$ profiles are also coherent and fall within ranges compatible with growth during the glacial Pleistocene, which is hard to reconcile with any major alteration. SEM imaging revealed homogenous, comparable external shell structure between modern coronulids and the Burica fossils (Fig. 1.11). In contrast, CASG 78449 displays textural and color indications of alteration, has considerable loss or morphing of delicate shell structure, and has a $\delta^{18}O$ profile substantially depleted relative to all other coronulids analyzed (Fig 1.9). SEM imaging of CASG 78449 displays evidence of dissolution, pitting, and crystalline overgrowth (Fig. 1.11).

Several different factors may influence calcite $\delta^{13}C$, including the incorporation of metabolic carbon, kinetic disequilibrium effects, temperature-dependent fractionation, and the $\delta^{13}C$ of dissolved inorganic carbon, which itself can be modified by upwelling or freshwater input. Interpreting $\delta^{13}C$ data is best done alongside accompanying $\delta^{18}O$ values (Killingley and Lutcavage 1983; Sadler et al. 2012; Killingley and Berger 1979; Bemis and Geary 1996). Depleted $\delta^{13}C$ values coupled with an enrichment in $\delta^{18}O$ may indicate time spent in an upwelling environment (Sadler et al. 2012; Bemis and Geary 1996), while relatively enriched $\delta^{13}C$ values may correspond to periods spent in more open ocean environments (Killingley and Lutcavage 1983). In our coronulid shells, the most enriched $\delta^{18}O$ values often coincide with some of the most depleted $\delta^{13}C$ values, whereas depleted $\delta^{18}O$ values are often paired with relatively enriched $\delta^{13}C$ values; this pattern may signify time that the host whale spent feeding in productive upwelling zones vs time spent migrating across open ocean environments or in breeding areas with little upwelling. While these broad patterns describing the relationship between $\delta^{18}O$ and $\delta^{13}C$ profiles are true for the majority of the coronulids we analyzed, they are not true for all of them, indicating that the other factors are likely playing a large role in determining coronulid shell $\delta^{13}C$.

It has been suggested that mysticetes first began to migrate in the Plio-Pleistocene (Slater et al. 2017; Marx and Fordyce 2015; Berger 2007) as productivity became increasingly seasonal (Ravelo et al. 2004), clustered within high-latitude waters (Barron et al. 2002; Barron 1998), and repeatedly redistributed by glacial-interglacial cycles (Matinez-Garcia et al. 2014; Kumar et al. 1995; Lisiecki et al. 2007), possibly providing a selective advantage for migration as a means of reliably accessing ephemeral and far-flung resources. Gigantism became established at the same time, allowing for more efficient long-distance travel and enabling mysticetes to better utilize pulses of intense productivity followed by long periods of fasting (Slater et al. 2017; Goldbogen et al. 2017; Williams 1999). Our findings demonstrate that migration has been established across multiple whale populations for at least the last several hundred thousand years. Isotopic analysis of other fossil coronulids – which are known from more than a dozen sites across six continents and from sediments dating back to the late Pliocene – provides a promising approach for answering long-standing questions about mysticete behavior and evolution. Combining fossil coronulid $\delta^{18}O$ profiles with paleoceanographic models and emerging proxies that can independently constrain seawater temperature and isotopic composition may provide further constraints on prehistoric migratory pathways.

Materials and Methods

Modern coronulid specimens were collected by members of NOAA's Marine Mammal Stranding Network at the San Diego Natural History Museum (SDNHM) and the California Academy of Sciences (CAS); several modern specimens were also loaned from the existing collections at the CAS. Some fossil specimens were loaned from the SDNHM and the CAS, and more fossil specimens were collected on the Burica Peninsula of Panama. Modern and fossil specimens from the CAS have specimen labels beginning with "CAS"; SDNHM fossil labels begin with "SDSNH," for the San Diego Society of Natural History.

Depending on the size of the shell, a Dremel hand drill or a New Wave Systems micromill was used to collect calcite samples from along the primary (vertical) growth axis of the shell.

Samples of 50-100 micrograms were collected at roughly 1mm intervals, then were analyzed at the Center for Stable Isotope Biogeochemistry at the University of California, Berkeley with a GV IsoPrime mass spectrometer with Dual-Inlet and MultiCarb systems. Several replicates of one international standard NBS19, and two lab standards CaCO3-I & II were measured along with every run of samples. Overall external analytical precision is ±0.07‰ for $\delta^{18}O$. Retrieved oxygen isotope profiles are interpreted using the balanomorph-specific paleotemperature equation of Killingley and Newman (13).

To assess if coronulid shells reliably record an isotopic signature of whale movements we compared isotope profiles from modern coronulids against expectations based on their host whales' known migratory route. To do this, we created gridded maps which predict what the average $\delta^{18}O$ of barnacle calcite formed at any point in the ocean should be during each month of the year. Barnacle calcite $\delta^{18}O$ is determined by both the temperature and $\delta^{18}O$ of the seawater in which it forms, as described by Killingley and Newman's equation (Killingley and Newman 1982):

$$t(^{\circ}C) = 22.14 - 4.37(\delta_C - \delta_W) + 0.07(\delta_C - \delta_W)^2$$

where δ_C denotes barnacle calcite $\delta^{18}O$ and δ_W denotes seawater $\delta^{18}O$. We downloaded global seawater $\delta^{18}O$ (Schmidt et al. 1999) and monthly seawater temperature (NOAA 2018) data derived from direct observations coupled with oceanographic models, then merged these datasets in R (R 2020). With the two variables determining barnacle shell $\delta^{18}O$ thus known, we then used the paleotemperature equation to back out predicted barnacle calcite $\delta^{18}O$ for each unit of a map. We created a series of maps indicating the expected $\delta^{18}O$ of barnacle calcite produced in each unit of the map grid; we generated these maps for each month of the year (Fig. 1.12). We then used these maps to assess whether the $\delta^{18}O$ profiles recovered from modern coronulid shells aligned with expectations based on the host whale's migration route. We used the $\delta^{18}O$ profile's three to four most enriched and most depleted consecutive values as expectations of where the whale should be during the summer feeding season and winter breeding season, respectively. Because our temperature data is monthly, the number of data points used was chosen so as to represent one month assuming constant growth rates of the barnacle. Because of the latitudinal difference in the whale's feeding and breeding regions, the barnacle experiences the coldest waters in the summer feeding season. Although this will also generally correspond with the lowest seawater $\delta^{18}O$, the temperature-dependent fractionation in barnacles (and other calcifying organisms) generates an enriched shell calcite $\delta^{18}O$ in cold temperatures and a depleted $\delta^{18}O$ in warm temperatures.

Fossils analyzed from California museum collections come from the Pleistocene-aged San Pedro Formation and Bay Point Formation of southern California (Wehmiller et al. 1977; Bryant 1987; Coates et al. 1992), along with one specimen from an unrecorded location in mainland Mexico. Further fossil specimens were collected from shallow marine sediments in the eastern Burica Peninsula of Panama, which were previously believed to belong to the Pliocene-aged Burica Formation; bulk samples from this unit were collected for analysis of calcareous nannoplankton assemblages to further constrain ages. Smear slides were prepared using standard techniques and viewed at a magnification of 1250 using a Zeiss Axioskop light microscope. Samples were also observed in a FEI Nova NanoSEM 630 FE scanning electron microscope in

the Pennsylvania State University Materials Characterization Laboratory. $\delta^{18}O$ profiles recovered from all fossil coronulids were qualitatively compared against the modern profiles in order to assess evidence of migration.

All fossil specimens were examined for macroscopic indications (color, texture) of alteration. External shell samples from modern coronulids and the Burica fossils were also imaged with a Hitachi TM-1000 scanning electron microscope for microscopic indications of alteration. We used inductively coupled plasma optical emission spectroscopy (ICP-OES) to compare the trace metal concentrations in the Burica fossils and CASG 78449. The smaller Bay Point and San Pedro fossils, loaned by the San Diego Natural History Museum, were not large enough to be subjected to these analyses without destroying the specimens.

Acknowledgements

Thanks to Tom Demere and Kesler Randall of the San Diego Natural History Museum, to Moe Flannery, Christina Piotrowski, and the late Jean Demouthe of the California Academy of Sciences, and to Nick Pyenson of the Smithsonian National Museum of Natural History for contributing specimens to this study. Thanks to Paul Taylor, Ethan Grossman, and Abigail Kelly for their help in the field. Thanks to Wenbo Yang, Todd Dawson, and Stefania Mambelli at the Center for Stable Isotope Biogeochemistry for their help with all isotope analysis. Thank you to the staff at the University of California Berkeley Electron Microscope Laboratory for advice and assistance in electron microscopy sample preparation and data collection. We thank Valerie and Bill Anders for their generous support. This study was supported by the NSF (EAR 1325683) and the National System of Investigators (SENACYT, Panamá) to A.O., and by funding from the Paleontological Society, the Geological Society of America, Sigma Xi, and the University of California Museum of Paleontology to L.T.

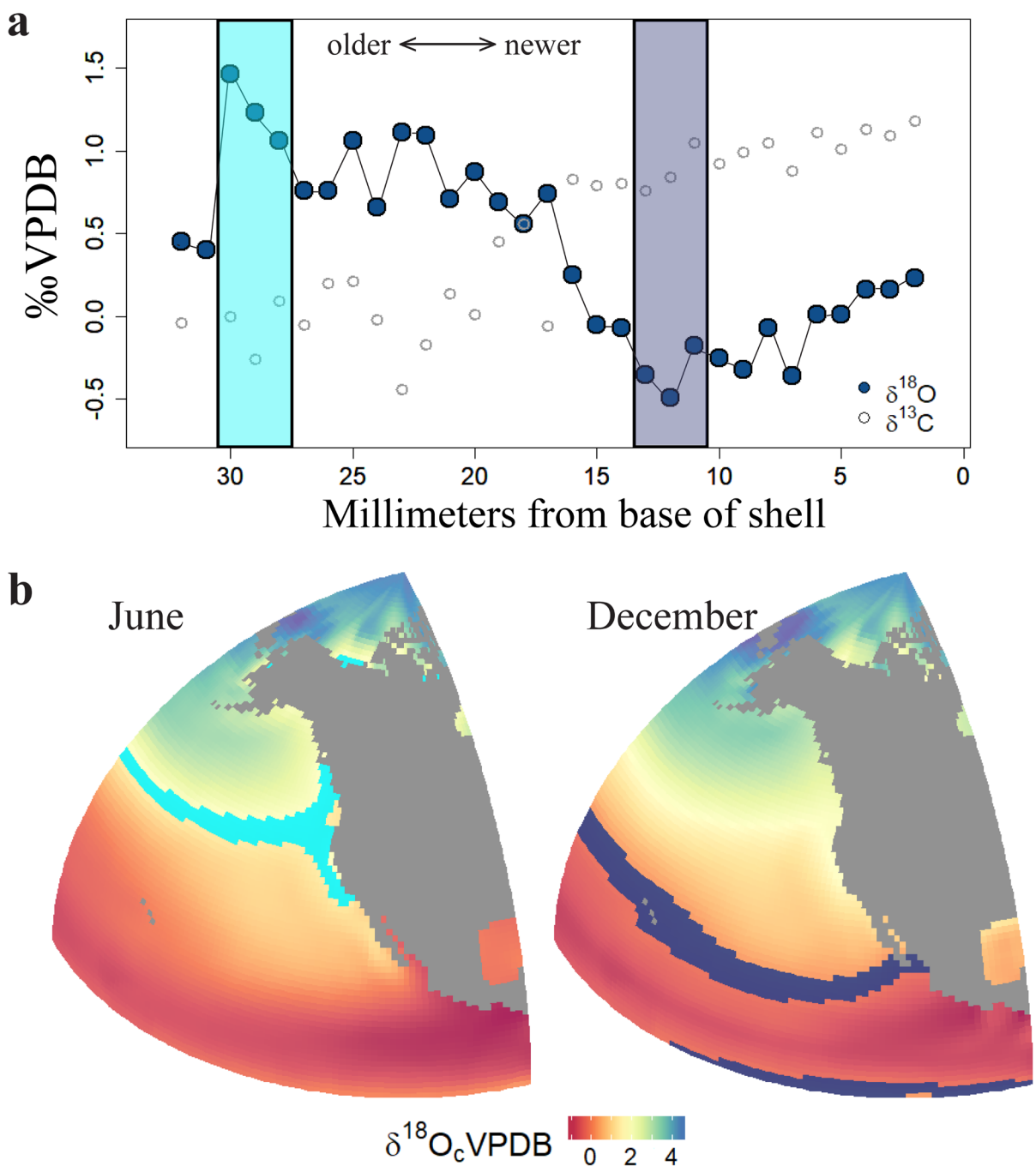

Fig. 1.1. $\delta^{18}O$ profile from UCMP 221031 (a), a modern *Coronula diadema*. UCMP 221031 was collected from a humpback whale that migrated between summer feeding areas along the coast of California and winter breeding areas near the southern Baja Peninsula. Shaded regions of the $\delta^{18}O$ profile in (a) correspond with shaded regions of plausibility for the whale's location during each season in (b). Analytical precision is ±0.07‰ for $\delta^{18}O$, and ±0.05‰ for $\delta^{13}C$.

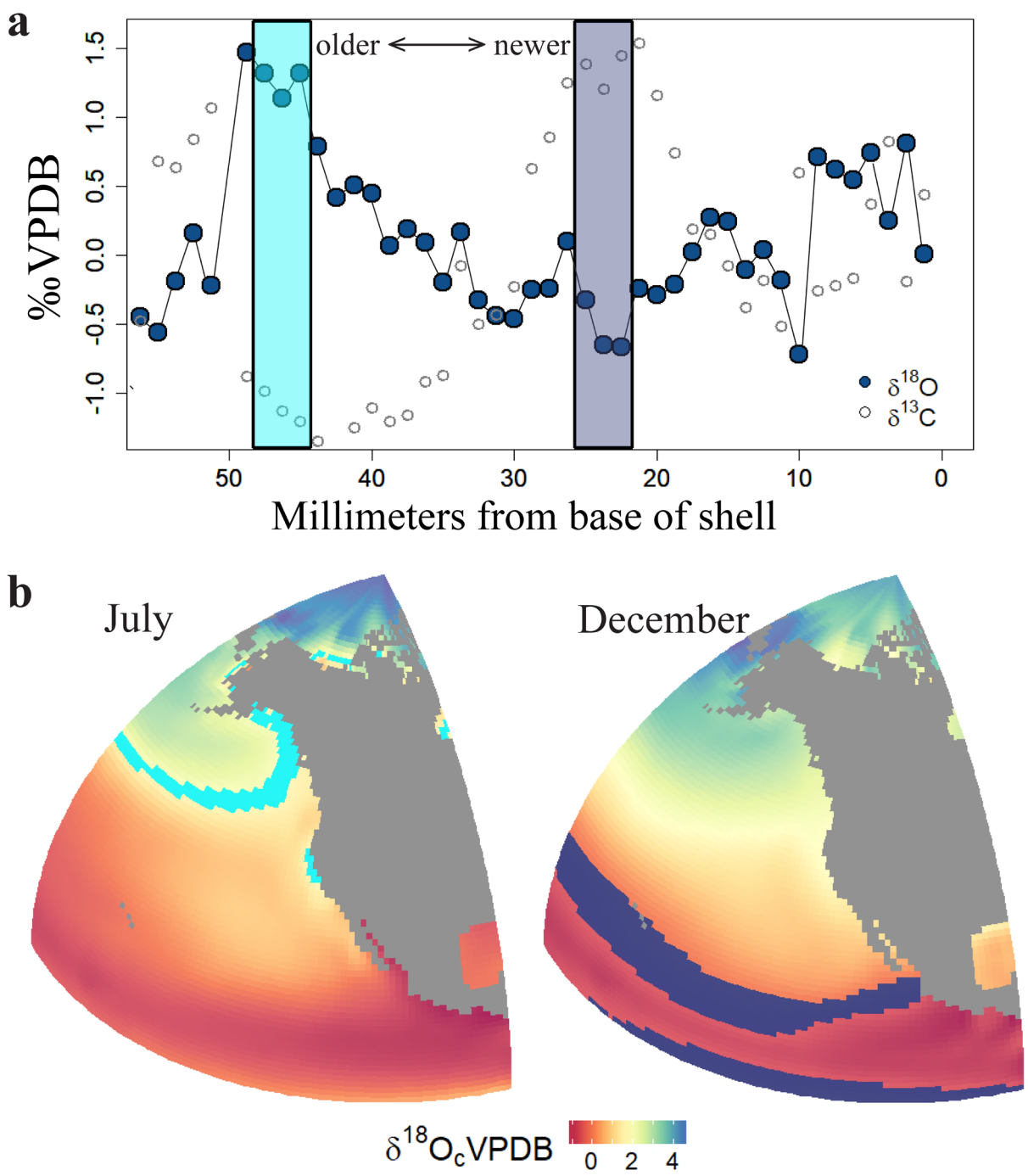

Fig. 1.2. $\delta^{18}O$ profile from CAS MAM 21691 (a), a modern *Coronula diadema*. CAS MAM 21691 was attached to a humpback whale that migrated between southeast Alaska and Hawaii. Shaded regions of the $\delta^{18}O$ profile in (a) align with regions of plausibility in (b).

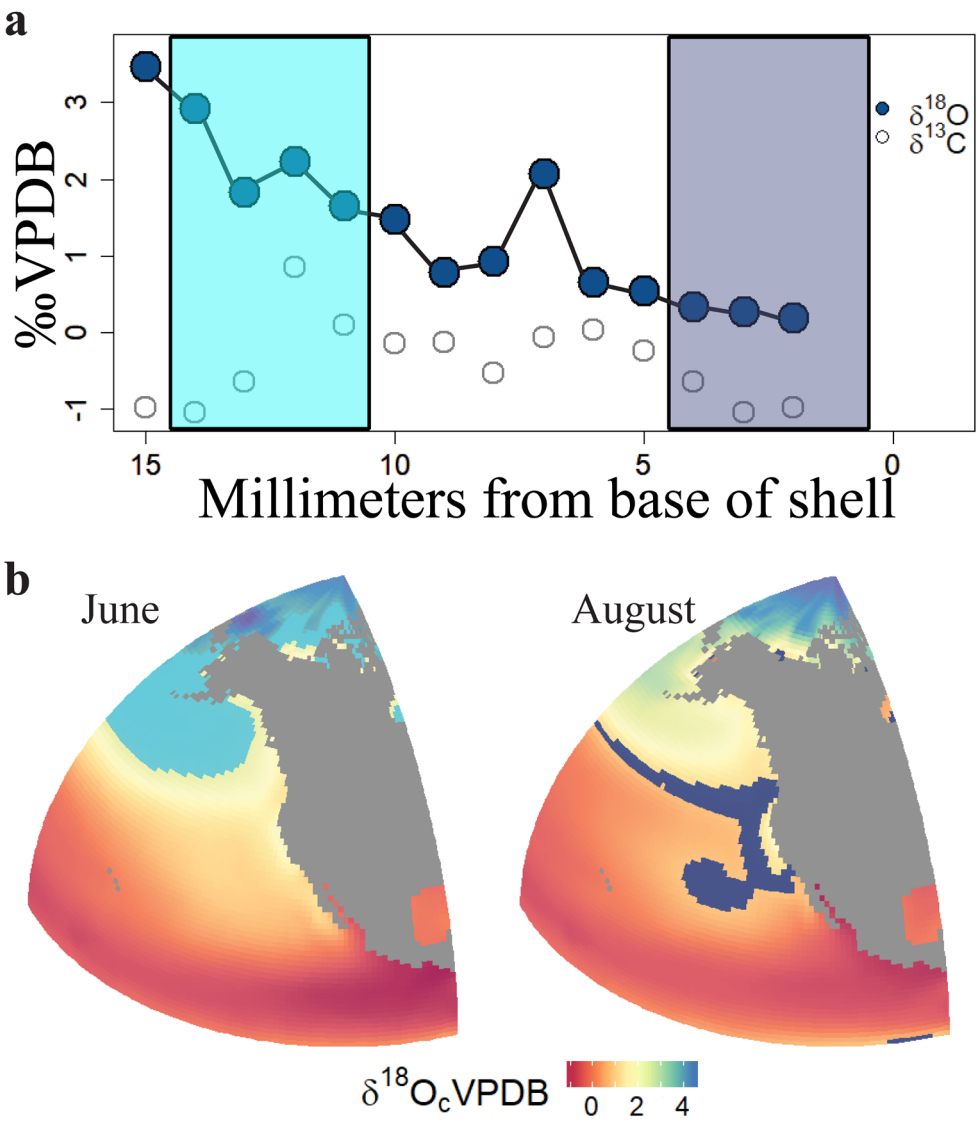

Fig. 1.3. $\delta^{18}O$ and $\delta^{13}C$ profile of CAS MAM 21149, a *Cryptolepas rhachianecti* collected from a gray whale that washed ashore in late August in northern California. Colored regions of the $\delta^{18}O$ profile (a) correspond with the colored regions of plausibility for the whale's location (b) during the feeding season and the final weeks before its discovery. The $\delta^{18}O$ profile is consistent with the whale having traveled south from the Bering Sea, where many gray whales feed in the summer.

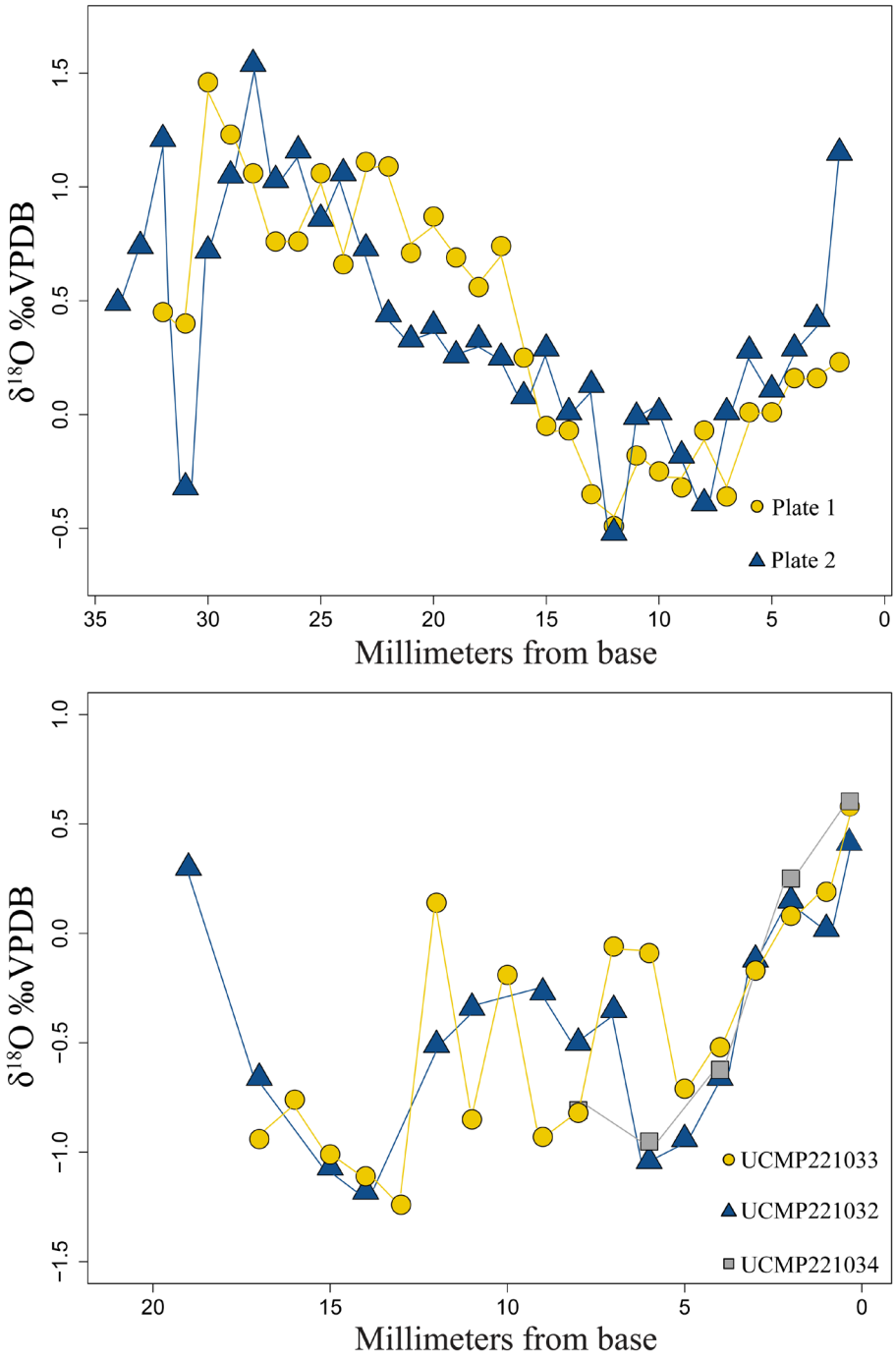

Fig 1.4. $\delta^{18}O$ profiles of two separate plates of UCMP 221031, a modern *Coronula diadema* (a). $\delta^{18}O$ profiles from UCMP 221032, 221033, and 221034, three modern *Coronula* collected from a single humpback whale (b). In (b) two barnacles were much larger than the other, and thus older. All three profiles were aligned such that each shell was taken to have ceased growing at the same time.

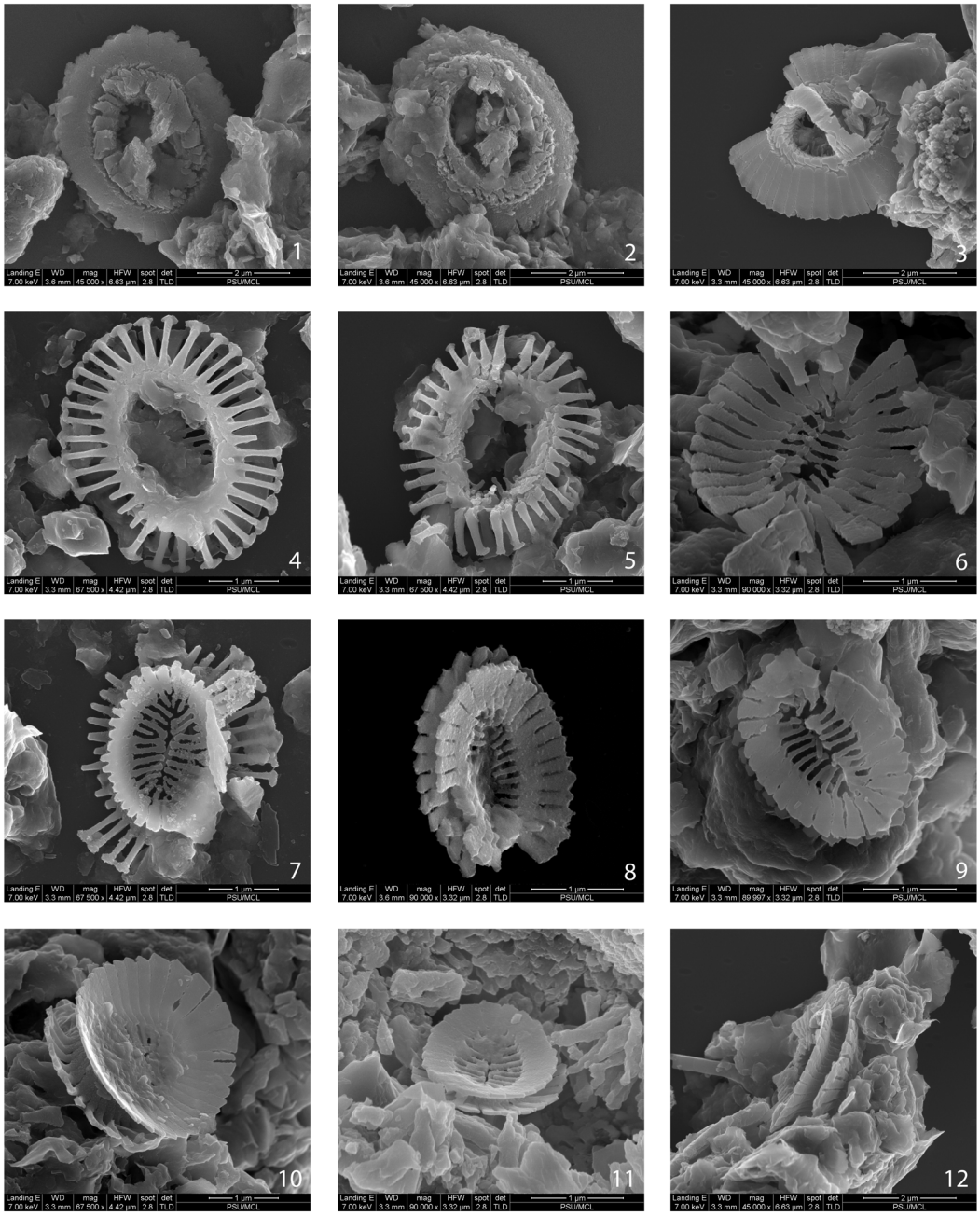

Fig. 1.5. Scanning electron micrographs of nannoplankton from Burica Peninsula sediments. The presence of *Emiliania huxleyi* indicates sediments are Pleistocene aged, and younger than ~270 kyr. 1: *Gephyrocapsa* sp. distal view, Sample 12-5. 2: *Gephyrocapsa sp*., proximal view, Sample 12-5. 3: *Gephyrocapsa sp*., distal view, Sample 167. 4-6, 7, 9, 10-12: *Emiliania huxleyi*, Sample 167; 4, 5: distal view; 6, 7, 9: proximal view; 10-12: side view. 8. *Emiliania huxleyi*, proximal view, sample 12-5. Scale bars for 1-3, 12 are 2 µm, remainder of plates scale bars are 1 µm. *Emiliania huxleyi* shows considerable variation in degree of preservation. *Image by Dr. Timothy Bralower, Penn State University.*

Specimen	Location	$\delta^{18}O$ max	$\delta^{18}O$ min	$\delta^{18}O$ range
UCMP 221031	California, USA (modern)	1.46	-0.49	1.95
CAS MAM 21691	Alaska, USA (modern)	1.47	-0.72	2.19
CAS MAM 21149	California, USA (modern)	3.47	0.19	3.28
UCMP 221032	California, USA (modern)	0.40	-1.18	1.58
UCMP 221033	California, USA (modern)	0.51	-1.24	1.75
UCMP 221034	California, USA (modern)	0.53	-0.95	1.48
UCMP 221029	Burica Peninsula, Panama	1.44	-0.88	2.32
UCMP 221028	Burica Peninsula, Panama	3.77	-0.02	3.79
UCMP 221022	Burica Peninsula, Panama	3.00	-0.79	3.79
UCMP 221030	Burica Peninsula, Panama	1.82	0.45	1.37
SDSNH 111656	Bay Point Fm, CA, USA	2.36	-0.15	2.51
SDSNH 114317	Bay Point Fm, CA, USA	1.93	-0.29	2.22
SDSNH 102564	Bay Point Fm, CA, USA	2.85	0.59	2.26
SDSNH 134747	Bay Point Fm, CA, USA	1.99	-1.49	3.48
SDSNH 30462	San Pedro Fm, CA, USA	2.00	0.31	1.69
SDSNH 50195	San Pedro Fm, CA, USA	2.70	0.91	1.79
CASG 78449	Unknown site, Mexico	0.65	-4.20	4.85

Table 1.1. A summary of $\delta^{18}O$ from modern and fossil coronulids compared in this chapter.

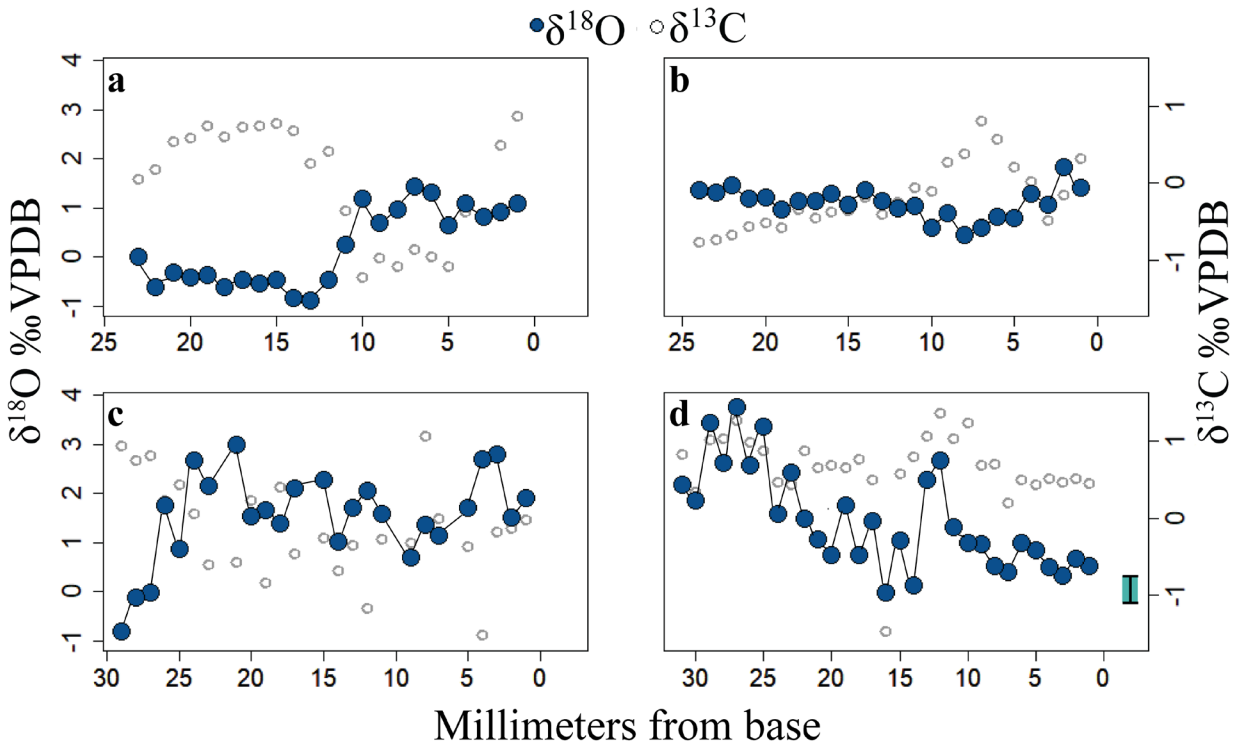

Fig. 1.6. $\delta^{18}O$ profiles from four Pleistocene-aged *C. diadema* fossils from the Burica Peninsula of Panama. Specimens are UCMP 221029 (a), 221030 (b), 221022 (c), and 221028 (d). Blue bar in the right of (d) indicates the range of $\delta^{18}O$ recorded in immobile bivalve shells from the same bedding plane as UCMP 221028. The variety of $\delta^{18}O$ profiles suggests that the whales were migrating to several different feeding regions. This is similar to the modern, where whales that winter off the coast of Panama migrate north to feeding areas from southern California to the Bering Sea and south to the Southern Ocean.

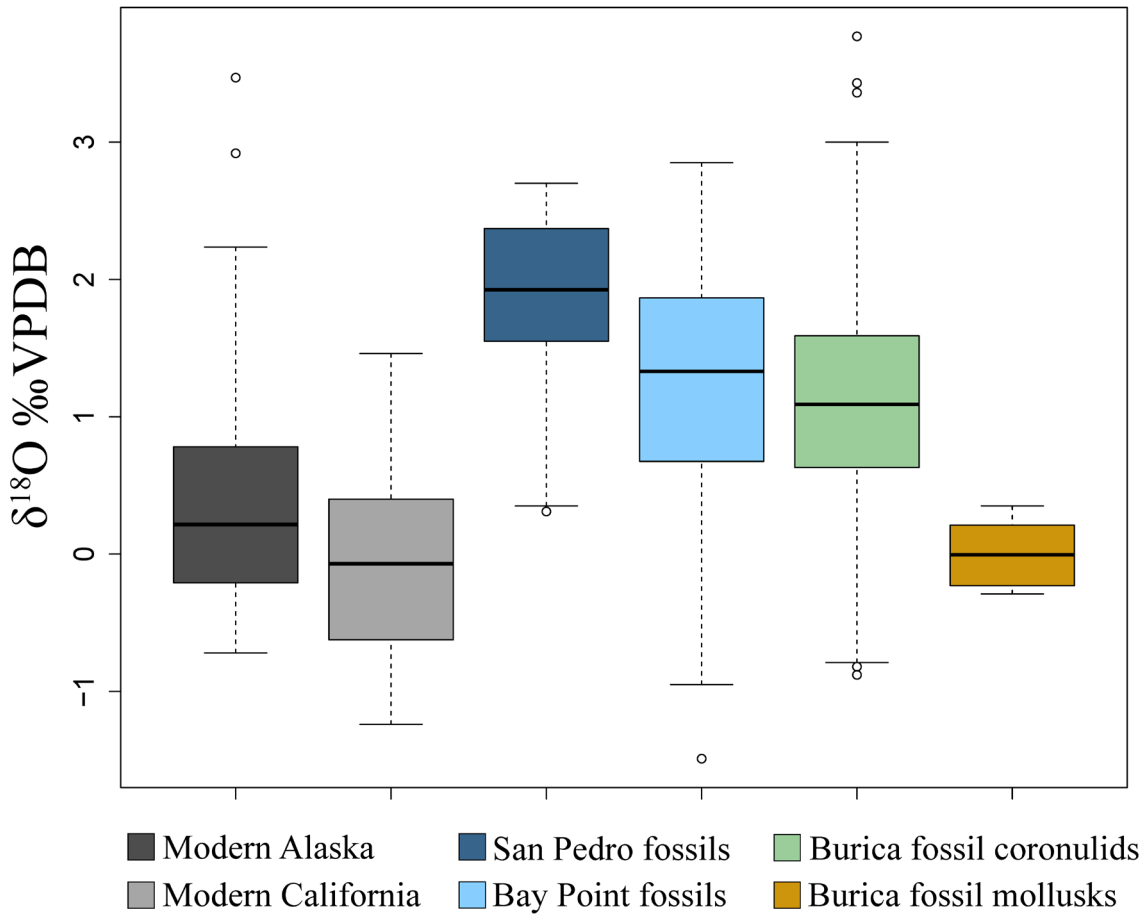

Fig. 1.7. Summary of $\delta^{18}O$ ranges recovered from modern coronulids, San Pedro fossil coronulids, Bay Point fossil coronulids, Burica fossil coronulids, and fossil mollusks collected from the same beds as the Burica coronulids, adjacent to UCMP 221028. Black lines represent median values and shaded boxes capture interquartile ranges (middle 50% of values). Whiskers indicate maximum and minimum values, besides outliers. Outliers (small circles) are defined as higher than 1.5 times the interquartile range above the upper quartile or lower than 1.5 times the interquartile range below the lower quartile. CAS MAM 21149 is included in the Alaska grouping due to its reconstructed migration from Alaska.

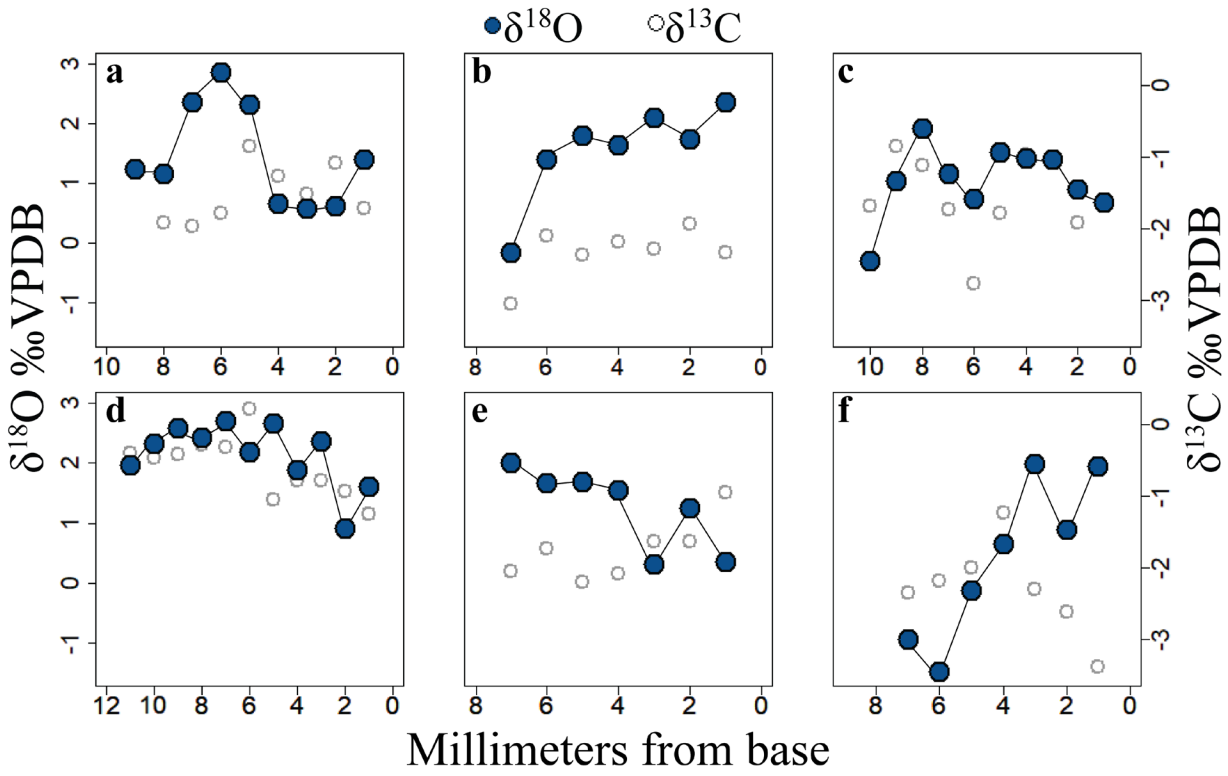

Fig. 1.8. $\delta^{18}O$ and $\delta^{13}C$ profiles from six Pleistocene-aged coronulid fossils from California. Four are *Coronula* (a-d) and two are *Cryptolepas* (e and f). Specimens come from the Bay Point Formation (a-c and f) and San Pedro Formation (d and e). Specimens are SDSNH 102564 (a), 111656 (b), 114317 (c), 50195 (d), 30462 (e), and 134747 (f).

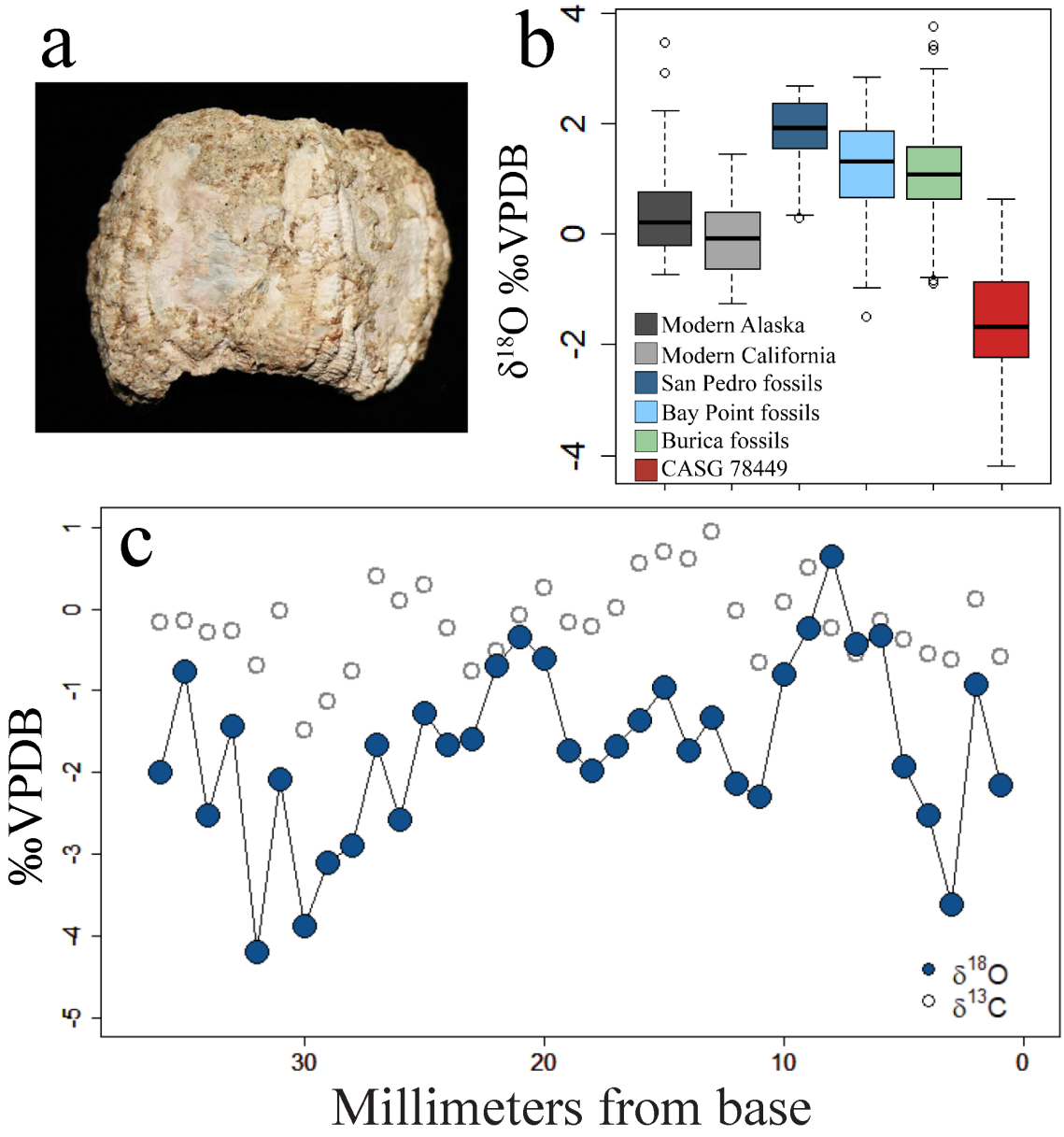

Fig. 1.9. CASG 78449 (a). The specimen displayed texture and color abnormalities indicative of alteration. The $\delta^{18}O$ profile yields values that are substantially depleted compared to all other modern and fossil specimens analyzed (b). $\delta^{18}O$ and $\delta^{13}C$ profile recovered from CASG 78449 (c).

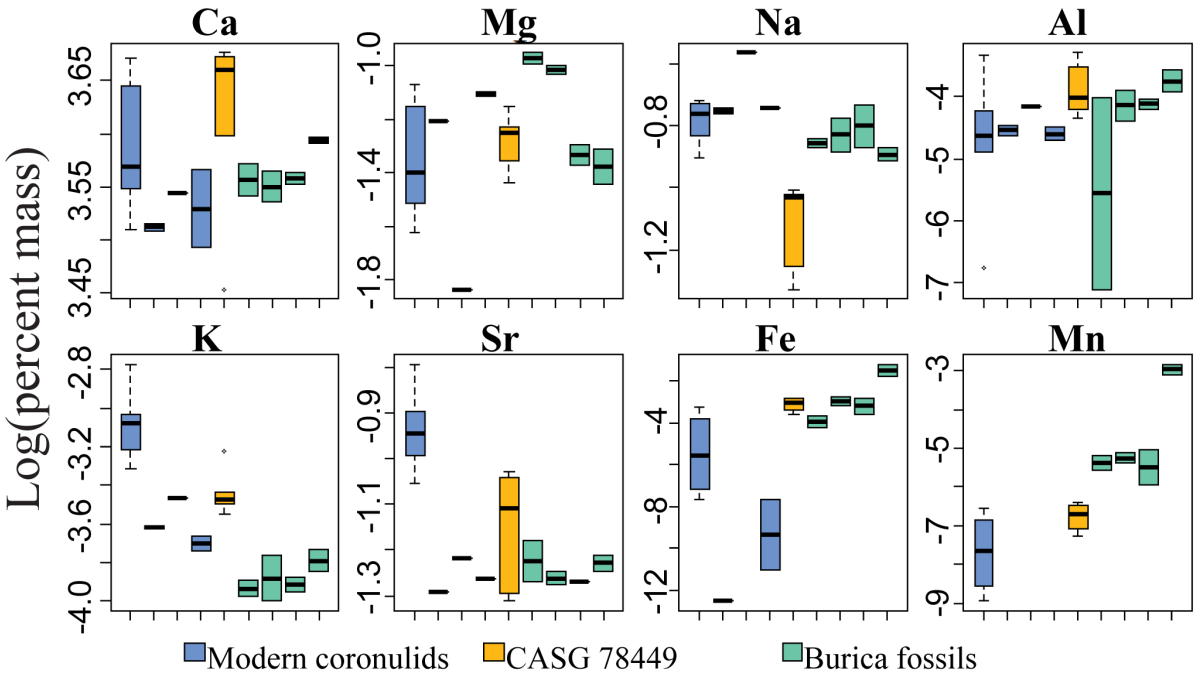

Fig. 1.10. Element concentrations from four modern coronulids, fossil CASG 78449, and the four Burica fossils, as revealed by ICP-OES. Modern specimens are (in order) UCMP 221031, 221032, 221033, and 221034. Burica fossils are (in order) UCMP 221029, 221022, 221028, and 220130.

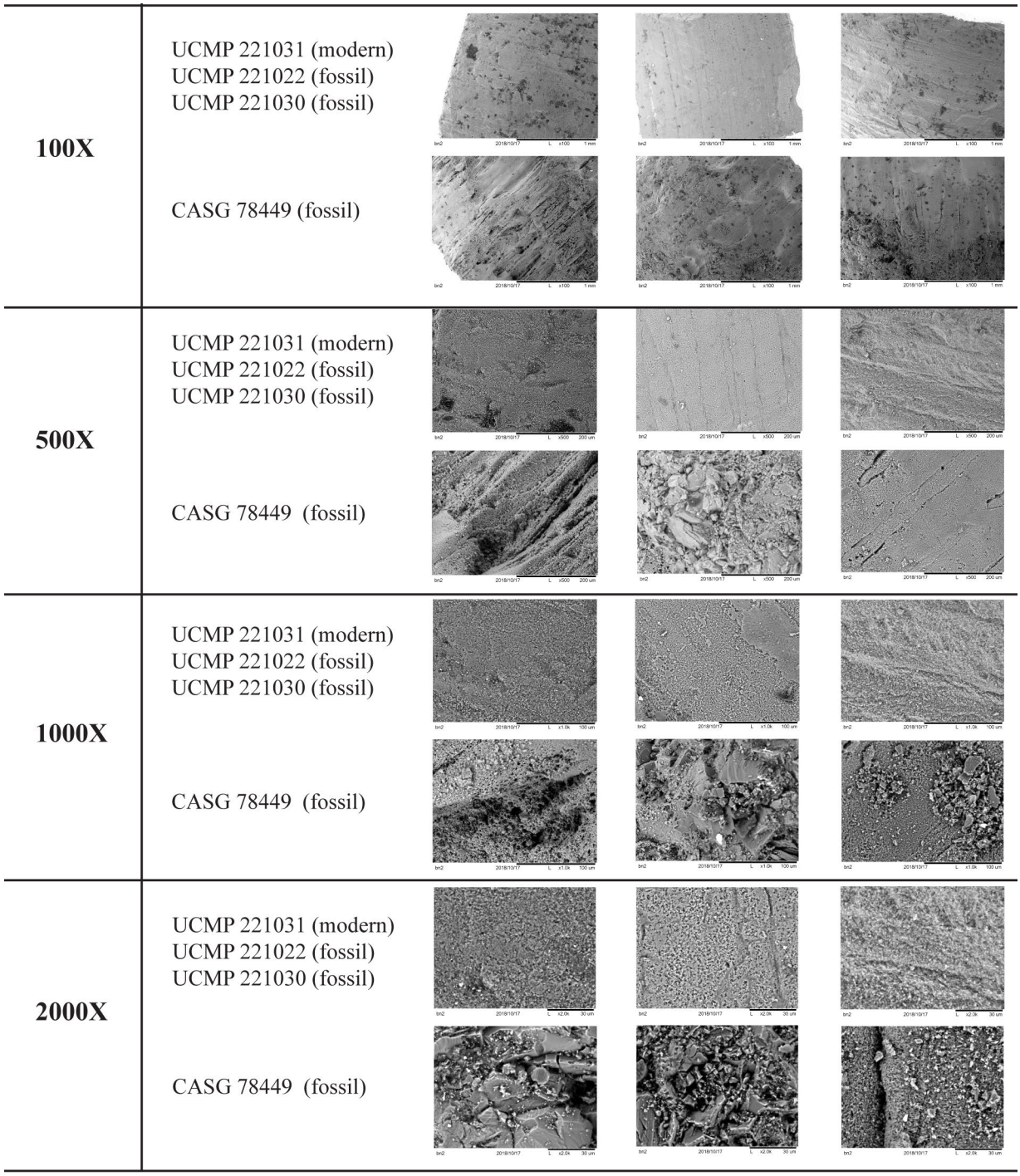

Fig. 1.11. Scanning electron micrographs of a modern coronulid, two Burica fossil coronulids, and CASG 78449. Modern and Burica samples were relatively homogeneous, while CASG 78449 displays a variety of morphologies, including evidence of pitting, dissolution, and crystalline overgrowth.

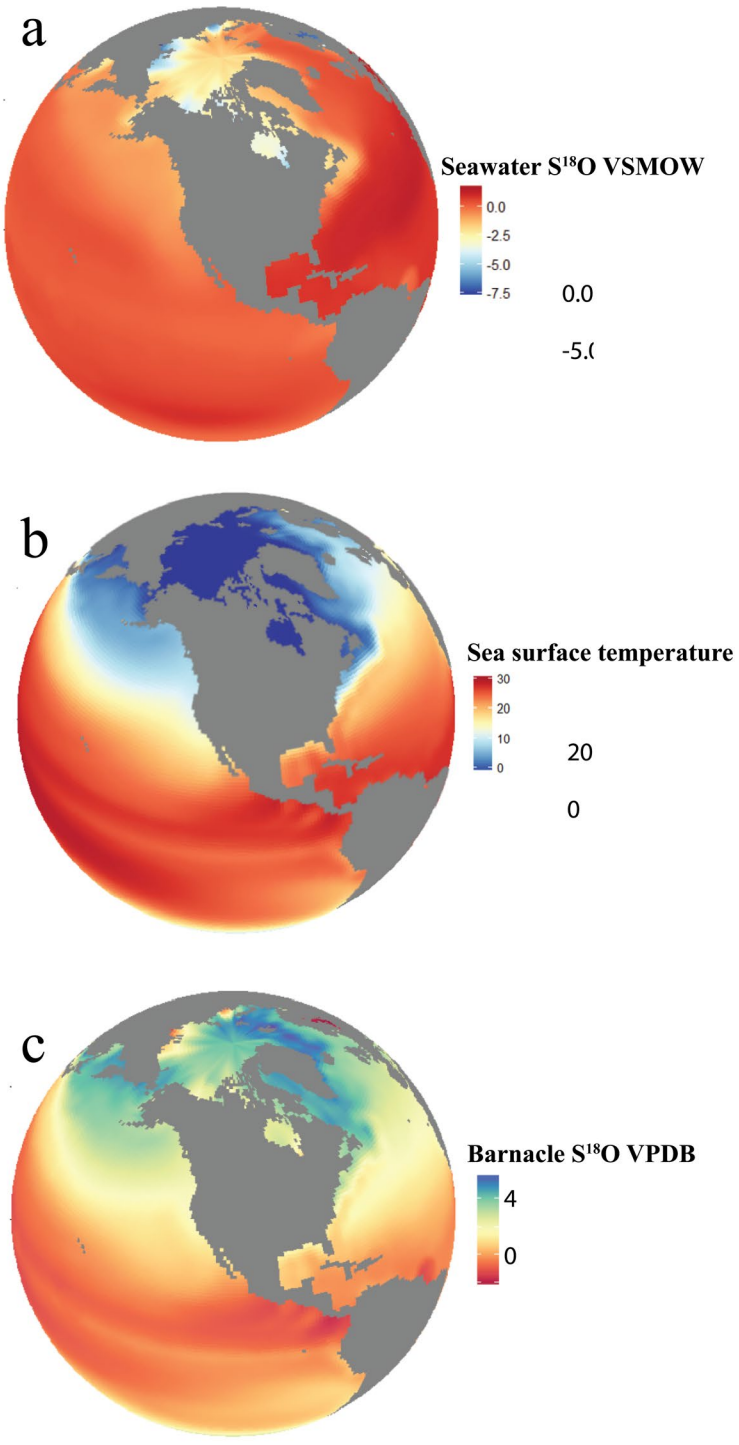

Fig. 1.12. Creation of expectations against which to compare modern coronulid $\delta^{18}O$ profiles is done by downloading sea surface $\delta^{18}O$ data (a; see Schmidt et al. 1999) and monthly temperature data (b; NOAA 2018). The barnacle-specific paleotemperature equation of Killingley and Newman (1982) was then used to calculate the expected $\delta^{18}O$ of barnacle calcite being produced in each unit of the map grid during a selected time interval (c).

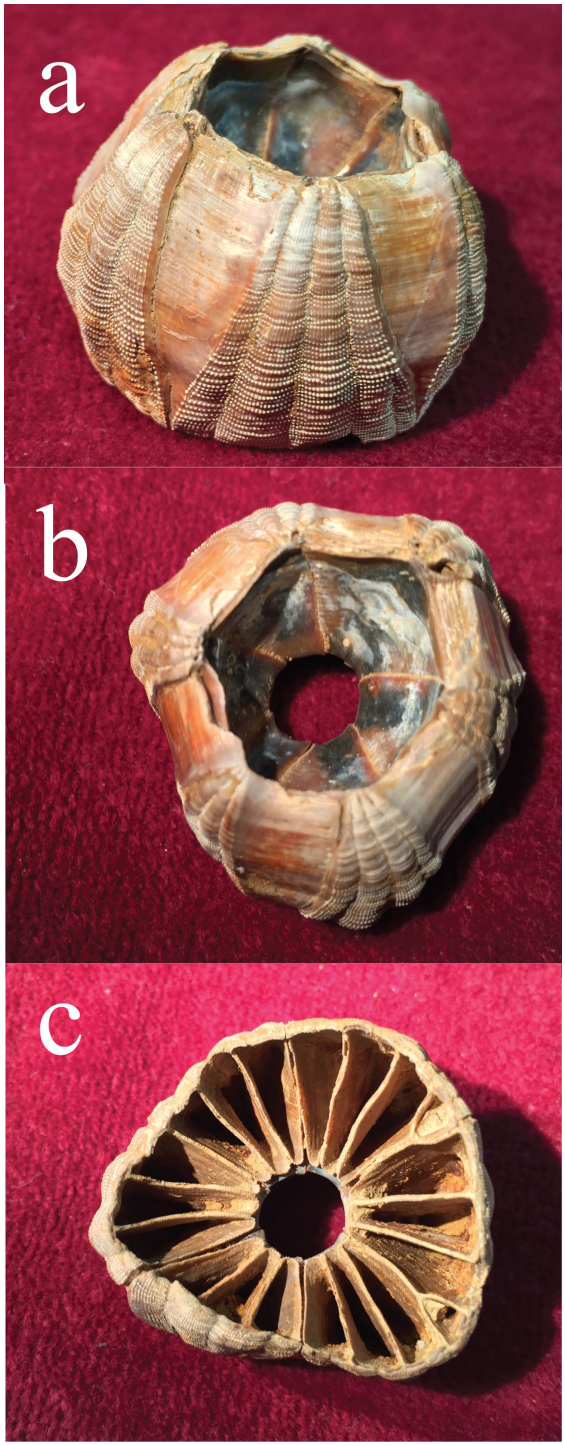

Fig. 1.13. Three views of *Coronula diadema* fossil UCMP 221030. The cavity seen in (a) and (b) would hold the body of the animal in life, and would be covered by a membranous sheath. The multiple chambers seen in (c) anchor the shell to the host by enclosing prongs of whale skin which extend from the shell's base to its apex.

Chapter II

Fossils of *Cryptolepas rhachianecti*, a commensal barnacle of gray whales, from Pleistocene-aged deposits in Ecuador

Abstract

Here we report the finding of two partial specimens of *Cryptolepas rhachianecti* (Cirripedia: Coronulidae), a coronulid barnacle known only to inhabit the skin of gray whales, in Pleistocene-aged sediments from the Canoa Basin, Ecuador. The historical range of gray whales includes the North Pacific and North Atlantic, but no historical or fossil evidence suggests their presence within the South Pacific. We explore the possibility that Pleistocene gray whales may have ranged into the southern Pacific Ocean.

Introduction

Coronuloidea consists of a superfamily of commensal barnacles adapted to live on a remarkable variety of organisms, including manatees, crabs, mollusks, snakes, turtles, and cetaceans (Hayashi et al. 2013). The whale-living barnacles, or coronulids (family Coronulidae) are the most recently derived lineage, having diverged from the other commensal barnacles within the past five million years (Hayashi 2013). This timing coincides with the onset of gigantism in baleen whales (Slater 2017, Marx and Fordyce 2015), and most coronulids make their home on the modern giants, though some species are occasionally seen on delphinids (Seilacher 2005, Hayashi et al. 2012).

As a group, the coronulids are relatively abundant throughout the modern oceans. The genus *Cryptolepas* is represented by the single extant species *Cryptolepas rhachianecti*, a host-specific inhabitant of the skin of gray whales (*Eschrichtius robustus*) (Swartz 2018, Hayashi et al. 2012, Seilacher 2005, Newman and Ross 1976, Newman and Abbott 1980, Bradford et al. 2011). Like its host, *Cryptolepas* has been previously known only from the northern hemisphere, both in the present day and within the fossil record. The most abundant coronulid in the oceans today is *Coronula diadema*, which lives attached to the skin of a more abundant and ubiquitous host, the humpback whale (*Megaptera novaeangliae*). Where whale barnacle fossils are found, they belong nearly exclusively to the genus *Coronula* (Beu 1971; Buckeridge 1983; Zullo 1969; Dominici et al. 2011; Fleming 1959; Collareta et al. 2016; Bianucci et al. 2006a; Bianucci et al. 2006b; Taylor et al. 2019) While fossil whale barnacles usually exist in small numbers wherever they are found, an exception to this general rule is the Canoa Basin of Ecuador, where dozens of coronulid fossils have been collected, previously all belonging to the genus *Coronula* (Bianucci 2006a; Bianucci et al. 2006b).

Here we report finding two partial shells of the gray whale barnacle *Cryptolepas rhachianecti* in Pleistocene-aged deposits from the Canoa Basin, Ecuador. To our knowledge these are the oldest known fossil specimens of *Cryptolepas*, the first occurrences of the genus in the southern hemisphere, and the first evidence of the gray whale lineage living in the southern hemisphere.

Geographic and stratigraphic framework

Specimens were collected in Pleistocene-aged sediments of the Canoa Basin, of the Cabo San Lorenzo area of the Manabi Province, Ecuador (1.2° S, 80.88° W). During the Plio-Pleistocene the Cabo San Lorenzo area was an uplifting island separated from mainland Ecuador by a shallow, narrow strait. Continued uplift eventually connected this island to mainland Ecuador via a land bridge. Glacial-interglacial oscillations caused the shoreline to advance and retreat multiple times, extending west of present-day La Plata Island during glacial periods, when sea level was lower (Di Celma et al. 2002; Di Celma et al. 2005; Cantamalessa and Di Celma 2004). During warmer interglacials, rising sea levels resulted in the shoreline retreating eastward to create a southwesterly-facing coastal embayment, the Canoa Basin (Fig. 2.1). Over time the basin has been progressively filled by roughly 120m of cyclically-stacked shallow marine strata (Di Celma et al. 2002; Di Celma et al. 2005).

Stratigraphic, sedimentological, paleoecological and taphonomic studies of the entire succession indicate it is composed of a series of glacio-eustatically driven parasequences capturing recurring periods of rising and falling sea levels, exposed along ~10km of coastline between Punta Canoa and Rio Callejon (Di Celma et al. 2002; Di Celma et al. 2005). The succession has been divided into the lower Canoa and upper Tablazo Formations, with the Canoa Formation being further divided by an angular uncomformity (Sheppard 1930; Pilsbry and Olsson 1941; Marchant 1961; Savoyat 1971; Baldock 1982; Whittaker 1988; Tsuchi et al. 1988; Di Celma et al. 2005). Older sediments in the basin have yielded Oligo-Miocene fossils, and the Miocene-aged Tosagua Formation lies just below the Lower Canoa (Cadena et al. 2018). The Lower Canoa rests uncomformably atop the Tosagua, and is composed of fine-grained, bluish-gray silty to sandy shales (Di Celma 2005). Above, the Upper Canoa consists of gray-brown silts to sands, overlain by the brown sands of the Tablazo Formation. Sediments in both formations are rich in fossils; taxa therein include bivalves, gastropods, echinoids, crustaceans, corals, and occasional vertebrate remains.

The Lower Canoa consists of four depositional sequences formed under the control of 40-kyr long sea level fluctuations (Di Celma et al. 2002; Di Celma et al. 2005; Cantamalessa and Di Celma 2004). Each sequence is bound below by an erosional surface, above which lies a basal hiatial shell bed followed by several meters of sparsely fossiliferous sediment (Di Celma et al. 2005). While the lowermost shell bed is quite taxa-rich and densely packed, whale barnacles are rare in the lowest two sequences and become more abundant thereafter. The Upper Canoa and Tablazo Formations are interpreted to be a continuous sedimentary record of two and six depositional sequences created under the control of 100-kyr sea level fluctuations (Di Celma et al. 2005). Here shell beds are found basally and mid-cycle, separated by sparsely fossiliferous siliciclastics, and exhibit within-habitat time averaging (Bianucci et al. 2006). The Tablazo Formation was described and is best known from the Santa Elena Province (approximately 120 Km to the south of this site), and has yielded mostly continental fossils (Hoffstetter 1952; Edmund 1965; Ficcarelli et al 2003; Lindsey and Lopez 2015; Cadena et al 2017), but also marine remains (Edmund 1965; Flores 2018). The Canoa and Tablazo Formations have previously yielded dozens of whale barnacles belonging to the species *Coronula diadema*, which lives on the skin of humpback whales, leading to the conclusion that the Canoa Basin was visited by migrating whales in the Pleistocene (Bianucci et al. 2006a; Bianucci et al. 2006b).

Description of taxa and specimens

Systematics:

Class Maxillopoda Dahl, 1956

Subclass Cirripedia Burmeister, 1834

Superorder Thoracica Darwin, 1854

Order Sessilia Lamarck, 1818

Suborder Balanomorpha Pilsbry, 1916

Superfamily Coronuloidea Newman and Ross, 1976

Family Coronulidae Leach, 1817

Genus *Cryptolepas* Dall*,* 1872

Cryptolepas rhachianecti Dall*,* 1872

Specimens UCMP 116131 and UCMP 116132 were both collected from the Upper Canoa Formation. Specimen UCMP 116131 is a single compartment, the radial lamellae mostly missing. Specimen UCMP 116131 is also represented by a single compartment, but in this case many of the radial lamellae are still intact (Fig 2.2). In both specimens several distinguishing characters are visible that identify the specimens as belonging to *Cryptolepas rhachianecti*; these include a transversely grooved sheath, the presence of four lamellar folds (plus two half folds, or sutural folds) on each compartment, irregularly branching radial lamellae where many branches do not reach the periphery, and where terminal ends of the lamellae that do not unite to form a solid outer wall (Pilsbry 1916, Davis 1972). These features distinguish *Cryptolepas* from *Coronula*, which has an ungrooved sheath, fewer lamellar folds, generally fewer branches arising from the folds (all of which reach the periphery), and a solid outer wall formed by the uniting of T-shaped terminal ends of the lamellar folds. In UCMP 116131 transverse grooving of the sheath is clearly visible, and from the outward-facing walls the eroded lamellar folds are clearly seen. Overall UCMP 116131 bears remarkable resemblance to a sub-fossil *Cryptolepas rhachianecti* specimen from the Netherlands reported by Bosselaers and Collareta (2016), and closely resembles a worn shell depicted by Pilsbry (1916; pl. 66, fig. 2). UCMP 116132 is more complete and less eroded; much of the lamellar folds are preserved, many irregular branches are present, and several branches clearly terminate well short of the periphery.

While fossils of the genus *Cryptolepas* are sparse, two species are now recognized in the fossil record: *C. rhachianecti*, reported here and as a (sub)fossil from the Netherlands (Bosselaers and Collareta 2016), and *C. murata*, reported from late Pleistocene deposits of California (Zullo 1961). *Cryptolepas* has traditionally been suggested to have derived from the *Cetopirus* lineage of coronulids, where the major differences in shell morphology seen in *Cryptolepas* are interpreted as degenerative changes related to the more embedded, protected station of the shell in the host's skin (Pilsbry 1916; Monroe 1981). A primary feature distinguishing *Cryptolepas rhachianecti* from *Cetopirus* and *Coronula* is the absence of a complete outer wall to the shell,

which in the latter two genera is formed by the merging of T-shaped flanges at the end of the lamellar folds and serves to create coring chambers which envelop prongs of the host's skin. Zullo interpreted *C. murata* as being an intermediate form, possessing most of the distinguishing features of *C. rhachianecti* while retaining an outer wall to the shell (Zullo 1961; Zullo 1969). Whether *C. murata* truly belongs to the genus *Cryptolepas* or *Cetopirus* has been questioned (Bosselaers and Collareta 2016), and the rarity of these fossils makes answering that question more difficult. *C. murata* shares several distinguishing features with *C. rhachianecti* that are lacking in *Cetopirus*. While *C. murata* shares with *Cetopirus* the outer wall formed by terminal flanges of the lamellar folds, it also shares with *C. rhachianecti* a greater number of primary lamellar folds, unsymmetrical internal branching of the lamellar folds, internal branches that fail to reach the periphery of the shell, a grooved sheath, a crenulate outer border to the radius, interlaminate septa that occur throughout the length of the lamellar folds, and radial septa that originate from one internal septum.

Discussion

To our knowledge these specimens represent the oldest known occurrence of *Cryptolepas rhachianecti*, and the first report of the species in the southern hemisphere. The oldest previously reported specimen of *C. rhachianecti* is a single compartment from late Quaternary deposits in the Netherlands (Bosselaers and Collareta 2016). Besides the Netherlands specimen, no other fossils of *C. rhachianecti* are known, most likely due to the fragile nature of the shell. Whereas other whale barnacles extrude far above the host's skin and are of necessity constructed robustly, *C. rhachianecti* lives deeply buried in the skin of gray whales, with the shell being largely supported by the skin of the host interweaving between the radial lamellae. This embedded, low-profile lifestyle of *C. rhachianecti* may be related to the suction-feeding habit of gray whales, which causes the whales to rub their skin on the seafloor. If *C. rhachianecti* shells protruded much more above the skin, they may risk being dislodged or destroyed via abrasion.

Today *C. rhachianecti* is found only in the North Pacific, where it is a host-specific symbiont of the gray whale (Newman and Ross 1976; Newman and Abbott 1980; Scarf 1986; Bradford et al. 2011; Hayashi 2012). Modern gray whales live in two distinct populations in the western and eastern North Pacific, though some interchange between these populations does occur (Cooke et al. 2007; LeDuc et al. 2002; IWC 2001). Gray whales also have both a fossil and historical record in the North Atlantic, but overharvesting led to the collapse of this population by sometime in the 18th century (Alter et al. 2015; Bosselaers and Collareta 2016; Noakes et al. 2013; Hufthammer et al. 2018; Rodrigues et al. 2018). Accordingly, it is reasonable to expect that *C. rhachianecti* also once ranged throughout the North Atlantic, and the Netherlands specimen supports this (Bosselaers and Collareta 2016). There are no historical or fossil records of gray whale populations in the equatorial Pacific or southern hemisphere, however, making the specimens we report particularly interesting.

The fragility of *C. rhachianecti* shells and their resulting scarcity in the fossil record suggests that the species must have been a common visitor of the ancient Canoa Basin, considering we found two specimens in only three days of fieldwork. Whale barnacles are thought to be mostly shed while host whales are in their winter breeding areas, and accumulations of fossil whale barnacle shells have been interpreted as representing ancient whale breeding areas

(Monroe 1981; Bianucci et al. 2006a; Bianucci et al. 2006b; Taylor et al. 2019). Our finding of *Cryptolepas rhachianecti* fossils raises the possibility that a Pleistocene gray whale population used the Canoa Basin as a winter breeding area. Extant gray whales in the eastern North Pacific spend their summer months feeding in cold, poleward waters, primarily in the Bering and Chukchi Seas, before migrating southward to warm, shallow, and sheltered waters along the coast of Baja California Sur to breed and raise their calves (Mate et al. 2015; Swartz et al. 2006). The Pleistocene Canoa Basin would have offered conditions similar to the lagoons and bays where modern gray whales overwinter, and the large number of *Coronula diadema* fossils found in the region suggest that the region at least served as an ancient breeding area for humpback whales (Bianucci 2006a). While humpback and gray whales do not typically winter together, they do sometimes seek out similar water depths and temperatures (Martins et al. 2000), and wintering populations of both species can be found only a few miles apart along the coast of present-day Baja California.

Oxygen isotope ratios of coronulid shells have been shown to record the movements of their host whales (Killingley 1980; Collaretta et al. 2018; Taylor et al. 2019). Isotopic analysis of the fossil shells revealed $\delta^{18}O$ ranges of 1.93‰ and 2.14‰ (Fig. 2.3). This is less than the 3.28‰ range seen in a modern-day *Cryptolepas rhachianecti* shell of similar size, despite the barnacle being attached to a whale that died while still more than 1,000 miles from its presumed destination; had the whale reached its known breeding ground, the $\delta^{18}O$ range would likely have increased by an additional 1‰ (Taylor et al. 2019). The smaller $\delta^{18}O$ range of the Canoa Basin fossils may reflect the fragmentary nature of the shells, or it may reflect real differences in the migratory extent of these animals as compared to their modern counterparts. If there was once a population of gray whales visiting the coast of Ecuador, then those whales have no directly comparable modern counterpart, but some insight may come from looking at the behavior of modern humpback whales that breed off the modern Ecuador coast (Sheidat et al. 2000; Felix F and Botero-Acosta N 2011). These modern humpbacks are known to migrate to feeding areas along the coast of Chile, within the Magellan Strait, and along the Antarctic Peninsula (Gibbons et al. 2003, Capella et al. 2008; Acevedo et al. 2007; Hucke-Gaete et al. 2013; Felix et al. 2012). It is also known that small numbers of modern gray whales don't migrate (Pyenson and Lindberg 2011; Calambokidis et al. 2002). The $\delta^{18}O$ ranges of these fossils are difficult to explain via annual variation in the immediate area, suggesting that the whales did migrate to some extent. The $\delta^{18}O$ maxima are also less enriched than would be expected if the host whales were traveling to Antarctica, however. It is plausible the whales may have migrated to the Chilean coast, as some modern humpbacks do (Gibbons et al. 2003, Capella et al. 2008; Acevedo et al. 2007; Hucke-Gaete et al. 2013; Felix et al. 2012), but also plausible that they may have migrated to any number of unknown ancient feeding grounds.

If a Pleistocene gray whale population once inhabited the South Pacific it has not survived to the present day. Humpback whales, on the other hand, still breed off the modern Ecuadorian coast. Compared to humpbacks, gray whales are less numerous, less ubiquitous, and more selective about areas they will feed or breed in. These differences may have made prehistoric gray whales comparatively rarer and more sensitive to change. While they are capable of generalist filter feeding like the other baleen whales, gray whales primarily prey on shallow, benthic invertebrate communities via suction feeding. This feeding habitat was greatly reduced

during glacial maxima, however, reducing carrying capacity for the species (Pyenson and Lindberg 2011). It's plausible that one of these disruptions could have winnowed a southern population beyond recovery, and that an intolerance for crossing warm equatorial waters coupled with fidelity of whale mothers to their natal lagoons has kept the species from recolonizing these areas in the modern day (Lindberg 1991; IWC 2001; Goerlitz et al. 2003). At least in the Canoa region, however, a primary cause of the loss of gray whales must have been the continual uplift of the Ecuador coast, which has eliminated the shallow embayments suitable for gray whale breeding. Gray whales only raise calves in sheltered lagoons and embayments, typically in waters of 10m or less (Gardner and Chavez-Rosales 2000; IWC 2001; Goerlitz et al. 2004). While previous periods of high sea level would have created such a suitable breeding habitat within the Canoa Basin, uplift of the Ecuadorian coast has resulted in the modern Canoa coast being dominated by cliffs, while Andean uplift has further eliminated shallow embayments along the South American coast (Lindberg 1991). Humpback whales, in contrast, will breed in a wider variety of water depths, and so may have been undisturbed by this loss of shallow habitat (Pack et al. 2017; Felix and Botero-Acosta 2011).

An alternative explanation is that *C. rhachianecti* once commonly occurred on a different host whale species. However, there is little support for this, as *C. rhachianecti* has never been observed to successfully inhabit any other species in the modern oceans. Settlement of coronulid larvae seems to be initiated by chemical cues from the preferred host's skin (Nogata and Matsumura 2006), while contact with other hosts initiate an immune response capable of shedding a barnacle (Ridgeway et al. 1997). Consequently, the most parsimonious explanation for the occurrence of *C. rhachianecti* fossils within the deposits is the prior presence of gray whales in the area.

With only a handful of *Cryptolepas* fossils known, our finding of *C. rhachianecti* fossils in the Canoa Basin makes the region a promising area for further study. As gray whale fossils themselves are also exceedingly rare, collecting and isotopically analyzing more *C. rhachianecti* fossils from the Canoa Basin may offer more insight into the behavior of this lost population of gray whales.

Materials and methods

Fossils were collected in September 2018 from sediments of the Upper Canoa Formation in the Canoa Basin, Ecuador, coordinates 1.1821ºS, 80.8622ºW. For isotopic analysis, a small Dremel handheld drill was used to collect calcite samples of 50-100 micrograms from along the primary (vertical) growth axis of the shell. Samples were analyzed at the Center for Stable Isotope Biogeochemistry at the University of California, Berkeley with a GV IsoPrime mass spectrometer with Dual-Inlet and MultiCarb systems. Several replicates of one international standard NBS19, and two lab standards CaCO3-I and II were measured along with every run of samples. Overall external analytical precision is ±0.07‰ for $\delta^{18}O$.

Barnacle calcite $\delta^{18}O$ is determined by both the temperature and $\delta^{18}O$ of the seawater in which it forms, as described by balanomorph-barnacle paleotemperature equation of Killingley and Newman's equation (1982):

$$t(ºC) = 22.14 - 4.37(\delta C - \delta W) + 0.07(\delta C - \delta W)^2$$

where δC denotes barnacle calcite $\delta^{18}O$ and δW denotes seawater $\delta^{18}O$. Because of latitudinal difference in the whale's feeding and breeding regions, the barnacle experiences the coldest waters in the summer feeding season. Although this will also generally correspond with the lowest seawater $\delta^{18}O$, the temperature-dependent fractionation in barnacles (and other calcifying organisms) generates an enriched shell calcite $\delta^{18}O$ in cold temperatures and a depleted $\delta^{18}O$ in warm temperatures.

Acknowledgements

Many thanks to Juan Abella of the Miquel Crusafont Catalan Institute of Paleontology and Jorge Morales of the Smithsonian Tropical Research Institute for their help in collecting fossils in Ecuador. I also want to thank Dave Strauss of the UCMP for his incredible work in photographing the specimens.

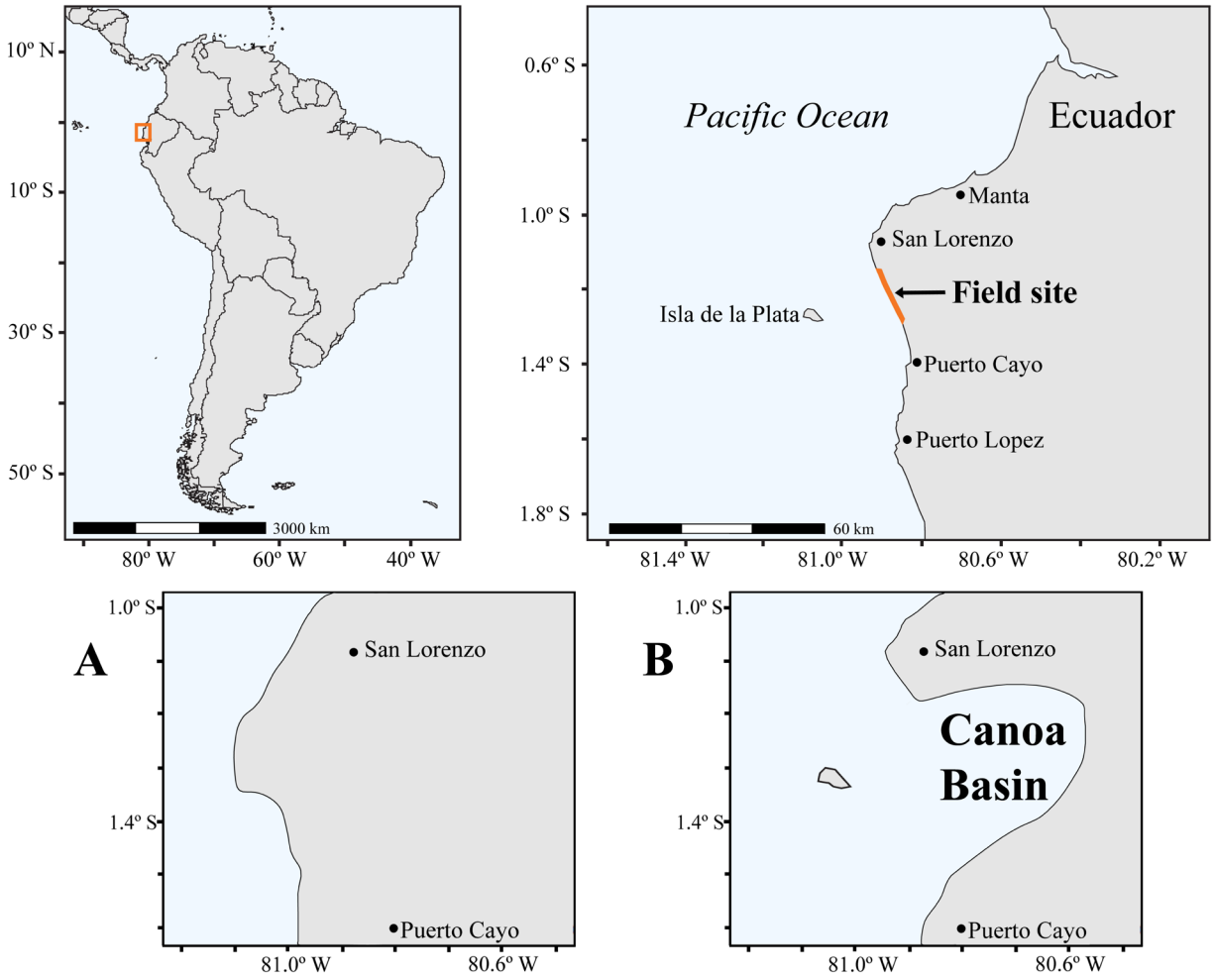

Fig. 2.1. Location of the Pleistocene-aged sediments of the Canoa Basin, Ecuador. During glacial lowstands the coastline extended west past present-day Isla de la Plata (A). During interglacial highstands the coastline moved east, creating a small coastal embayment, the Canoa Basin (B).

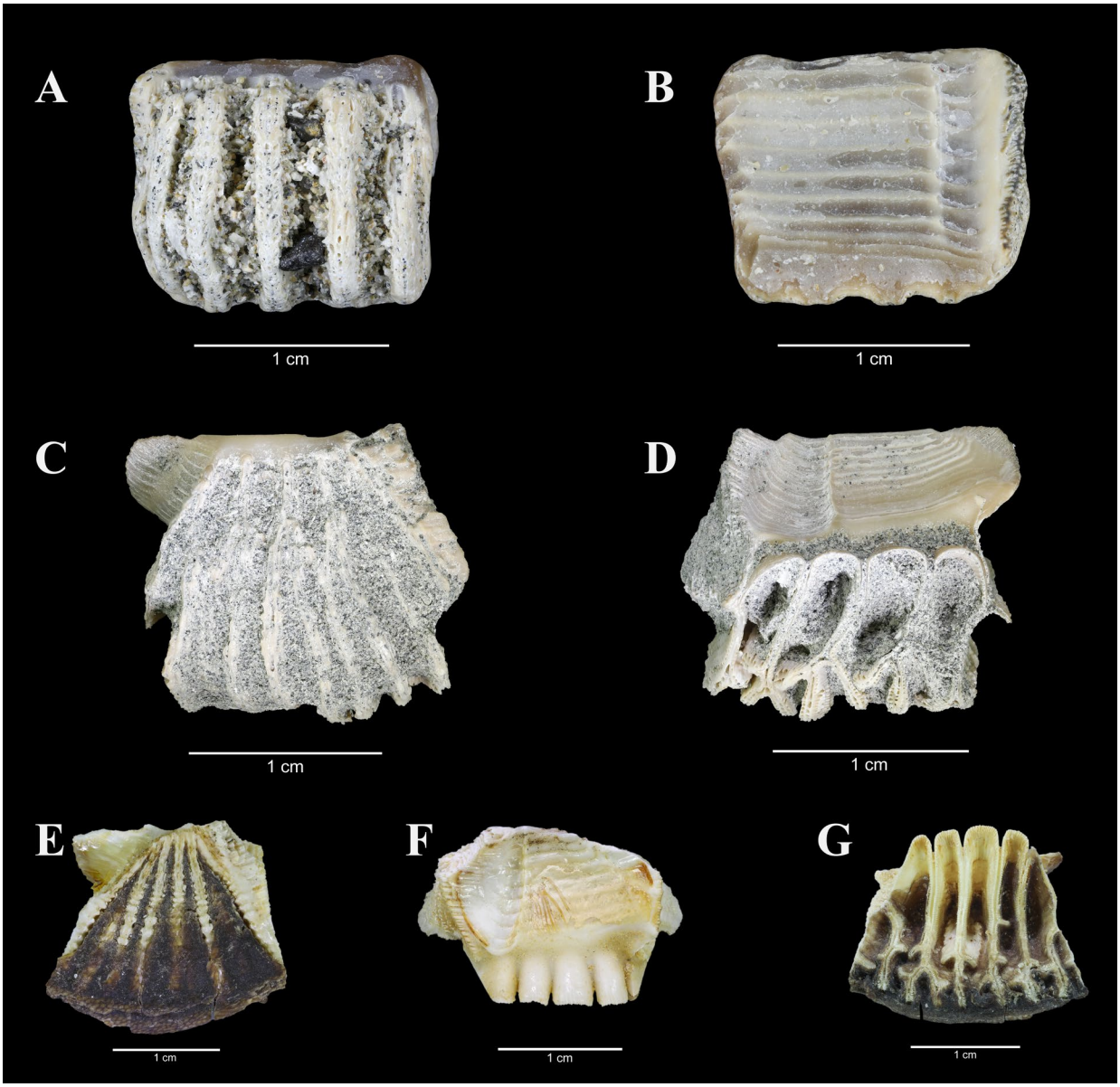

Fig. 2.2. Fossil *Cryptolepas rhachianecti* shells UCMP 116131 (A, B) and UCMP 116132 (C, D) from Pleistocene sediments of the Canoa Basin, Ecuador, alongside modern *C. rhachianecti* shell UCMP 34678 (E, F, G). Fragile folds of shell are supported by whale skin in life (dark material seen in E, F, and G); the folds of UCMP 116132 survived by support from sediment (C). The grooved sheath (B, D, F), 4-6 lamellar folds (A, D, G), blind-ended folds which do not reach the periphery (D, G), and lack of an external wall formed by fusion of the folds can be seen.

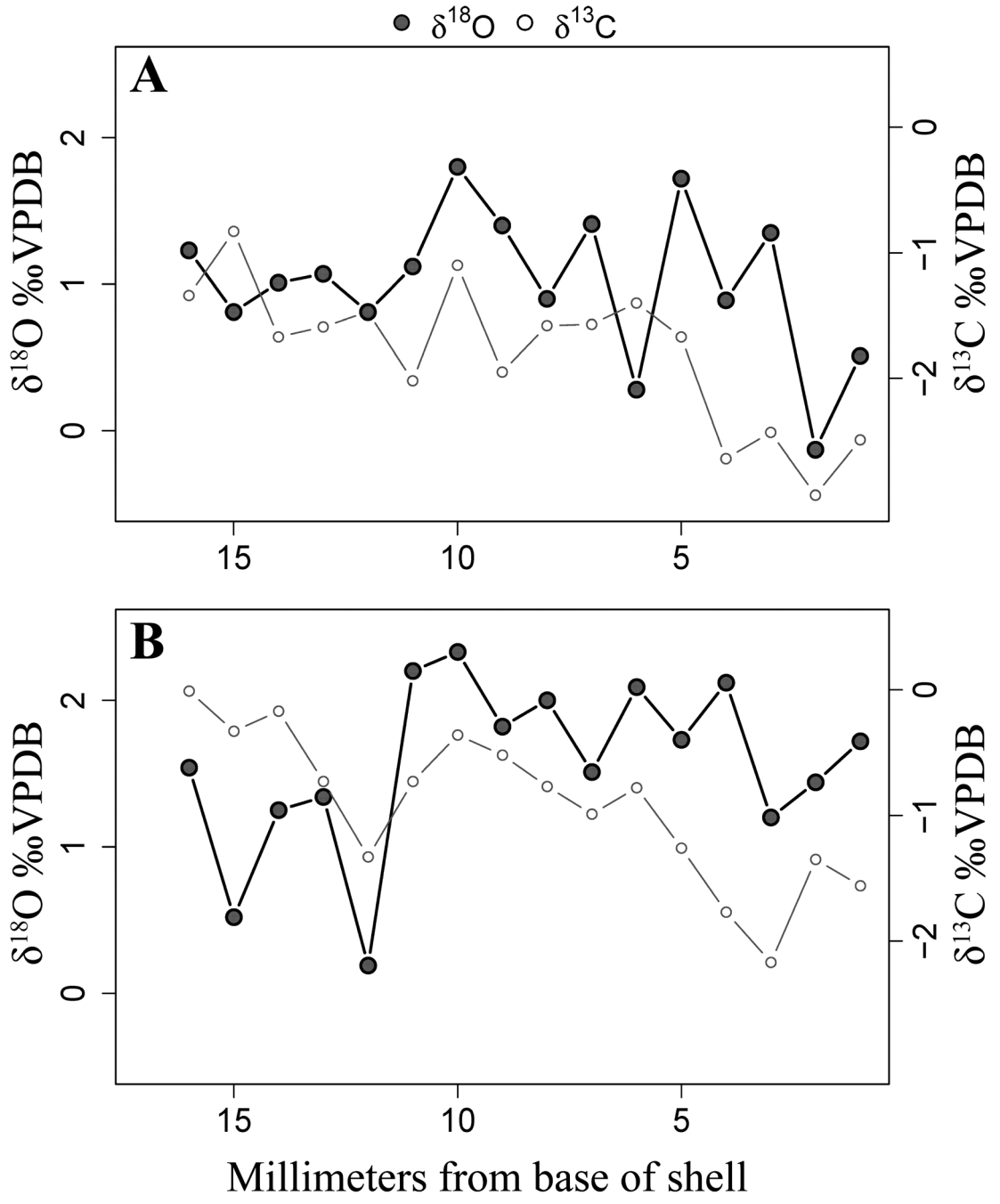

Fig. 2.3. $\delta^{18}O$ and $\delta^{13}C$ profiles collected from along the primary growth axis of UCMP 116131 (A) and UCMP 116132 (B). $\delta^{18}O$ of barnacle shells is determined by the temperature and isotopic composition of the seawater in which it was located during each growth interval. Both shells display $\delta^{18}O$ ranges similar to those seen in barnacles collected from modern, migrating whales, suggesting that the hosts of these barnacles also migrated. Analytical precision is ±0.07‰ for $\delta^{18}O$, and ±0.05‰ for $\delta^{13}C$.

Chapter III

Using paleoceanographic models and isotopes from fossil coronulid barnacles to constrain the migrations of Pleistocene whales visiting the Canoa Basin, Ecuador

Abstract

Modern mysticete whales migrate toward high latitudes to exploit seasonal productivity booms before returning to lower latitudes where they breed each winter, and their need to access high prey densities in order to sustain their great mass ties these animals to the most productive patches of the ocean. Constraining the onset, ubiquity, and potential routes of prehistoric whale migrations could provide insight into mysticete evolution and the spatiotemporal distribution of productivity in the ancient ocean. Here we explore the use of multiple isotope systems in fossil whale barnacles, combined with paleoceanographic temperature and isotope models, to constrain the migratory behaviors of Pleistocene whales visiting the Canoa Basin, Ecuador. Our results indicate that most of these whales were migrating, and that they favored feeding grounds different from the majority of their modern counterparts.

Introduction

Annual cycles in temperature, sunlight, and food abundance determine key aspects of many organisms' ecology, including annual migration patterns. Mysticete whales undertake the longest of all mammalian migrations, taking advantage of seasonally productive, high-latitude waters in summer months before retreating to tropical waters to mate and raise their calves in the winter (Calambokidis et al. 2009; Acevedo et al. 2007; Capella et al. 2008; Cooke et al. 2007; Rasmussen et al. 2007). In the eastern Pacific, these migration routes often take whales from winter breeding areas off the coast of Mexico, Central America, and northern South America to summer feeding waters in the Gulf of Alaska, upwelling zones along the Pacific coast of North America, and several regions in the Southern Ocean. Mysticete migration has been hypothesized to have begun in the Plio-Pleistocene, when global oceans increasingly characterized by seasonal upwelling and patchy productivity distributions may have selectively favored lineages capable of making long-distance migrations (Berger 2007; Marx and Fordyce 2015). While the role that migration has played in mysticete evolution is still an open question, it is clear that migratory behavior is tightly linked to ocean temperature and productivity patterns, as changes in either result in corresponding changes in whales' timing of migration, choice of feeding area, and choice of breeding area (Berger 2007). Temperature tolerances and depth help determine breeding site suitability, while the energetics of their feeding mechanisms constrain the whales to seeking out the most productive patches of the world's oceans (Slater et al. 2017; Calambokidis et al. 2009).

Understanding the ubiquity of mysticete migration through time and constraining where ancient whales were (or were not) migrating to can provide insight into both the importance of migration to the group's evolutionary history and the spatiotemporal distributions of productivity in the prehistoric oceans. Analyzing variation in stable isotope ratios across sequential layers of a continually-growing tissue provides a mechanism by which to constrain the movements of

individual animals (McMahon et al. 2014), but applying such a technique to prehistoric animals requires a tissue with a high preservation potential that will not be prone to diagenetic alteration. Tooth enamel is one such tissue, and variation in oxygen isotopes across enamel growth layers has been used to reconstruct the movements of both living and extinct organisms (Fricke et al. 2011; Britton et al. 2009; Evans et al. 2019).

While baleen whales have no enamel, several species frequently carry heavy loads of coronulid barnacles on their skin. Coronulids build continuously-growing shells of high-magnesium calcite by adding new growth material at the shell base, with each growth increment capturing isotopic tracers of its formation water. Shell $\delta^{18}O$ is primarily determined by seawater $\delta^{18}O$ and temperature, and has been used to reconstruct modern migrations as well as to infer the presence of migration in prehistoric mysticete populations (Killingley 1980; Collareta et al. 2018; Taylor et al. 2019). When reacted with acid, carbonates produce a CO_2 gas, within which the abundance of the "clumped" isotopologue of mass 47 (CO_2 molecules containing both a ^{13}C and ^{18}O substitution) is determined primarily by the temperature of the carbonate's formation water (Ghosh et al. 2006), thus constraining one variable impacting shell $\delta^{18}O$. Analyzing shell $\delta^{18}O$ requires only 15-100µg of material per sample site, however, whereas a minimum of 24mg is needed for multiple replicates of 8mg each in analyzing shell Δ_{47}, which means that $\delta^{18}O$ sampling can be done at a much higher resolution along a shell's growth axis (Center 2020; Spence and Kim 2015). Thus each technique has its strength: control by fewer variables in one, and a higher sampling resolution in the other. Used together, analysis of fossil coronulid $\delta^{18}O$ and Δ_{47} provides a framework for assessing plausible movement patterns of prehistoric whales.

Here we investigate using $\delta^{18}O$ and Δ_{47} data from fossil whale barnacles, combined with paleoceaonographic temperature and seawater $\delta^{18}O$ models, to constrain the migratory paths of prehistoric mysticete whales. This work focuses on large shells of *Coronula diadema*, the common barnacle of the humpback whale lineage, collected from Pleistocene deposits of the Canoa Basin, Manabi Province, Ecuador.

Geographic and stratigraphic framework

During the Plio-Pleistocene a subsiding basin formed in the area surrounding present-day Cabo San Lorenzo, Ecuador, as a result of the Carnegie Ridge colliding with the Ecuador Trench (Di Celma et al. 2002; Di Celma et al. 2005; Bianucci et al. 2006a). At this time Cabo San Lorenzo itself was an uplifting island separated from the mainland by a shallow strait, but continued uplift created a land bridge connecting the island to the mainland (Di Celma et al. 2005). This then divided the Manta Basin to the north from the Canoa Basin to the south (Cantalemessa and Di Celma 2004; Di Celma et al. 2002; Di Celma et al. 2005; Bianucci et al. 2006a). During interglacial highstands the Canoa Basin was a coastal embayment, while during glacial lowstands the shoreline extended much further west (Bianucci et al. 2006a)

The basin has been subsequently filled by roughly 120m of stacked shallow marine strata which are today primarily exposed along 10km of coastal cliffs between Punta Canoa and Rio Callejon (Cantalemessa and Di Celma 2004; Di Celma et al. 2002; Di Celma et al. 2005). The Canoa Formation rests unconformably on Miocene-aged sediments of the Tosagua Formation, and is divided into two units: a lower unit composed of bluish-gray silt and shale and an upper

unit of gray-brown silt and sand, divided by an angular uncomformity (Di Celma et al. 2005; Di Celma et al. 2002; Cantalemessa and Di Celma 2004). Above the upper unit of the Canoa lies the brown sands of the Tablazo Formation. Direct geochronologic and biostratigraphic constraints are lacking, so chronology of the sequences is based on altitude, geomorphology, and geometric data (Cantalamessa and Di Celma 2004). The most intensive study of the area integrated sedimentological, paleoecological, taphonomic, and stratigraphic data to establish that the formations are composed of recurrent glacially-driven cyclothems, with each deposit capturing an interglacial highstand (Di Celma et al. 2002; Di Celma et al. 2005; Cantalamessa and Di Celma 2004). The upper unit of the Canoa Formation and the Tablazo Formation are together interpreted as eight depositional sequences formed by 100-kyr sea level fluctuations, while the lower unit of the Canoa Formation is interpreted as four depositional sequences formed by 40-kyr sea level fluctuations (Di Celma et al. 2002; Di Celma et al. 2005; Cantalamessa 2004; Bianucci et al. 2006a). The uppermost Tablazo has previously been correlated to Marine Isotope Substage 5e based on association with terraces on Isla de Plata (Clapperton 1993), but radiometric or biostratigraphic constraints are needed to constrain the ages of the various sequences, which collectively span a considerable amount of time. The work of Di Celma, however, firmly established the formations as representing Pleistocene-aged glacio-eustatically driven cyclothems (Di Celma et al. 2002; Di Celma et al. 2005; Cantalamessa and Di Celma 2004).

Depositional sequences in both formations contain shell beds at their base and sometimes mid-cycle. The Tablazo Formation is also mapped in the Santa Elena Province, 120 Km to the south, where it has yielded mostly terrestrial fossils (Hoffstetter 1952; Edmund 1965; Ficcarelli et al. 2003; Lindsey and Lopez 2015; Cadena et al. 2017), but also some marine fossils (Edmund 1965; Flores 2018). In the Canoa region exposures, shell beds of both the Canoa and Tablazo Formations yield bivalves, gastropods, echinoids, crustaceans, and corals, as well as occasional vertebrate remains, including fragmentary cetacean skeletal elements. Each shell bed within the Upper Canoa and Tablazo Formation have been interpreted as representing a time-averaged accumulation from a temporally persistent community, while those within the Lower Canoa are accumulations of organisms from a variety of habitats (Bianucci et al. 2006a). The formations also hold the world's largest known accumulation of fossil whale barnacles, primarily belonging to the species *Coronula diadema*, which in the modern day attaches to the skin of humpback whales (*Megaptera novaeangliae*) (Bianucci et al. 2006a, Bianucci et al. 2006b).

Material

A total of 90 fossil whale barnacles were collected during three days of fieldwork carried out in September of 2018. Of these, 88 specimens belong to *Coronula diadema;* the other two belong to the species *Cryptolepas rhachianecti*, which is only known to attach to the skin of gray whales (*Eschrichtius robustus*). *Coronula diadema* is easily identifiable, and several features establishing the species identity are seen in our specimens, including the crown-shaped shell, cup-shaped body chamber, convex ribs with beaded transverse crenulations, and the thick compound radii that are as wide near the apex as the parietes are at the base. The majority of the shells we collected are complete, with all six plates articulated. Shells range in size from only 5mm to more than 80mm measured along the curve of the shell.

Selecting which fossils would be targeted for isotopic analysis was a multi-stage process. Of the 90 barnacles collected, 46 come from boulders which have detached from the exposed cliffs. While the color and grain size of the boulders' sediments often allowed correlation with the in-place sediment on the exposure, these barnacles were eliminated from consideration. Next, $\delta^{18}O$ profiles were collected from several barnacles. Barnacles that had a $\delta^{18}O$ profile with clear peaks (most enriched portions of the profile) and troughs (most depleted portions of the profile) were marked as the most promising for Δ_{47} analysis. The $\delta^{18}O$ "peak" and "trough" likely represent the coldest and warmest waters, respectively, that the barnacle grew in. Thus the ^{18}O-enriched shell layers are hypothesized to correspond to the cold, high-latitude waters where the whale fed in the summer, while the ^{18}O-depleted regions are hypothesized to correspond to the warm, low-latitude waters where the whale spent its winter. The goal was to identify barnacles with enough shell material to permit collecting of the necessary 24 – 40mg of shell material needed to produce 3 – 5 replicates at each site for Δ_{47} analysis while staying within the confines of the $\delta^{18}O$ peak or trough as much as possible.

Results

$\delta^{18}O$ profiles were collected from a total of 17 Canoa Basin fossils, three of which were then selected for clumped isotope analysis. $\delta^{18}O$ data were compared against expectations of what barnacle $\delta^{18}O$ composition would be if the host whales had visited known feeding sites of the modern Ecuadorian whale population, which includes locations primarily along the Antarctic Peninsula, but also the western coast of Chile (IWC 2015; Gibbons et al. 2003; Hucke-Gaete et al. 2013; Acevedo et al. 2007; Capella et al. 2008). Expected barnacle $\delta^{18}O$ is calculated from the barnacle-specific paleotemperature equation of Killingley and Newman (1982). Barnacle $\delta^{18}O$ profiles were first compared against expectations based on modern ocean temperature and isotopic composition, and then against paleoclimate models of both. $\delta^{18}O$ profiles from all 17 barnacles show an average range in $\delta^{18}O$ of 2.86‰. This range in shell $\delta^{18}O$ is comparable to that seen in previously analyzed modern and fossil coronulids, where such a range has been interpreted as evidence of migration (Figs. 3.1, 3.2, 3.3; Collareta et al. 2018; Taylor et al. 2019). $\delta^{13}C$ data, measured and reported alongside, is impacted by more variables, and is best interpreted alongside $\delta^{18}O$, where depleted $\delta^{13}C$ corresponding with enriched $\delta^{18}O$ may signify time spent in an upwelling zone (Figs. 3.1, 3.2, 3.4; Killingley and Lutcavage 1983; Sadler et al. 2012; Killingley and Berger 1979).

Set against modern climate, none of the $\delta^{18}O$ profiles are consistent with migration to Antarctica. Most are consistent with migration to various locations along the Chilean coast, however (Figs. 3.5, 3.6). Specimen UCMP116135 records a peak in the $\delta^{18}O$ profiles which reaches notably beyond the upper limits of expectation for Chilean waters, while UCMP116156's $\delta^{18}O$ profile peaks notably below the lower limit of expectation for Chilean waters.

Barnacle $\delta^{18}O$ was next compared against expectations based on modeled GISS interglacial seawater $\delta^{18}O$ and seawater temperature from ten models of Pleistocene interglacial conditions: GISS, IPSL, NESM3, CNRM, FGOALS-f3, FGOALS-g3, NorESM2, NorESM1-F, MIROC, and CESM (Otto-Bliesner et al. 2020; Bauer and Tsigardis 2020; Boucher et al. 2020; Cao et al, 2018; Voldoire et l. 2019; He et al. 2020; Li et al. 2020; Seland et al. 2020; Guo et al. 2019; Hajima et al. 2010; Danabasoglu et al. 2019). The full range of temperatures predicted by

all models was considered in constraining plausible migration paths. The results are consistent with modeling based on modern ocean data, and do not support most barnacles' host whales having migrated to Antarctica (Figs. 3.5, 3.6, 3.7, 3.8). Results do appear consistent with the majority of these barnacles' hosts having migrated to Chile, however (Figs. 3.7, 3.8). Again, UCMP116156 seems unlikely to have grown in waters as cold as that of the Chilean coast, while UCMP116135 has a $\delta^{18}O$ profile with several values reaching beyond the upper limits of expectation for Chilean waters, the most enriched of which is consistent with travel to Antarctica when interpreted against the warmer climate models.

Specimens UCMP116161, UCMP116157, and UCMP116135 were selected for clumped isotope analysis. The high-resolution $\delta^{18}O$ profiles for these barnacles showed $\delta^{18}O$ ranges of 2.31‰, 3.34‰, and 5.79‰, respectively. Compared against the modern ocean, $\delta^{18}O$ profiles are most consistent with the host of UCMP116161 having migrated to northern or central Chile, the host of UCMP116157 having migrated to central or southern Chile, and the host of UCMP116135 having moved to southernmost Chile (Figs. 3.9, 3.10). Compared against paleoclimate models, these results remain consistent, except that interpretation of UCMP116135 is more nuanced; the composite average paleoclimate model predicts the host whale having likely migrated to southern Chile, while individual models cannot rule out the whale having visited the Antarctic Peninsula.

Samples for Δ_{47} analysis were taken centered on areas of the shells correlating with the most enriched and most depleted portions of the $\delta^{18}O$ profiles (Fig. 3.11). As anticipated, Δ_{47} analysis revealed colder formation water temperatures correlating with enriched portions of the $\delta^{18}O$ profile, and warmer formation water temperatures correlating with depleted portions of the $\delta^{18}O$ profile (Table 3.1). To interpret temperature data, a mixing model was used to account for the fact that sampling for clumped isotope analysis requires three orders of magnitude more calcite per sample than does sampling for $\delta^{18}O$, resulting in Δ_{47} samples averaging across, or mixing, calcite from multiple growth layers. Results are again consistent with the host whales of UCMP116161 and UCMP116157 having migrated to feeding areas along the coast of Chile, with clumped isotope samples indicating small to moderate amounts of mixing. Clumped isotope samples from UCMP116135 are likely moderately to heavily mixed, which could be expected based on the narrowness of the $\delta^{18}O$ profile's peak. Δ_{47} results lend greater support to the host whale having migrated to southern Chile than to Antarctica; the temperature signal is similar to that seen in both UCMP116161 and UCMP116157 (whereas travel to Antarctica would predict a considerably colder temperature), and it is difficult for our mixing model to account for the temperature and $\delta^{18}O$ combination measured (Fig. 3.12).

Overall, $\delta^{18}O$ profiles from fossil barnacles are most consistent with the majority of host whales having migrated to feeding areas along the coast of Chile. All of these $\delta^{18}O$ profiles except for one are not compatible with plausible migrations to Antarctica. We cannot rule out travel to Antarctica for UCMP116135, but Δ_{47} analysis suggests that UCMP116135's host whale more likely migrated to southernmost Chile.

Discussion

Prior work has established that the coast of Ecuador has likely served as a breeding ground for humpback whales for hundreds of thousands of years (Bianucci et al. 2006a); our work here

clarifies plausible migration routes for members of this population. The hypothesis that Pleistocene whales bred in the Canoa Basin is largely based on the immense number of fossil whale barnacles the site has yielded. Modern observations suggest that the barnacles reproduce when their host whales are clustered together in warm, tropical waters over the winter, and that old, large barnacles often get dislodged during this same time (Feliz et al. 2006; Best 1991; Seilacher 2005). The tendency of barnacles to dislodge during the whales' breeding season has been suggested to arise from biologically programmed reactions to changes in water temperature, because of surface activity like breaching and fin-slapping, or due to increased whale-to-whale contact (Felix et al. 2006; Dawbin 1988). The hypothesis is further strengthened by the fact that modern humpback whales still gather along the Ecuador coast to breed in the present day (Felix and Haase 2001; Felix and Botero-Acosta 2011; Shediat et al. 2000).

In the late whaling and early post-whaling eras the scientific literature recognized the feeding grounds of southeastern Pacific humpback whales to be the waters west of the Antarctic Peninsula (Omura 1953; Mackintosh 1965; Olavarría et al. 2000; Gibbons et al. 2003). As the population has rebounded from whaling-era lows, however, the number of whales feeding in Chilean waters has continued to increase, leading some to suggest that this has historically been a more important feeding area than was previously recognized (Gibbons et al. 2003; Hucke-Gaete et al. 2013). This has been supported by historical records of whales in the area dating back six centuries, and by whaling records that indicate successful hunts in the region during the humpback's traditional feeding months (Gibbons et al. 2003; Hucke-Gaete et al. 2013). Today healthy populations of whales are seen feeding from as far north as the waters surrounding Chiloe Island (42ºS) to at least the Strait of Magellan, where their increasing numbers led to the creation of the Francisco Coloane Coastal-Marine Protected Area in 2003 (IWC 2015; Gibbons et al. 2003; Hucke-Gaete et al. 2013; Acevedo et al. 2007; Capella et al. 2008).

Isotopic analysis of fossil whale barnacles offers the best proxy for constraining the migratory behavior of individual prehistoric mysticete whales, which themselves have no tissue (such as enamel) that would lend itself to similar analyses. Combining $\delta^{18}O$ and Δ_{47} of fossil barnacles give both high resolution ($\delta^{18}O$ sampling) and the ability to collect data influenced by a single variable (Δ_{47}), where each method offers something the other lacks (barnacle $\delta^{18}O$ is influenced by two variables, while barnacle Δ_{47} offers lower resolution sampling). $\delta^{13}C$ data, reported herein, is more difficult to interpret and may be influenced by multiple factors, including the incorporation of metabolic carbon, kinetic disequilibrium effects, temperature-dependent fractionation, and the $\delta^{13}C$ of dissolved inorganic carbon, which itself can be modified by up-welling or freshwater input. $\delta^{13}C$ is best interpreted alongside $\delta^{18}O$ data, where depleted $\delta^{13}C$ concurrent with enriched $\delta^{18}O$ may indicate time spent in an upwelling zone, while enriched $\delta^{13}C$ values may indicate time spent in open-ocean environments (Sadler et al. 2012; Killingley and Berger 1979; Bemis and Geary 1996). For several specimens, this potential upwelling signal coincides with what is interpreted as the whale's feeding season (e.g., Figs. 3.3 and 3.4, panel O).

$\delta^{18}O$ and Δ_{47} analyses of fossil whale barnacles reveal little support for most Pleistocene Ecuadorian whales having migrated to Antarctica, but instead support the hypothesis that Chilean fjords have historically been an important feeding area for this population, at least during warm interglacial periods. Where such a population of whales could have fed during a glacial lowstand cannot be addressed here, as the Canoa Basin sediments only contain fossils from warmer

interglacials. Specimen UCMP116156 is interesting in that its $\delta^{18}O$ profile suggests the host whale never traveled to especially cold waters. It is possible that this barnacle's host stayed within the region year-round. A small number of humpback whales are known to do this; these whales are believed to be feeding within the Humboldt Current, as has been observed in the recovering fin whale population (Felix and Olavarria 2012; Toro et al. 2016). While rare, this non-migratory behavior is known to occur in other populations of humpback whales and in some gray whales (Best et al. 1995; Craig and Herman 2003; Pyenson and Lindberg 2011). For all of the barnacles analyzed, it is also possible, of course, that the host whales were undertaking migrations completely different from that seen in any of their modern counterparts. While no whales from Ecuador are known to migrate towards northern hemisphere feeding grounds in the modern day, the stable isotopic constraints provided by this work are also consistent with some locations in the northern hemisphere.

Specimen UCMP116135 is the largest barnacle analyzed, and its full $\delta^{18}O$ profile, displaying multiple enriched and depleted segments, suggests the possibility of having recorded multiple migratory cycles. The longevity of coronulids is unknown, though it has been suggested that the barnacles live only one to three years (Best 1991; Monroe 1981). To date, isotopic analysis lends some support to this hypothesis: of the more than 30 total fossil and modern coronulids analyzed here and elsewhere (Taylor et al. 2019; Collareta et al. 2018; Killingley 1980), none thus far (besides potentially UCMP116135) have a $\delta^{18}O$ profile that suggests more than two annual cycles as judged by a progression of the $\delta^{18}O$ profile through multiple enriched (whales' feeding season) and depleted (whale's breeding season) segments. This could reflect a truly short lifespan for the barnacles, or it could reflect the fact that coronulids erode at their apex such that the oldest layers of large barnacles are often no longer present. The multiple maxima of UCMP116135 are short-lived, however, which makes collecting enough calcite for Δ_{47} analyses difficult without considerable mixing of the signal across multiple growth layers. Higher-resolution analyses could help resolve these questions. The most enriched segments of UCMP116135's $\delta^{18}O$ profile extend beyond the limit of expectations for Chilean waters, and displays three separate peaks that are each more enriched than the $\delta^{18}O$ maximum of any other barnacle analyzed here, plus a fourth peak more enriched than the $\delta^{18}O$ maximum of all but one other barnacle. We cannot rule out that the host whale migrated toward the Antarctic Peninsula, though Δ_{47} data lend greater support to the whale having migrated to southernmost Chile. The brief periods of highly enriched $\delta^{18}O$ could plausibly reflect the whale consistently migrating early in the austral spring, thus encountering colder waters than many of its counterparts.

Evidence from isotopic analysis of fossil whale barnacles indicates that whales visiting the Pleistocene coast of Ecuador were migrating primarily to feeding regions along the coast of Chile. This is different from the modern day, where the majority of Ecuadorian humpbacks migrate to Antarctica, though increasing numbers are feeding in Chilean fjords as the population grows (IWC 2015; Gibbons et al. 2003; Hucke-Gaete et al. 2013; Acevedo et al. 2007; Capella et al. 2008). Our results suggest these Chilean fjords have served as an important feeding ground for southeastern humpback whales during prior interglacial periods, and demonstrate the benefit of combining $\delta^{18}O$ and Δ_{47} analyses of fossil whale barnacles to constrain the movements of prehistoric whales. An important component of future work will be developing tighter constraints on the ages of the sediments, and thereafter incorporating relevant models of seawater

temperature and $\delta^{18}O$ in order to interpret the behavior of prehistoric whales across multiple interglacial cycles.

Methods

For analysis of shell $\delta^{18}O$, a handheld Dremel drill was used to collect calcite samples of 50-100 micrograms from along the shell's primary (vertical) growth axis. Samples were analyzed at the Center for Stable Isotope Biogeochemistry at the University of California, Berkeley with a GV IsoPrime mass spectrometer with Dual-Inlet and MultiCarb systems. Several replicates of one international standard NBS19, and two lab standards CaCO3-I & II were measured along with every run of samples. Overall external analytical precision is ±0.07‰ for $\delta^{18}O$. Barnacle calcite $\delta^{18}O$ is determined by both the temperature and $\delta^{18}O$ of the seawater in which it forms, as described by Killingley and Newman's equation (1982):

$$t(^{o}C) = 22.14 - 4.37(\delta C - \delta W) + 0.07(\delta C - \delta W)^2$$

where δC denotes barnacle calcite $\delta^{18}O$ and δW denotes seawater $\delta^{18}O$. Because of latitudinal difference in the whale's feeding and breeding regions, the barnacle experiences the coldest waters in the summer feeding season. Although this will also generally correspond with the most ^{18}O-depleted seawater the animal will experience (due to less evaporation than in the tropics, which favors the lighter $\delta^{18}O$ entering the gas), the temperature-dependent fractionation in barnacles (and other calcifying organisms) generates an enriched shell calcite $\delta^{18}O$ in cold temperatures and a depleted $\delta^{18}O$ in warm temperatures. We downloaded modern global seawater surface $\delta^{18}O$ (Schmidt et al. 1999) and monthly seawater temperature (NOAA) data derived from direct observations coupled with oceanographic models, then merged these datasets in R (see Appendix III).

We used temperature data from ten separate paleoclimate models available for the last interglacial for our Pleistocene comparisons. Paleoclimate models used were GISS, IPSL, NESM3, CNRM, FGOALS-f3, FGOALS-g3, NorESM2, NorESM1-F, MIROC, and CESM (Otto-Bliesner et al. 2020; Bauer and Tsigardis 2020; Boucher et al. 2020; Cao et al, 2018; Voldoire et l. 2019; He et al. 2020; Li et al. 2020; Seland et al. 2020; Guo et al. 2019; Hajima et al. 2010; Danabasoglu et al. 2019). Model boundary conditions are listed in Otto-Bliesner et al. (2020), Table 1. A composite average model was created after interpolating each individual model onto the same grid using the R package "Akima" (see Appendix III). We compared interpolated data against that from the modern in grid cells where modern data was available, and in places where the modern Ecuadorian whale population is known to breed (Ecuador) or feed (coastal regions from Northern Chile through the Antarctic Peninsula). GISS Pleistocene interglacial seawater $\delta^{18}O$ data was interpolated onto the same coordinates. The warmest and coldest model values at each region of interest were used as our upper and lower limits when calculating expected barnacle $\delta^{18}O$. The peak of the $\delta^{18}O$ profile, expected to correspond to the whale's summer feeding season, was defined as most enriched, consecutive three points from each barnacle's $\delta^{18}O$ profile; these values are used as the constraints when plotting maps of plausible migrations (Figs. 3.6, 3.8, 3.9, 3.10). Paleoclimate models averaged temperature data across the height of the feeding season (December - February).

The benefit of using both $\delta^{18}O$ sampling and Δ_{47} sampling is that the $\delta^{18}O$ data provides higher resolution, while the Δ_{47} data is influenced by a single variable (temperature), rather than two. When comparing $\delta^{18}O$ and Δ_{47} from barnacle shells it is necessary to account for impacts of the different sample size used in each method. Analyzing a shell's $\delta^{18}O$ requires only 50µg per sample, and thus a high-resolution profile can be made by sampling at roughly every millimeter along the shell's primary growth axis, whereas clumped isotope analysis requires 24 – 40mg of material per sample site for 3 – 5 replicates of 8mg each. As a result, clumped isotope samples average a signal over multiple layers of shell growth (or across multiple points from the $\delta^{18}O$ profile), and this must then be accounted for when interpreting Δ_{47} results, as it means that the "true" maximum or minimum temperature the barnacle experiences is unlikely to be captured. We used a mixing model that assessed what mixture of shell calcite, if any, could simultaneously account for the $\delta^{18}O$ values measured from high-resolution (bulk isotope) sampling, the measured Δ_{47}, and the $\delta^{18}O$ measured during clumped isotope analysis. Here the paleoclimate model outputs were used to constrain potential temperature endmembers that the barnacle might have experienced. When evaluating the mixing model, the warmest and coldest paleoclimate model outputs were used to constrain the range of temperature a barnacle might have experienced via growing in different locations. One endmember is known, in that the barnacle did spend some time in the waters of the Canoa Basin. For other potential endmembers we used paleoclimate model temperatures for regions where the modern Ecuadorian whales are known to migrate, asking if prehistoric whales migrating to these same locations could explain our results or not.

Carbonate clumped isotope thermometry eliminates one variable (seawater $\delta^{18}O$ composition) that determines barnacle calcite $\delta^{18}O$, because the Δ_{47} signal is determined by formation water temperature (Ghosh et al. 2006; Affek et al. 2008; Passey et al. 2010; Huntington et al. 2010; Eiler 2011; Lechler et al. 2013; Huntington and Lechler 2015; Methner et al. 2016). Carbonate clumped-isotope measurements were made in the Stolper lab at the University of California, Berkeley on a Thermo 253 Plus IRMS purified. CO_2 was extracted and purified using an automated gas purification system identical to that described in Passey et al. (2010). The He stream used for purification is also Grade 5.0 (99.999%). 8mg of carbonate sample were used. Isotopic measurements are made at masses 44-49 amu as well as a half mass cup at 47.5 amu (e.g., Fiebig et al. 2019). Measurements are made in blocks of 10 cycles and each block is replicated 9 times yielding internal measurement precisions for Δ_{47} of ~0.012‰ typically. Samples can increase in Δ_{47} values by up to 0.035‰ over the course of the measurement due to subtle re-equilibration in the source (the effect is most observable for 1000°C heated gases). This is corrected for by noting the trend of measured Δ_{47} values vs. time and projecting all values to the starting acquisition time.

Measured isotopic compositions ($\delta^{18}O$ and $\delta^{13}C$ values) are calculated based on the Brand parameters. The commonly observed dependence of Δ_{47} values on bulk compositions (as given by δ^{47} values) is first corrected for using a pressure base line correction derived from measured intensities at the mass 47.5 cup. A residual dependence of Δ_{47} on measured δ^{47} values (typical slope of 0.0005 ‰/‰) is corrected for by measuring CO_2 samples with a variation in δ^{47} values of ~ -3 to 42‰ (relative to the working gas) heated to 1000°C (Huntington et al. 2009; Dennis et al. 2011). Following this, Δ_{47} values are corrected to the so-called Absolute Reference Frame (ARF), also called the carbon dioxide equilibrium scale (CDES) after Dennis et al. (2011) based

on measured differences in samples equilibrated at 25°C or heated to 1000°C vs. that expected based on theory. An acid digestion correction of 0.082‰ is then added to all samples to place them into a 25°C acid-digestion reference frame (Bernasconi et al. 2018). Finally, samples are corrected based on measured vs. expected values of the ETH 1-4 standards using the values given in Bernasconi et al. (2018). At least four replicates of all four ETH standards measured over one month are used for the secondary ETH correction following transfer of the raw measurements to the ARF.

Measured $\delta^{18}O$ and $\delta^{13}C$ of samples are corrected based on differences in measured values of the ETH standards vs. values given in Bernasconi et al. (2018). Finally, $\delta^{18}O$ values were corrected using an acid fractionation factor for $\delta^{18}O$ ($^{18}R_{CaCO3}/^{18}R_{CO2} = 1.00821$ at 90 ºC; Swart et al., 1991). We measured three secondary standards to assess the accuracy and long-term precision of $\delta^{18}O$, $\delta^{13}C$, and Δ_{47} measurements. We measured an in-house marble (CAR1), in-house travertine (TRV1) and the international IAEA-603 standard. Carbonate samples were measured three to five times across at least three analytical weeks. All samples were replicated across multiple calibration sessions.

Acknowledgements

Many thanks to Juan Abella of the Miquel Crusafont Catalan Institute of Paleontology and Jorge Morales of the Smithsonian Tropical Research Institute for their help in collecting fossils in Ecuador. Thanks to Daniel Stolper and Andrew Turner of the Stolper Lab at UC Berkeley and Dan Ibarra of Brown University for their work in measuring clumped isotope samples, and for their patience and mentoring as I learned these systems. Many thanks to Wenbo Yang, Stefania Mambelli, and Todd Dawson for their work at the CSIB and their long-term support of my research.

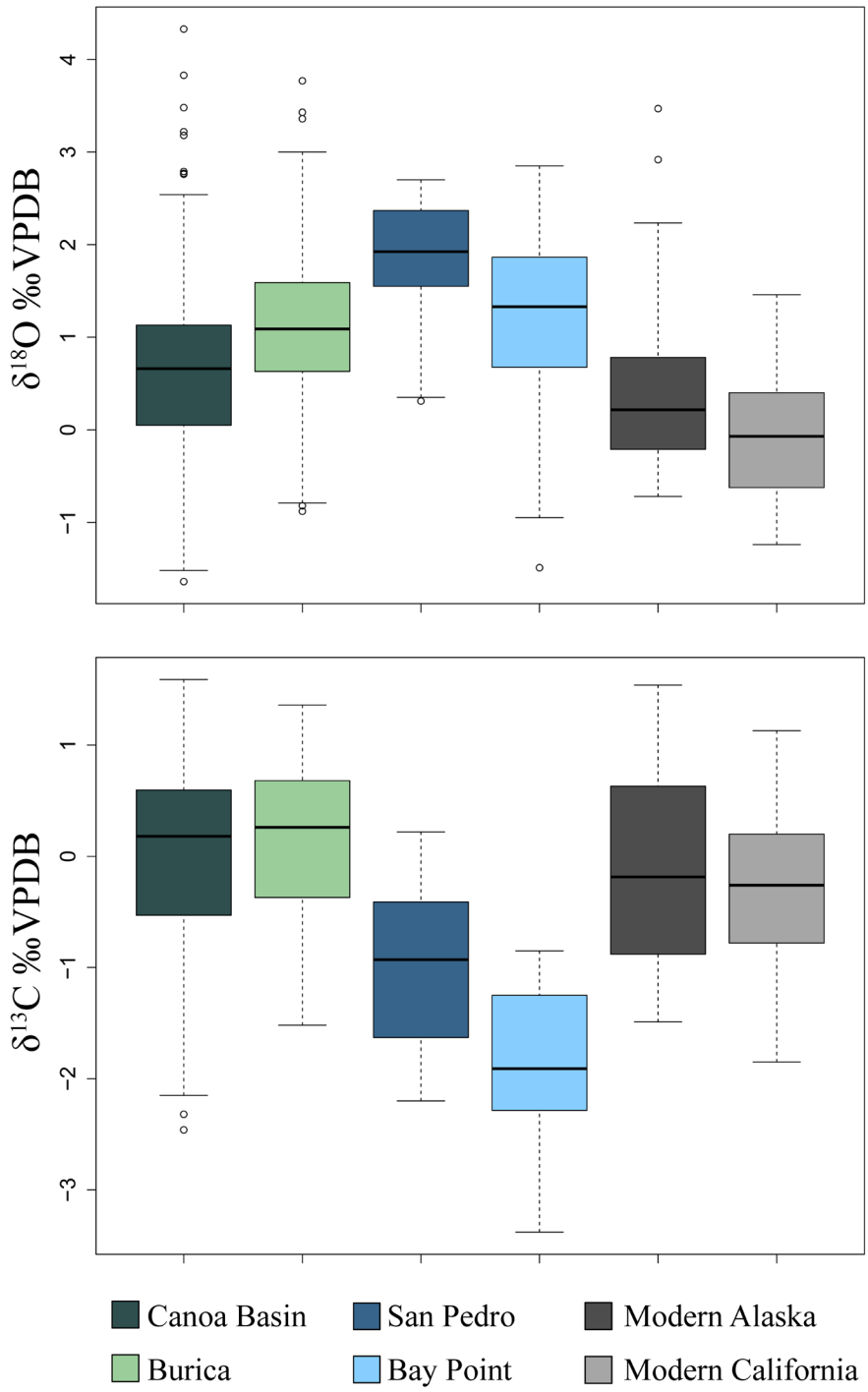

Fig. 3.1. Ranges of $\delta^{18}O$ and $\delta^{13}C$ from Canoa Basin coronulids compared to previously analyzed groups of specimens. Black lines represent median values and shaded boxes capture interquartile ranges (middle 50% of values). Whiskers indicate maximum and minimum values, besides outliers. Outliers (small circles) are defined as higher than 1.5 times the interquartile range above the upper quartile or lower than 1.5 times the interquartile range below the lower quartile.

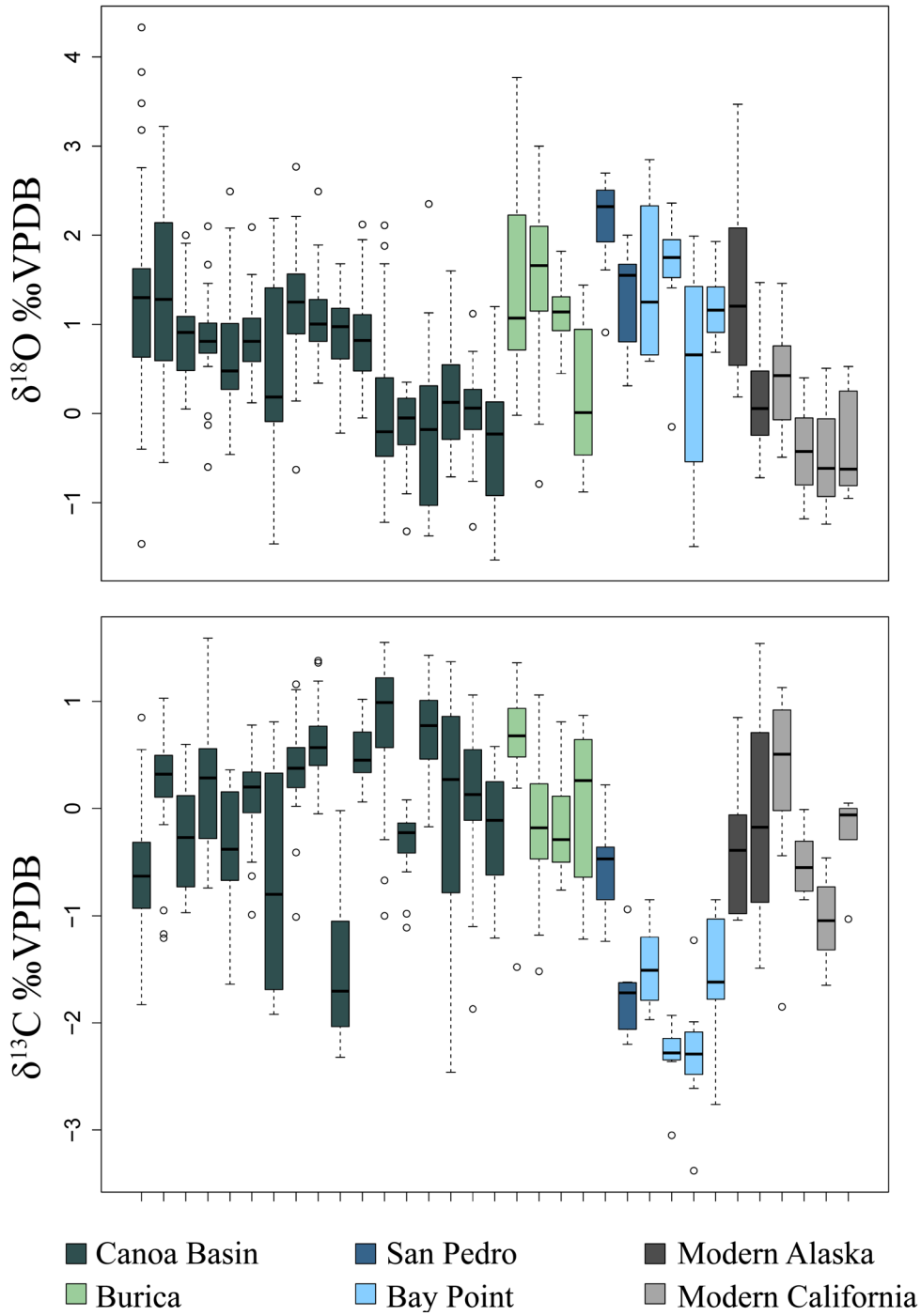

Fig. 3.2. Individual $\delta^{18}O$ and $\delta^{13}C$ values for Canoa Basin coronulids compared against previously analyzed specimens. Black lines represent median values and shaded boxes capture interquartile ranges (middle 50% of values). Whiskers indicate maximum and minimum values, besides outliers. Outliers (small circles) are defined as higher than 1.5 times the interquartile range above the upper quartile or lower than 1.5 times the interquartile range below the lower quartile.

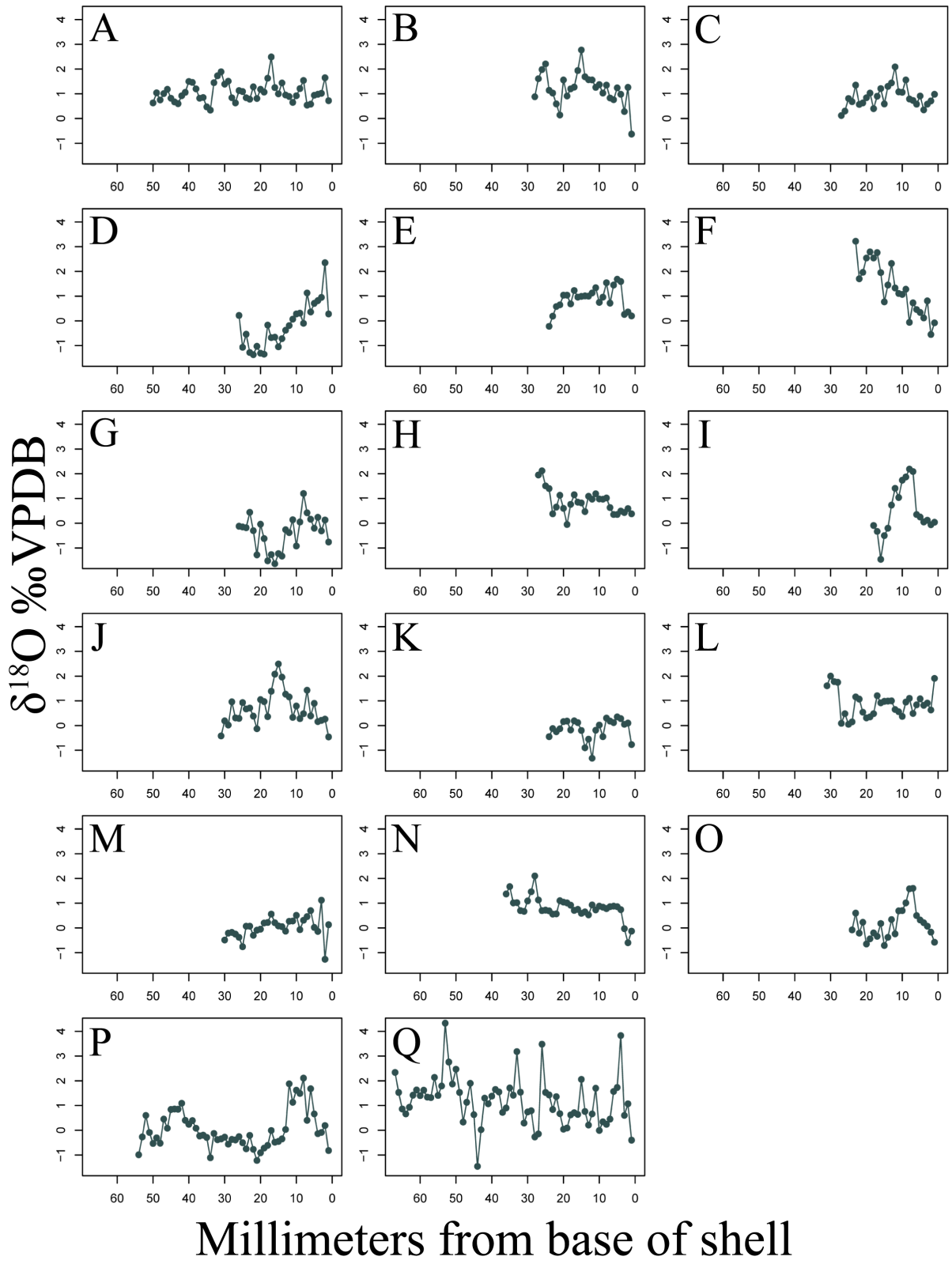
A
B
C
D
E
F
G
H
I
J
K
L
M
N
O
P
Q
δ18O ‰VPDB
Millimeters from base of shell

Fig 3.3. $\delta^{18}O$ profiles from all barnacles analyzed in this study. Specimens are UCMP116168 (A), UCMP116138 (B), UCMP116137 (C), UCMP116166 (D), UCMP116165 (E), UCMP116143 (F), UCMP116141 (G), UCMP116171 (H), UCMP116140 (I), UCMP116139 (J), UCMP116156 (K), UCMP116153 (L), UCMP116178 (M), UCMP115144 (N), UCMP16161 (O), UCMP116157 (P), and UCMP116135 (Q).

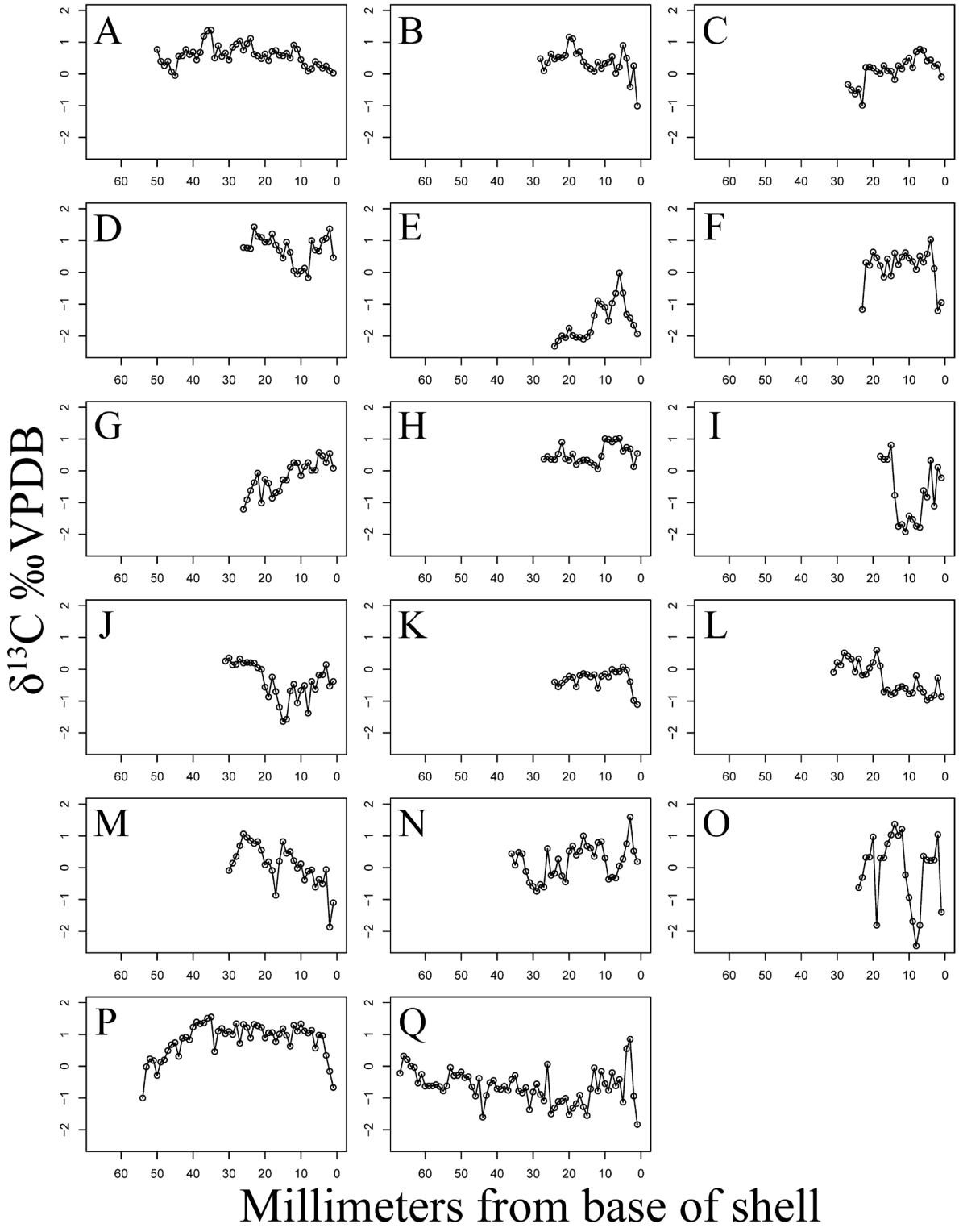
A
B
C
D
E
F
G
H
I
J
K
L
M
N
O
P
Q
δ13C ‰VPDB
Millimeters from base of shell

Fig 3.4. $\delta^{13}C$ profiles from all barnacles analyzed in this study. Specimens are UCMP116168 (A), UCMP116138 (B), UCMP116137 (C), UCMP116166 (D), UCMP116165 (E), UCMP116143 (F), UCMP116141 (G), UCMP116171 (H), UCMP116140 (I), UCMP116139 (J), UCMP116156 (K), UCMP116153 (L), UCMP116178 (M), UCMP115144 (N), UCMP16161 (O), UCMP116157 (P), and UCMP116135 (Q).

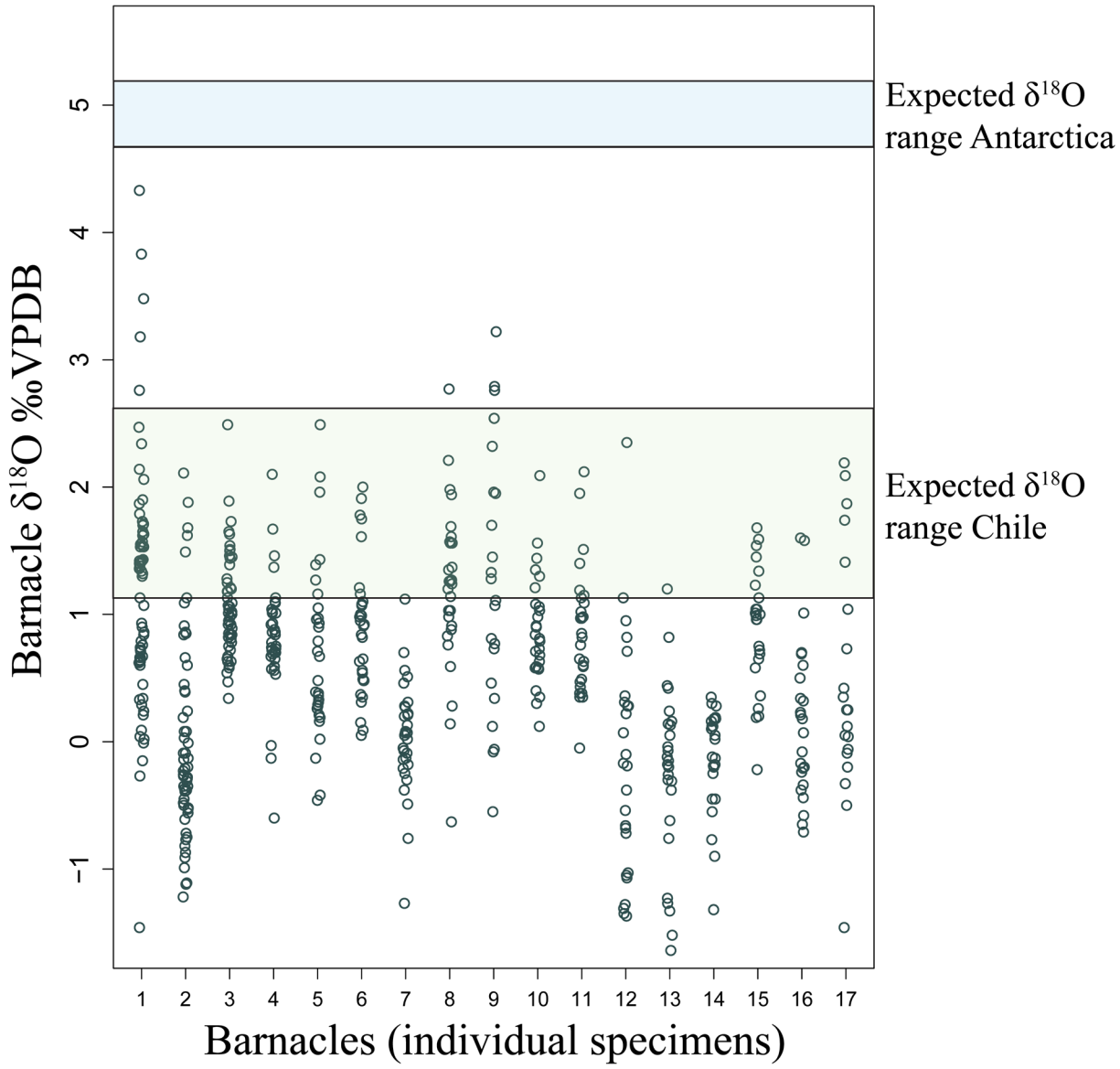

Fig. 3.5. Comparison of $\delta^{18}O$ from fossil whale barnacles against expected ranges for those migrating to known feeding areas on the coast of Chile and Antarctica, using modern seawater temperature and $\delta^{18}O$ data. Each column of points is the entire $\delta^{18}O$ record recovered from one barnacle plotted together. The upper limits of most $\delta^{18}O$ ranges fall within the expectations of whales traveling to Chile. One barnacle (UCMP161135, column 1) has a $\delta^{18}O$ range notably beyond the upper limits of expectation for Chilean waters, and another (UCMP116156, column 14) seems to have never traveled as far as Chile.

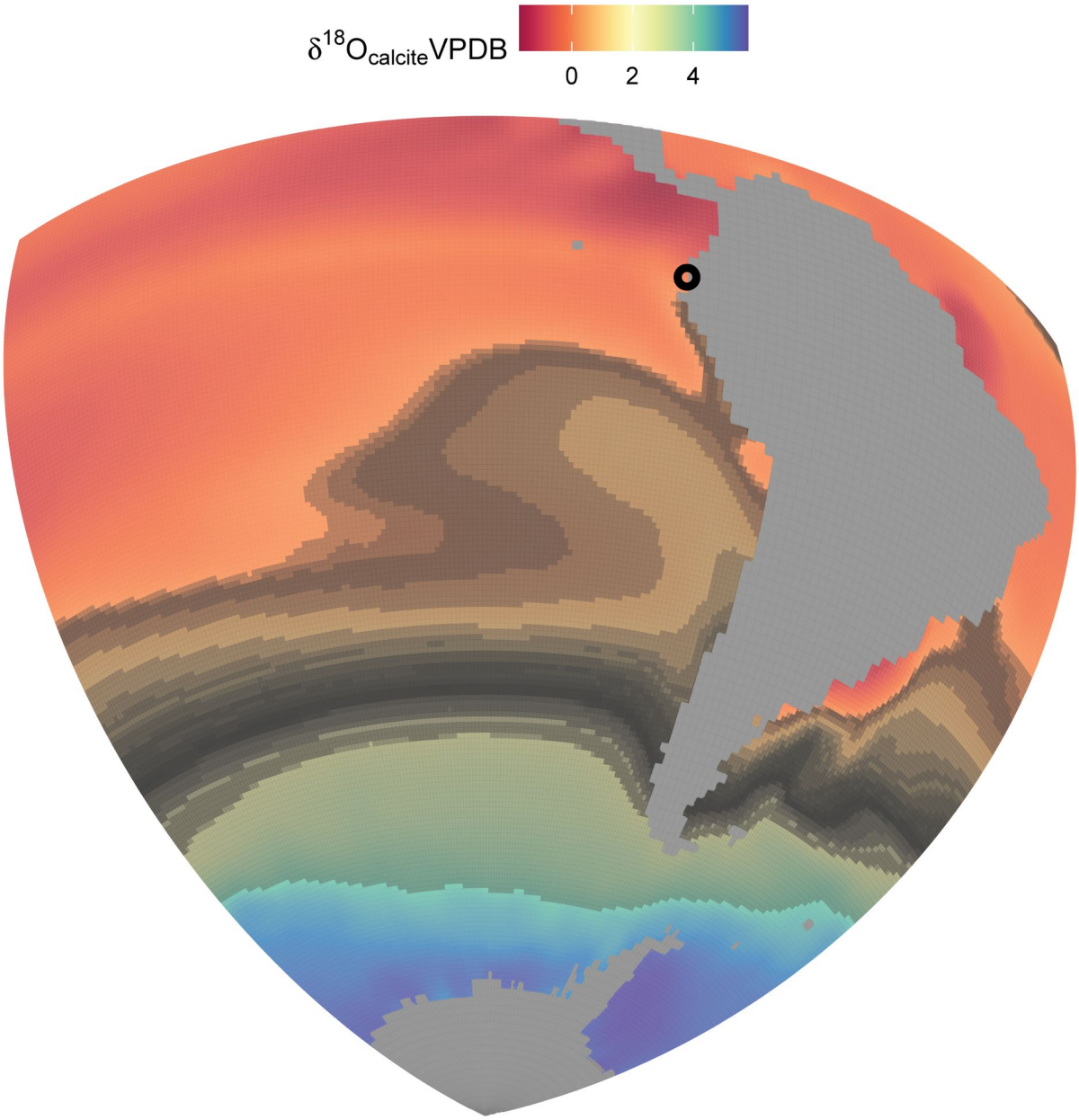

Fig. 3.6. Plausible migration destinations for the host whales of fossil specimens analyzed here based on modern seawater isotopic composition and temperature in the middle of the feeding season (January) of modern southern hemisphere whales. Each gray layer represents the region of the ocean that can plausibly account for the peak of a barnacle's $\delta^{18}O$ profile, with the peak taken as the most enriched, consecutive three points along the profile. The least enriched profile indicates the host whale may have not traveled far from its breeding site, the most enriched profile indicates the host whale migrated to or beyond the southernmost tip of South America, and the majority of $\delta^{18}O$ profiles indicate the host whales migrated to the coast of Chile. The black circle indicates the coast of Ecuador.

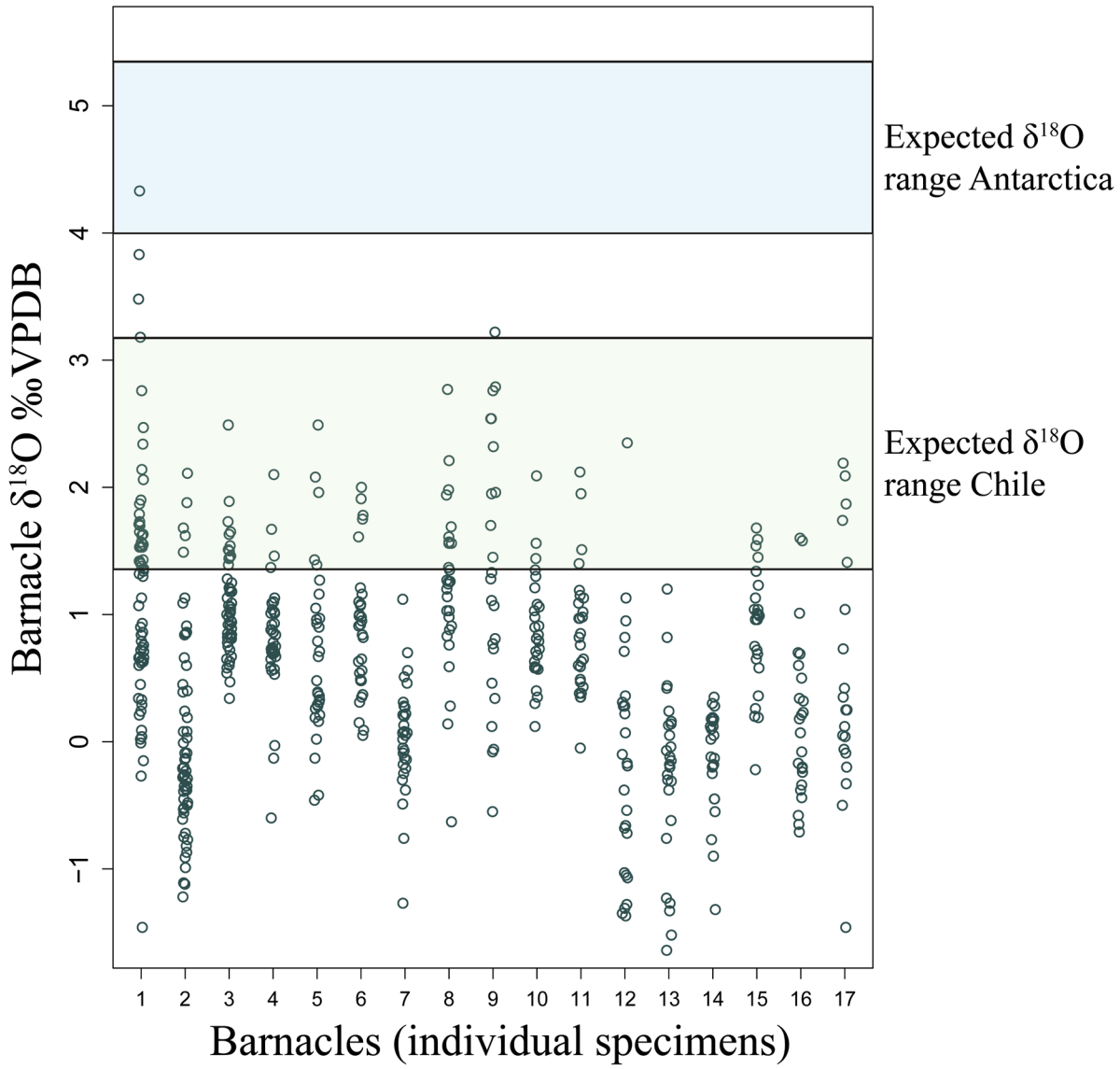

Fig. 3.7. Comparison of $\delta^{18}O$ from fossil whale barnacles against expected ranges for those migrating to known feeding areas on the coast of Chile and Antarctica, using paleoclimate seawater temperature and $\delta^{18}O$ data. Each column of points is the entire $\delta^{18}O$ record recovered from one barnacle plotted together. Ranges of expected barnacle $\delta^{18}O$ are constrained by the warmest and coldest of the paleoclimate models used. The upper limits of most $\delta^{18}O$ ranges fall within the expectations of whales traveling to Chile, while two appear to fall just beneath it. One barnacle (UCMP161135, column 1) has a maximally enriched $\delta^{18}O$ value consistent with travel to Antarctica. As was the case when comparing against modern temperature data, one barnacle (UCMP116156, column 14) appears to have never traveled as far as Chile.

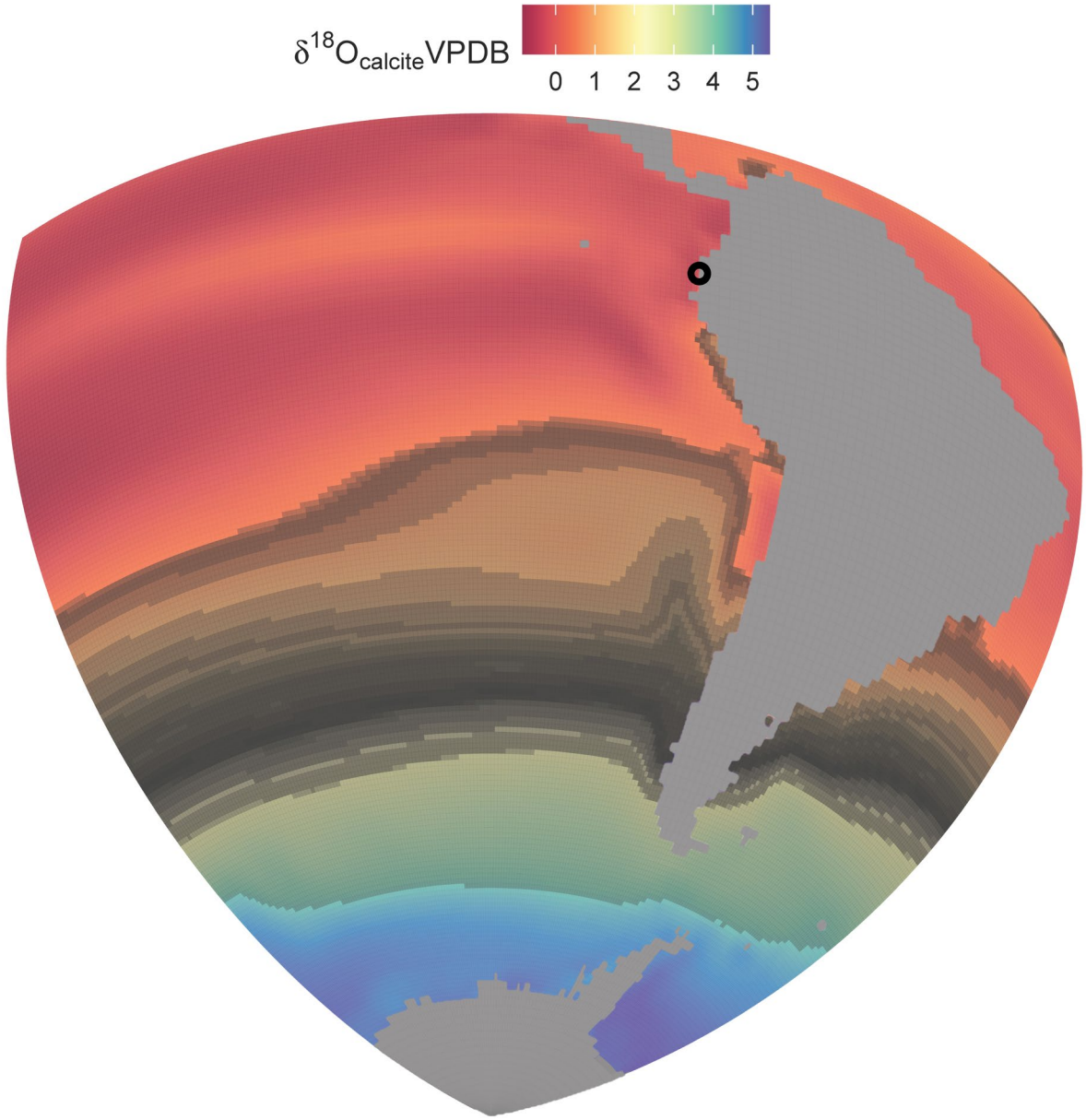

Fig. 3.8. Plausible migration destinations for the host whales of fossil specimens analyzed here based on paleoclimate modeled seawater temperature and isotopic composition. Temperature modeled here is the composite average of ten paleoclimate models for the middle of the austral summer, when modern southern hemisphere whales are at the peak of their feeding season. Each gray layer represents the region of the ocean that can plausibly account for the peak of one barnacle's $\delta^{18}O$ profile, with the peak taken as the most enriched, consecutive three points along the profile. The least enriched profile indicates the host whale may have not traveled far from its breeding site, the most enriched profile indicates the host whale migrated to or beyond the southernmost tip of South America, and the majority of $\delta^{18}O$ profiles indicate the host whales migrated to the coast of Chile. The black circle indicates the coast of Ecuador.

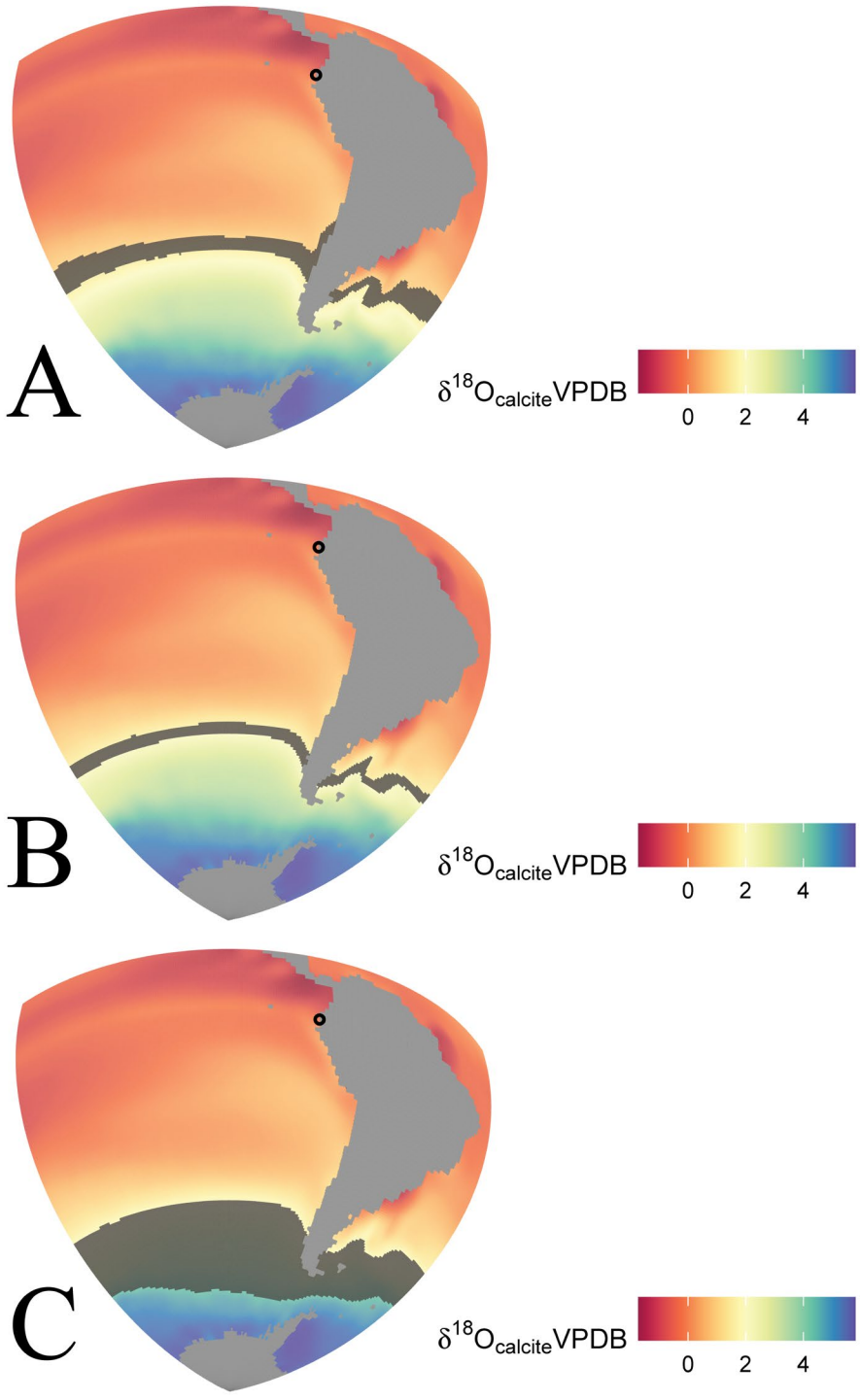

Fig. 3.9. Plausible migration destinations for the host whale of UCMP116161 (A), UCMP116157 (B), and UCMP116135 (C) based on modern seawater isotopic composition and temperature in the middle of the feeding season (January) of modern southern hemisphere whales. Black circles indicate the Ecuador coast.

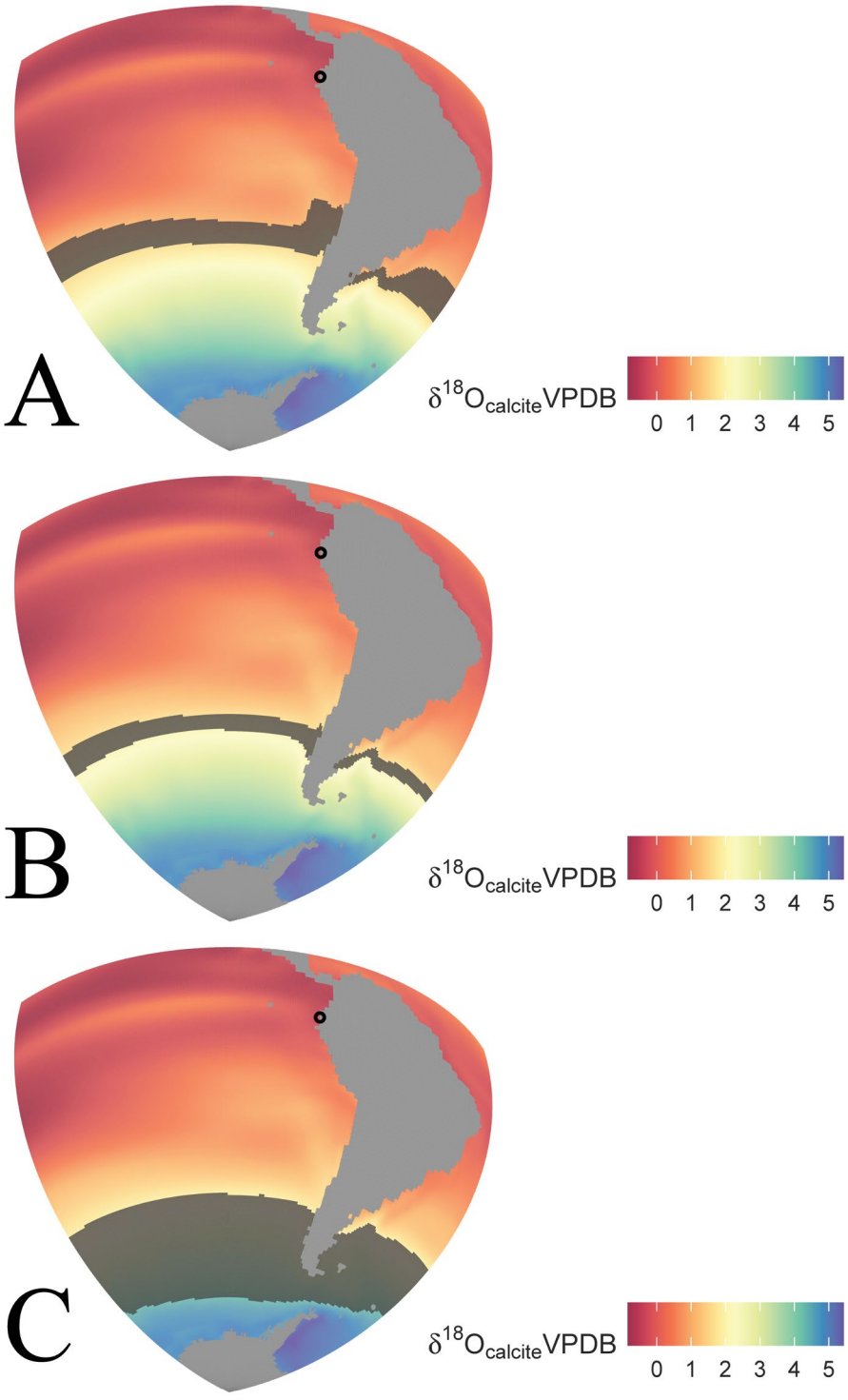

Fig. 3.10. Plausible migration destinations for the host whale of UCMP116161 (A), UCMP116157 (B), and UCMP116135 (C) based on paleoclimate seawater temperature and $\delta^{18}O$ models, where temperature is for the peak of the austral summer feeding season and is the composite average of ten separate models. Black circles indicate the Ecuador coast.

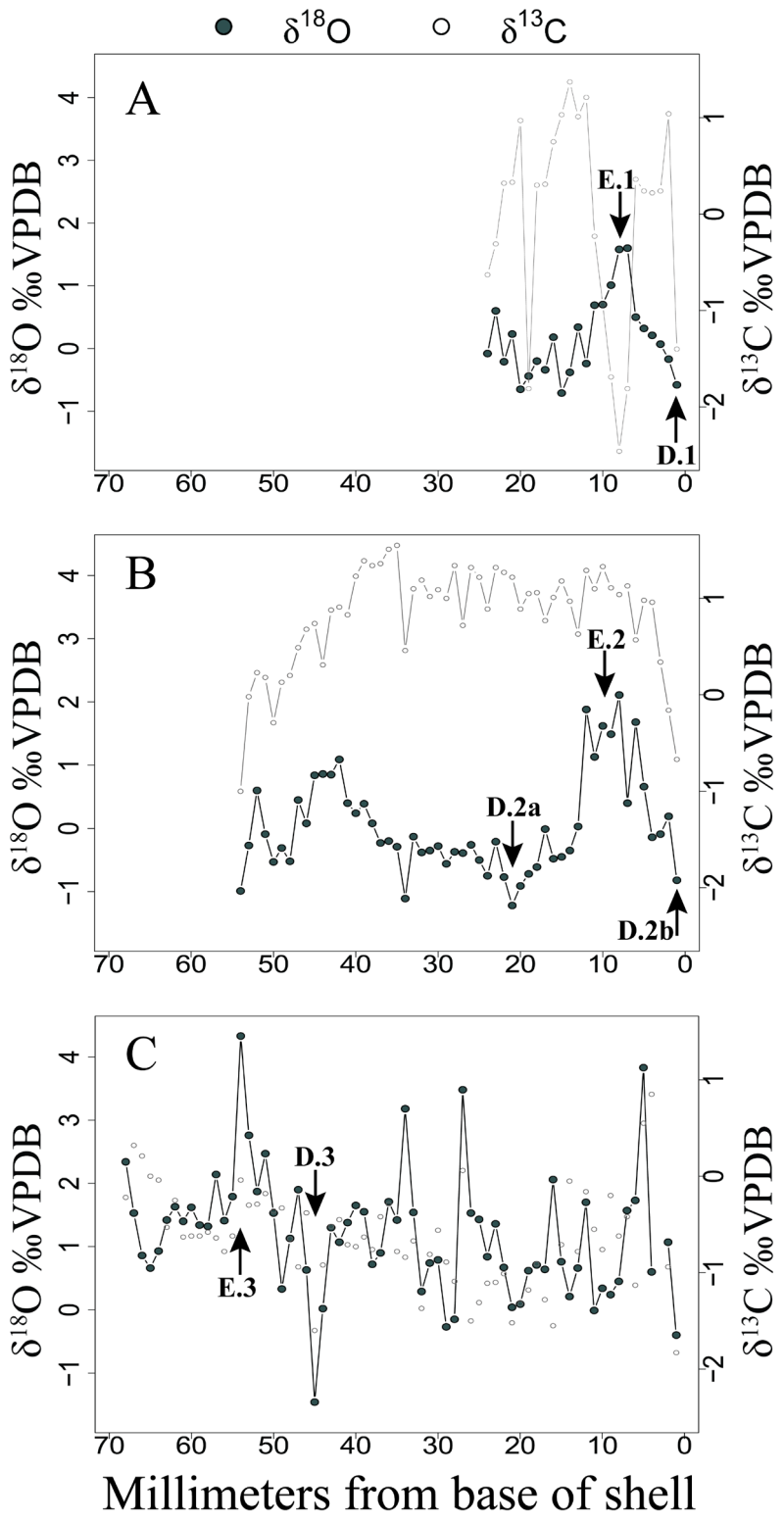

Fig. 3.11. $\delta^{18}O$ and $\delta^{13}C$ profiles for UCMP116161 (A), UCMP116157 (B), and UCMP116135 (C). Arrows mark where clumped isotope samples were centered ("e"= enriched, "d"= depleted).

Specimen	Sample site	Temperature	$\delta^{18}O$	$\delta^{18}O$ s.d.
UCMP116161	E.1	20.26	1.79	0.0071
UCMP116161	E.1	15.10	1.56	0.0064
UCMP116161	E.1	17.09	1.73	0.0027
UCMP116161	E.1	18.26	1.74	0.0052
UCMP116161	D.1	21.77	-0.21	0.0078
UCMP116161	D.1	20.58	-0.19	0.0065
UCMP116161	D.1	23.92	-0.34	0.0062
UCMP116157	E.2	17.94	0.48	0.0052
UCMP116157	E.2	18.21	0.27	0.0059
UCMP116157	E.2	20.04	0.27	0.0041
UCMP116157	E.2	13.25	0.27	0.0043
UCMP116157	E.2	15.52	0.37	0.0039
UCMP116157	D.2a	22.52	-0.51	0.0057
UCMP116157	D.2a	20.09	-0.52	0.0065
UCMP116157	D.2a	16.58	-0.47	0.0035
UCMP116157	D.2a	21.43	-0.55	0.0057
UCMP116157	D.2b	21.09	-0.52	0.0050
UCMP116157	D.2b	25.94	-0.52	0.0049
UCMP116157	D.2b	25.04	-0.64	0.0061
UCMP116157	D.2b	24.64	-0.70	0.0058
UCMP116135	E.3	18.06	1.69	0.0079
UCMP116135	E.3	20.99	1.52	0.0050
UCMP116135	E.3	19.62	1.51	0.0057
UCMP116135	E.3	16.45	1.59	0.0073
UCMP116135	D.3	24.93	0.43	0.0090
UCMP116135	D.3	19.13	0.30	0.0070
UCMP116135	D.3	21.60	0.38	0.0061
UCMP116135	D.3	21.26	0.46	0.0095

Table 3.1. Measured temperature and calculated $\delta^{18}O$ from analysis of clumped isotopes taken at 2-3 samples sites each of UCMP116161, UCMP116157, and UCMP116135.

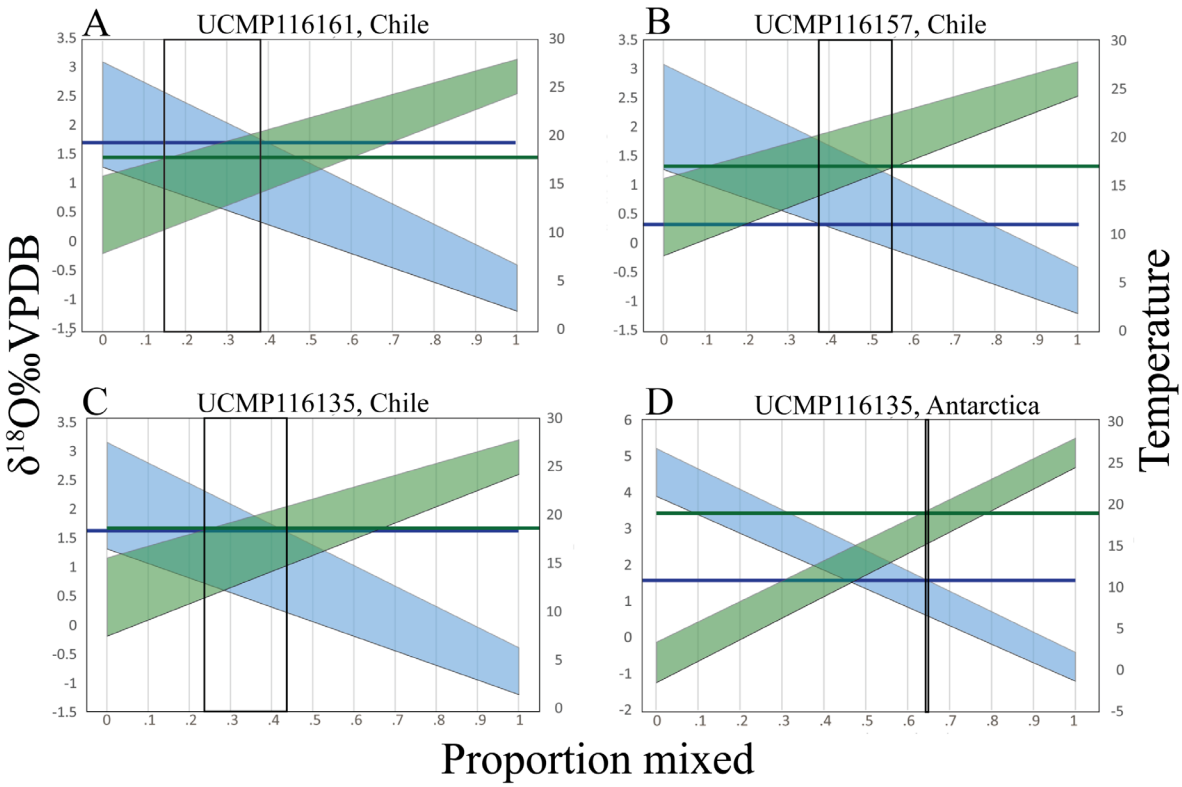

Fig. 3.12. A mixing model used to assist in interpreting clumped isotope temperature results. For each graph, a green line represents the measured temperature and a blue line represents the $\delta^{18}O$ calculated from clumped isotope samples. The x-axis represents the degree of mixing between the cold (whale's feeding region) and warm (Canoa region) end members, where "0" means the sample is composed of only the cold end member, and "1" means the sample was composed of only the warm end member. Shaded regions constrain the upper and lower limits of temperature for the heart of the feeding season (December-January) and calculated barnacle $\delta^{18}O$ as determined by the warmest and coldest paleoclimate outputs. For a barnacle which has moved between these potential end members, the measured temperature and barnacle $\delta^{18}O$ can be explained by regions where the green line and blue line are simultaneously within their regions of plausibility, outlined by vertical black boxes. For UCMP116161 (A) and UCMP116157 (B), their measurements are consistent with small to moderate amounts of mixing if both barnacles had indeed traveled to the Chilean coast. For UCMP116135, the measured temperature and calculated $\delta^{18}O$ are easily consistent with the barnacle having traveled to Chilean waters (C). Results from UCMP116135 might plausibly be consistent with travel to Antarctica (D), but only within a very narrow range of heavy mixing (see panel D; note the y-axis scale changes from panel C to D).

References

Acevedo J, Rasmussen K, Felix F, Castro C, Llano M, Secchi E, Saborio MT, Aguayo-Lobo A, Haase B, Sheidat M, Dalla-Rosa L, Olavarria C, Forestell P, Acuna P, Kaufman G, and Pastene LA (2007). Migratory destinations of humpback whales from the Magellan Strait feeding ground, southeast pacific. *Marine Mammal Science*, 23(2): 453-463. DOI: 10.1111/j.1748-7692.2007.00116.x

Affek HP and Eiler JM (2006). Abundance of mass 47 CO_2 in urban air, car exhaust, and human breath. *Geochemica et Cosmochimica Acta*, 70(1): 1-12.

Affek HP, Bar-Matthews M, Ayalon A, Matthews A, and Eiler JM (2008). Glacial/interglacial temperature variations in Soreq cave speleothems as recorded by 'clumped isotope' thermometry. *Geochemica et Cosmochimica Acta*, 72(22): 5351-5360.

Alter SE, Meyer M, Post K, Czechowski P, Gravlund P, Gaines C, Rosenbaum HC, Kaschner K, Turvey ST, van der Plicht J, Shapiro B, and Hofreiter M (2015). Climate impacts on transocean dispersal and habitat in gray whales from the Pleistocene to 2100. *Molecular Ecology*, 24(7): 1510-1522.

Anderson DT. Barnacles: Structure, function, development and evolution. Berlin: Springer, 1993.

Barron JA (1998). Late Neogene changes in diatom sedimentation in the North Pacific. *Journal of Asian Earth Sciences*, 16(1): 85-95.

Barron JA, Lyle M, and Koizumi T (2002). Late Miocene and early Pliocene biosiliceous sedimentation along the California margin. *Revista Mexicana de Ciencias Geológicas*, 19(30): 161-169.

Bartoli G, Sarnthein M, Weinelt M, Erlenkeuser H, Garbe-Schonber D, and Lea DW (2005). Final closure of Panama and the onset of northern hemisphere glaciation. *Earth and Planetary Science Letters*, 237(1-2): 33-44.

Bauer SE and Tsigardis K (2020). Description of the GISS-E2-1-G. *Journal of Advances in Modeling Earth Systems*, 2020.

Bemis BE and Geary DH (1996). The usefulness of bivalve stable isotope profiles as environmental indicators: Data from the eastern Pacific Ocean and the southern Caribbean Sea. *PALAIOS*, 11(4): 328- 339.

Benson SR, Croll DA, Marinovic BB, Chavez FP, and Harvey JT (2002). Changes in the cetacean assemblage of a coastal upwelling ecosystem during El Nino 1997–98 and La Nina 1999. *Progress in Oceanography*, 54: 279- 291.

Berger WH (2007). Cenozoic cooling, Antarctic nutrient pump, and the evolution of whales. *Deep-Sea Research II*, 54, 2399-2421.

Bernasconi SM, Muller IA, Bergmann KD, Breitenbach SFM, Fernandez A, Hodell DA, Jaggi M, Meckler AN, Millan I, and Ziegler M (2018). Reducing uncertainties in carbonate clumped isotope analysis through consistent carbonate-based standardization. *Geochemistry, Geophysics, Geosystems*, 19(9): 2895-2914.

Best PB (1991). The presence of coronuline barnacles on a southern right whale Eubalaena australis. *South African Journal of Marine Science*, 11(1): 585-587.

Best PB, Sekiguchi K, and Findlay KP (1995). A suspended migration of humpback whales *Megaptera novaeangliae* on the west coast of South Africa. *Marine Ecology, Progress Series*, 118(1–3): 1–12.

Beu AG (1971). Further fossil whale barnacles from New Zealand. *New Zealand Journal of Geology and Geophysics*, 14, 898- 904.

Bianucci G, Di Celma C, Landini W, and Buckeridge J (2006a). Palaeoecology and taphonomy of an extraordinary whale barnacle accumulation from the Plio-Pleistocene of Ecuador. *Palaeogeography, Palaeoclimatology, Palaeoecology*, 242, 326- 342.

Bianucci G, Landini W, and Buckeridge J (2006b). Whale barnacles and Neogene cetacean migration routes. *New Zealand Journal of Geology and Geophysics*, 49, 115-120.

Bosselaers M and Collareta A (2016). The whale barnacle Cryptolepas rhachianecti (Cirripedia: Coronulidae), a phoront of the grey whale Eschrichtius robustus (Cetacea: Eschrichtiidae) from a sandy beach in The Netherlands. *Zootaxa*, 4145(3): 331-338.

Boucher O, Servonnat J, Albright AL, Aumont O, Balkanski Y, Bastrikov V, Bekki S, Bonnet R, Bony S, Bopp L, Braconnot P, Brockmann P, Cadule P, Caubel A, Cheruy F, Codron F, Cozic A, Cugnet D, D'Andrea F, Davini P, de Lavergne C, Denvil S, Deshayes J, Devilliers M, Ducharne A, Dufresne J-L, Dupont E, Ethe C, Fairhead L, Falletti L, Flavoni S, Foujols M-A, Gardoll S, Gastineau G, Ghatas J, Grandpeix J-Y, Guenet B, Guez L, Guilyardi E, Guimberteau M, Hauglustaine D, Hourdin F, Idelkadi A, Joussaume S, Kageyama M, Khodri M, Krinner G, Lebas N, Levavasseur G, Levy C, Li L, Lott F, Lurton T, Luyssaert S, Madec G, Madeleine J-B, Maignan F, Marchand M, Marti O, Mullul L, Meurdesoif Y, Mignot J, Musat I, Ottle C, Peylin P, Planton Y, Polcher J, Rio C, Rochetin N, Rouet C, Sepulchre P, Sima A, Swingedouw D, Thieblemont R, Traore AK, Vancoppenolle M, Vial J, Vialard J, Viovy N, and Vuichard N (2020). Presentation and evaluation of the IPSL-CM6A-LR climate model. *Journal of Advances in Modeling Earth Systems,* 12, e2019MS002010.

Bradford AL, Weller DW, Burdin AM and Brownell Jr. RL (2011). Using barnacle and pigmentation characteristics to identify gray whale calves on their feeding grounds. *Marine Mammal Science*, 27 (3): 644–651.

Bralower TJ, Leckie RM, Sliter WV, and Thierstin HR (1995). An integrated Cretaceous microfossil biostratigraphy. *Geochronology Time Scales and Global Stratigraphic Correlation, SEPM Special Publications No. 54*, ISBN 1-5676-02407.

Brand U and Veizer J (1980). Chemical diagenesis of a multicomponent carbonate system – 1: trace elements. *Journal of Sedimentary Petrology*, 50(4): 1219-1236.

Britton K, Grimes V, Dau J, and Richards MP (2009). Reconstructing faunal migrations using intra-tooth sampling and strontium and oxygen isotope analyses: a case study of modern caribou (*Rangifer tarandus granti*). *Journal of Archaeological Science*, 36(5): 1163-1172.

Bryant ME (1987). Emergent marine terraces and quaternary tectonics, Palos Verdes Peninsula, California, in Geology of the Palos Verdes Peninsula and San Pedro bay, SEPM Guidebook, edited by PJ Fischer et al., pp 63-78, Society of Economic Paleontologists and Mineralogists, Tulsa, OK.

Buckeridge JS (1983). Fossil barnacles (Cirripedia: Thoracica) of New Zealand and Australia. *New Zealand Geology Survey Paleontological Bulletin*, 50, 1- 151.

Cadena E, Abella J, and Gregori M (2017). New findings of Pleistocene fossil turtles (Geoemydidae, Kinosternidae and Chelydridae) from Santa Elena Province, Ecuador. *PeerJ*, 5:e3215; DOI 10.7717/peerj.3215

Cadena E, Abella J, and Gregori M (2018). The first Oligocene sea turtle (Pan-Cheloniidae) record of South America. *PeerJ*, 6:e4554;DOI 10.7717/peerj.4554

Calambokidis J, Falcone EA, Quinn TJ, Burdin AM, Clapham PJ, Ford JKB, Gabriele CMG, LeDuc R, Mattila D, Rojas-Bracho L, Straley JM, Taylor BL, Urbán J, Weller D, Witteveen BH, Yamaguchi M, Bendlin A, Camacho D, Flynn K, Havron A, Huggins J, and Maloney N (2009). SPLASH: Structure of Populations, Levels of Abundance and Status of Humpback Whales in the North Pacific. Final Report for Contract AB133F-03-RP-0078. Prepared for the U.S. Department of Commerce.

Calambokidis J, Steiger G, Straley J, Herman L, and Cerchio S (2001). Movements and population structure of humpback whales in the North Pacific. *Marine Mammal Science*, 17(4): 769- 794.

Calambokidis J, Steiger GH, Curtice C, Harrison J, Ferguson MC, Becker E, DeAngelis M, and Van Parijs SM (2015). Biologically important areas for selected cetaceans within U.S. waters – west coast region. *Aquatic Mammals*, 41(1): 39-53.

Cantalamessa G and Di Celma C (2004). Origin and chronology of Pleistocene marine terraces of Isla de la Plata and of flat, gently dipping surfaces of the southern coast of Cabo San Lorenzo (Manabi, Ecuador). *Journal of South American Earth Sciences*, 16, 633-648.

Cao J, Wang B, Young-Min Y, Ma L, Li J, Sun B, Bao Y, He J, Zhou X, and Wu L (2018). The NUIST Earth System Model (NESM) version 3: description and preliminary evaluation, *Geoscientific Model Development*, 11, 2975–2993.

Capella JJ, Gibbons J, Florez-Gonzalez L, Llano M, Valladres C, Sabaj V, and Vilina YA (2008). Migratory round-trip of individually identified humpback whales at the Strait of Magellan: clues on transit times and phylopatry to destinations. *Revista Chilena de Historia Natural*, 81, 547-560.

Center for Stable Isotope Biogeochemistry (CSIB). 2020. "Analyses: Carbon and Oxygen (Carbonates)." https://nature.berkeley.edu/stableisotopelab/analyses/organic-analysis/carbon-13c-and-oxygen-18o-in-carbonates/

Clapperton, Chalmers M. (Chalmers Moyes) (1993). Quaternary geology and geomorphology of South America. Elsevier, Amsterdam ; New York.

Coates AGC, Jackson JB, Collins LS, Cronin TM, Dowsett HJ, Bybell LM, Jung P, and Obando JA (1992). Closure of the Isthmus of Panama: The near-shore marine record of Costa Rica and western Panama. *Geological Society of America Bulletin*, 104, 814-828.

Collareta A, Margiotta S, Varola A, Catanzariti R, Bosselaers M, and Bianucci G. (2016) A new whale barnacle from the early Pleistocene of Italy suggests an ancient right whale breeding ground in the Mediterranean. *Comptes Rendus Palevol*, 15(5): 473–481.

Collareta A, Regattieri E, Zanchetta G, Lambert O, Catanzariti R, Bosselaers M, Covelo P, Varola A, and Bianucci G (2018). New insights on ancient cetacean movement patterns from oxygen isotope analyses of a Mediterranean Pleistocene whale barnacle. *Neues Jahrbuch für Geologie und Paläontologie – Abhandlungen*, 288(2):143-159.

Cooke JG, Weller DW, Bradford AL, Burdin AM, and Brownell RL (2007). Population assessment of the western gray whales in 2007. Presented to the International Whaling Commission Scientific Committee, Anchorage, AK.

Craig AS and Herman LM (2003). Sex differences in site fidelity and migration of humpback whales (*Megaptera novaenagliae*) to the Hawaiian Islands. *Canadian Journal of Zoology*, 75, 1923–33.

Danabasoglu G, Lamarque J-F, Bacmeister J, Bailey DA, DuVivier AK, Edwards J, Emmons LM, Fasullo J, Garcia R, Gettelman A, Hannay C, Holland MM, Large WG, Lauritzen PH, Lawrence DM, Lenaerts JTM, Lindsay K, Lipscomb WH, Mills MJ, Nele R, Oleson KW, Otto-Bliesner B, Phillips AS, Sacks W, Tilmes S, van Kampenhout L, Vertenstein M, Bertini A, Dennis J, Deser C, Fischer C, Fox-Kemper B, Kay JE, Kinnison D, Kushner PJ, Larson WE, Long MC, Mickelson S, Moore JK, Nienhouse E, Polvani L, Rasch PJ, and Strand WG (2020). The Community Earth System Model Version 2 (CESM2). *Journal of Advances in Modeling Earth Systems*, 12, e2019MS001916. https://doi.org/10.1029/2019MS001916

Davis CW (1972). Studies on the barnacles epizoic on marine vertebrates. MA thesis, California State University, San Francisco, 60 pp.

Dawbin DH (1988). Baleen whales. Pages 44-65 in R. Harrison and M. Bryden, eds. Whales, dolphins, and porpoises. Facts on File, New York, NY.

Dennis KJ, Affek HP, Passey BH, Schrag DP, and Eiler JM (2011). Defining an absolute reference frame for 'clumped' isotope studies of CO2. *Geochemica et Cosmochimica Acta*, 75(22): 7117-7131.

Detjen M, Sterling E, & Gomez A (2015). Stable isotopes in barnacles as a tool to understand green sea turtle (*Chelonia mydas*) regional movement patterns. *Biogeosciences*, 12, 7081- 7086.

Di Celma C, Ragaini L, Cantalamessa G, and Curzio P (2002). Shell concentrations as tools in characterizing sedimentary dynamics at sequence-bounding unconformities: examples from the lower unit of the Canoa Formation (Late Pliocene, Ecuador). *Geobios*, 35, 72-85.

Di Celma C, Ragaini L, Cantalamessa G, and Landini W (2005). Basin physiography and tectonic influence on sequence architecture and stacking pattern: Pleistocene succession of the Canoa Basin (central Ecuador). *GSA Bulletin*, 117(9/10): 1226-1241.

Dominici S, Bartalini M, Benvenuti M, and Balestra B (2011). Large kings with small crowns: a Mediterranean Pleistocene whale barnacle. *Bollettino della Societa Paleontologica Italiana*, 50(2): 95- 101.

Edmund AG (1965). A late pleistocene fauna from the Santa Elena Peninsula, Ecuador. Toronto: Royal Ontario Museum, Life Sciences Division, 350 pp.

Eiler JM, (2007). "Clumped-isotope" geochemistry – The study of naturally-occurring, multiply-substituted isotopologues. *Earth and Planetary Science Letters*, 262, 309–327.

Eiler JM, (2011). Paleoclimate reconstruction using carbonate clumped isotope thermometry. *Quaternary Science Reviews*, 30, 3575– 3588.

Evans J, Pearson MP, Madgwick R, Sloane H, and Albarella U (2019). Strontium and oxygen isotope evidence for the origin and movement of cattle at Late Neolithic Durrington Walls, UK. *Archaeological and Anthropological Sciences*, 11, 5181-5197.

Felix F & Haase B (2001). The humpback whale off the coast of Ecuador, population parameters and behavior. *Journal of Marine Biology and Oceanography*, 36(1): 61- 74.

Felix F and Botero-Acosta N (2011). Distribution and behaviour of humpback whale mother-calf pair during the breeding season off Ecuador. *Marine Ecology Progress Series*, 426, 277-287.

Felix F and Olavarria C (2012). Genetic diversity and population structure of humpback whales (*Megaptera novaeangliae*) from Ecuador based on mitochondrial DNA analyses. *Journal of Cetacean Research and Management*, 12(1): 71-77.

Felix F, Bearson B, and Falconi J (2006). Epizoic barnacles removed from the skin of a humpback whale after a period of intense surface activity. *Marine Mammal Science*, 22(4): 979-984.

Ficcarelli G, Coltorti M, Moreno-Espinosa M, Pieruccini PL, Rook L, and Torre D (2003). A model for the Holocene extinction of the mammal megafauna in Ecuador. Journal of South American Earth Sciences, 15, 835-845.

Fiebig J, Bajnai D, Loffler N, Methner K, Krsnik E, Mulch A, and Hofman S (2019). Combined high-precision Δ_{48} and Δ_{47} analysis of carbonates. *Chemical Geology*, 522(20): 18-191.

Fleming CA (1959). A Pliocene whale barnacle from Hawke's Bay, New Zealand. New Zealand *Journal of Geology and Geophysics*, 2, 242- 247.

Flores FF (2018). Estudio poblacional del Tiburón Blanco (Carcharodon carcharias,Linnaeus, 1758), del yacimiento Pleistoceno de Quebrada Tiburón (Atahualpa, Santa Elena, Ecuador). Graduate Thesis. Universidad Estatal Península de Santa Elena, Ecuador

Fricke HC, Hencecroth J, and Hoerner ME (2011). Lowland–upland migration of sauropod dinosaurs during the Late Jurassic epoch. *Nature*, 480, 513-515.

Gardner SC and Chavez-Rosales S (2000). Changes in the relative abundance and distribution of gray whales (*Eschrichtius robustus*) in Magdalena Bay, Mexico during and El Nino event. *Marine Mammal Science*, 16(4): 728-738.

Ghosh P, Adkins J, Affek H, Balta B, Guo W, Schauble EA, Schrag D, and Eiler JM (2006). 13C-18O bonds in carbonate minerals: A new kind of paleothermometer. *Geochimica et Cosmochimica Acta*, 70, 1439–1456.

Gibbons J, Capela JJ, and Valladares C (2003). Rediscovery of a humpback whale (*Megaptera novaeangliae)* feeding ground in the Straits of Magellan, Chile. *Journal of Cetacean Research and Management*, 5(2): 203-208.

Goerlitz DS, Urban J, Roja-Bracho L, Belson M, and Schaeff CM (2004). Miochondrial DNA variation among Eastern North Pacific gray whales (Eschichtius robustus) on winter breeding grounds in Baja California. *Canadian Journal of Zoology*, 81, 1965-1972.

Goldbogen J, Cade D, Calambokidis J, Friedlaender A, Potvin J, Segre P, and Werth A (2017). How Baleen Whales Feed: The Biomechanics of Engulfment and Filtration. *Annual Review of Marine Science*, 9(1): 367-386.

Guo C, Bentsen M, Bethke I, Ilicak M, Tjiputra J, Toniazzo T, Schwinger J, and Otterå OH (2019). Description and evaluation of NorESM1-F: a fast version of the Norwegian Earth System Model (NorESM). *Geoscientific Model Development*, 12, 343–362.

Guzman HM, Capella JJ, Valladares C, Gibbons J, and Condit R (2020). Humpback whale movements in a narrow and heavily-used shipping passage, Chile. *Marine Policy*, 118, DOI: 10.1016/j.marpol.2020.103990.

Hajima T, Watanabe M, Yamamoto A, Tatebe H, Noguchi MA, Abe M, Ohgaito R, Ito A, Yamazaki D, Okajima H, Ito A, Takata K, Ogochi K, Watanabe S, and Kawamiya M (2020). Development of the MIROC-ES2L Earth system model and the evaluation of biogeochemical processes and feedbacks. *Geoscientific Model Development*, 13, 2197–2244.

Hayashi R (2012). Atlas of the barnacles on marine vertebrates in Japanese waters including taxonomic review of superfamily Coronuloidea (Cirripedia: Thoracica). *Journal of the Marine Biological Association of the United Kingdom*, 92(1): 107–127.

Hayashi R, Chan BKK, Simon-Blecher N, Watanabe H, Guy-Haim T, Yonezawa T, Levy Y, Shuto T, and Achituv Y (2013). Phylogenetic position and evolutionary history of the turtle and whale barnacles (Cirripedia: Balanomorpha: Coronuloidea). *Molecular Phylogenetics and Evolution*, 67, 9-14.

He B, Yu U, Bao Q, Lin P, Liu H, Li J, Wang L, Liu Y, Wu G, Chen K, Guo Y, Zhao S, Zhang X, Song M, and Xie J (2020). CAS FGOALS-f3-L model dataset descriptions for CMIP6 DECK experiments. *Atmospheric and Oceanic Science Letters*, 13:6, 582-588.

Hoffstetter R (1952). Les Mammife res Pleistocenes de la Republique de l'Equateur. *Mémoires de la Société Géologique de France*: Serie 66:1_391.

Hoppe KA, Koch PL, Carlson RW, and Webb SD (1999). Tracking mammoths and mastodons: Reconstruction of migratory behavior using strontium isotope ratios. *Geology*, 27(5): 439-442.

Hoppe KA and Koch PL (2007). Reconstructing the migration patterns of late Pleistocene mammals. *Quaternary Research*, 68, 347-352.

Hucke-Gaete R, Haro D, Torres-Florez JP, Montecinos Y, Viddi F, Bedrinana-Romano L, Nery MF, and Ruiz J (2013). A historical feeding ground for humpback whales in the eastern South Pacific revisited: the case of northern Patagonia, Chile. *Aquatic Conservation: Marine and Freshwater Ecosystems*, 23, 858-867.

Hufthammer AK, Arntsen L, Kitchener AC, and Buckley M (2018). Grey whale (*Eschrichtius robustus*) in Norweigan waters 2000 years ago. *Palaeogeography, Palaeoclimatology, Palaeoecology*, 495, 42-47.

Huntington KW and Lechler AR (2015). Carbonate clumped isotope thermometry in continental tectonics. *Tectonophysics*, 647-648, 1-20.

Huntington KW, Eiler JM, Guo W, Boniface M, Yeung LY, Thiagarajan N, Passey B, Tripati A, Daeron M, and Came R (2009). Methods and limitations of 'clumped' CO_2 isotope ($\Delta 47$) analysis by gas-source isotope ratio mass spectrometry. *Journal of Mass Spectrometry*, 44(9): 1318-1329.

Huntington KW, Wernicke BP, and Eiler JM (2010). Influence of climate change and uplift on Colorado Plateau paleotemperatures from carbonate clumped isotope thermometry. *Tectonics*, 29(3): TC3005.

International Whaling Commission (2001). Report of the Scientific Committee, Annex F: Sub-Committee on Bowhead, Right and Gray Whales. Tromso, Norway, 30 May to June 11 2001.

International Whaling Commission (2015). Report of the Scientific Committee. Meeting 66a, San Diego, California, 22 May to 3 June 2015.

Jacobs D, Haney T, & Louie KD (2004). Genes, diversity, and geologic process on the Pacific coast. Annual Review in Earth and Planetary Science, 32, 601- 652.Land LS (1967). Diagenesis of skeletal carbonates. *Journal of Sedimentary Petrology*, 37(3): 914-930.

Kellogg R (1929). What is known of the migration of some of the whalebone whales. *Smithsonian Institution Annual Report,* 1928:467–494.

Kelson JR, Huntington KW, Schauer AJ, Saenger C, and Lechler AR (2017). Toward a universal carbonate clumped isotope calibration: Diverse synthesis and preparatory methods suggest a single temperature relationship. *Geochemica et Cosmochimica Acta*, 197, 104-131.

Khim BK, Krantz DE, Cooper LW, and Grebmeier JM (2003). Seasonal discharge of estuarine freshwater to the western Chukchi Sea shelf identified in stable isotope profiles of mollusk shells. *Journal of Geophysical Research*, 108, 3300-3309.

Killingley JS (1980). Migrations of California gray whales tracked by Oxygen-18 variations in their epizoic barnacles. *Science*, 207, 759-760.

Killingley JS and Berger WH (1979). Stable isotopes in a mollusk shell: Detection of upwelling events. *Science*, 205(4402): 186- 188.

Killingley JS and Lutcavage M (1983). Loggerhead turtle movements reconstructed from 18O and 13C profiles from commensal barnacle shells. *Estuarine, Coastal, and Shelf Science*, 16, 345–349.

Killingley JS and Newman WA (1982). 18O fractionation in barnacle calcite: a barnacle paleotemperature equation. *Journal of Marine Research*, 40(3): 893-902.

Kumar N, Anderson RF, Mortlock RA, Froelich PN, Kubik P, Dittrich-Hannen B, and Suter M (1995). Increased biological productivity and export production in the glacial Southern Ocean. *Nature*, 378(6558): 675-680.

Lechler AR, Niemi NA, Hren MT, and Lohmann KC (2013). Paleoelevation estimates for the northern and central proto-Basin and Range from carbonate clumped isotope thermometry. *Tectonics*, 32, 295–316.

LeDuc RG, Weller DW, Hyde J, Burden AM, Rosel PE, Brownell RL, Wursig B, and Dizon AE (2002). Genetic differences between western and eastern gray whales (Eschrichtius robustus*). Journal of Cetacean Research and Management*, 4(1): 1-5.

Li L, Yu Y, Tang Y, Lin P, Xie J, Song M, Don L, Zhou T, Liu L, Wang L, Pu Y, Xiaolong C, Chen L, Xie Z, Liu H, Zhang L, Huang X, Feng T, Zheng W, Xia K, Liu H, Liu J, Wang Y, Wang L, Jia B, Xie F, Wang B, Zhao S, Yu Z, Zhao B, and Wei J. (2020). The flexible global ocean-atmosphere-land system model grid-point version 3 (fgoals-g3): description and evaluation. *Journal of Advances in Modeling Earth Systems*, 12, e2019MS002012. https://doi.org/10.1029/2019MS002012.

Lindberg DL (1991). Marine biotic interchange between the northern and southern hemispheres. *Paleobiology*, 17(3): 308-324.

Lindsey EL and Lopez EX (2015). Tanque Loma, a new late-Pleistocene megafaunal tar seep locality from southwest Ecuador. *Journal of South American Earth Sciences*, 57, 61-82. DOI 10.1016/j.jsames.2014.11.003

Lisiecki LE and Raymo ME (2007). Plio–Pleistocene climate evolution: Trends and transitions in glacial cycle dynamics. *Quaternary Science Reviews*, 26(1-2): 56-69.

Marchant S (1961). A photogeological analysis of the structure of the western Guayas province, Ecuador: With discussion of the stratigraphy and Tablazo Formation, derived from surface mapping. *Geological Society [London] Journal*, 117, 215–233.

Mackintosh, N.A. 1965. *The Stocks of Whales*. Fishing News (Books) Ltd, London. 232pp.

Marlow JR, Lange CB, Wefer G, and Rosell-Mele A (2000). Upwelling intensification as part of the Pliocene-Pleistocene climate transition. *Science*, 290(5500): 2288-2291.

Martinez-Garcia A, Sigman DM, Ren H, Anderson RF, Straub M, Hodell DA, Jaccard SL, Eglinton TI, and Haug GH (2014). Iron Fertilization of the Subantarctic Ocean During the Last Ice Age. *Science*, 343(6177): 1347-1350.

Martins CCA, Morete ME, Engel MH, Freitas AC, Secchi ER, and Kina PG (2000). Aspects of habitat use patterns of humpback whales in the Abrolhos Bank, Brazil, breeding ground. *Memoirs of the Queensland Museum*, 47, 563-570.

Marx FG, and Fordyce RE (2015). Baleen boom and bust: a synthesis of mysticete phylogeny, diversity and disparity. *Royal Society Open Science*, 2, 140434.

Mate BR, Ilyashenko VY, Bradford AL, Vertyankin VV, Tsidulko GA, Rozhnov VV, and Irvine LM (2015). Frasier TR, Koroscil SM, White BN, and Darling JD (2011). Assessment of population substructure in relation to summer feeding ground use in the eastern North Pacific gray whale. *Endangered Species Research*, 14, 39-48.

Matthews CJD, Longstaffe FJ, and Ferguson SH (2016). Dentine oxygen isotopes (δ18O) as a proxy for odontocete distributions and movements. *Ecology and Evolution*, 6(14): 4643-4653.

McMahon KW, Hamady LL, and Thorrold, SR (2013). A review of ecogeochemistry approaches to estimating movements of marine animals. *Limnology and Oceanography*, 58(2): 697-714.

Methner K, Fiebig J, Wacker U, Umhoefer P, Chamberlain CP, and Mulch A (2016). Eocene-Oligocene proto-Cascades topography revealed by clumped (Δ_{47}) and oxygen isotope ($\delta^{18}O$) geochemistry (Chumstick Basin, WA, USA). *Tectonics*, 35(3): 546-564.

Monroe R (1981). Studies in the Coronulidae (Cirripedia): Shell morphology, growth, and function, and their bearing on subfamily classification. *Memoirs of the Queensland Museum*, 20(2): 237-251.

Moore GW and Kennedy MP (1975). Quaternary Faults at San Diego Bay, California. *Journal of Research of the U.S. Geological Survey*, 3(5): 589-595.

Nash SMB, Schlabach M, & Waugh C (2013). Metabolic concentration of lipid soluble organochlorine burdens in southern hemisphere humpback whales through migration and fasting. *Environmental Science and Technology*, 47, 9404− 9413.

Newman WA and Abbott DP (1980). Cirripedia: the barnacles. Intertidal Invertebrates of California. Stanford University Press, Stanford, 504–535.

Newman WA and Ross A (1976). Revision of the balanomorph barnacles; including a catalog of the species. *San Diego Society of Natural History Memoir*, 9, 1–108.

NOAA Optimum Interpolation (OI) Sea Surface Temperature (SST) V2 (NOAA_OI_SST_V2) data provided by the NOAA/OAR/ESRL PSD, Boulder, Colorado, USA. https://www.esrl.noaa.gov/psd/.

Noakes SE, Pyenson ND, and McFall G (2013). Late Pleistocene gray whales (Eschrichtius robustus) offshore Georgia, U.S.A., and the antiquity of gray whale migration in the North Atlantic Ocean. *Palaeogeography, Palaeoclimatology, Palaeoecology*, 392, 502-509.

Nogata Y and Matsumura K (2005). Larval development and settlement of a whale barnacle. *Biology Letters*, 2(1): 92-93.

Olavarría BC, Baker CS, Medrano GL, Aguayo LA, Caballero GS, Flórez-Gonzàlez L, Capella AJ, Rosenbaum HC, Garrigue C, Greaves J, Bannister JL, Jenner M, and Jenner C (2000). Stock identity of Antarctic Peninsula humpback whales inferred from mtDNA variation. Paper SC/52/IA15 presented to the IWC Scientific Committee, June 2000, in Adelaide, Australia.

Omura H (1953). Biological study on the humpback whales in the Antarctic whaling areas IV and V. Sci. Rep. Whales Res. Inst., Tokyo 8:81-101.

Otto-Bliesner BL, Brady EC, Zhao A, Brierley C, Axford Y, Capron E, Govin A, Hoffman J, Isaacs E, Kageyama M, Scussolini P, Tzedakis PC, Williams C, Wolff E, Abe-Ouchi A, Braconnot P, Ramos Buarque S, Cao J, de Vernal A, Guarino MV, Guo C, LeGrande AN, Lohmann G, Meissner K, Menviel L, Nisancioglu K, O'ishi R, Salas Y Melia D, Shi X, Sicard M, Sime L, Tomas R, Volodin E, Yeung N, Zhang Q, Zhang Z, and Zheng W (in review, 2020). Large-scale features of Last Interglacial climate: Results from evaluating the lig127k simulations for CMIP6-PMIP4. *Climate of the Past*, https://doi.org/10.5194/cp-2019-174.

Pack AA, Hermn L, Craig AS, Spitz SS, Waterman JO, Herman E, Deakos MH, Hakala S, and Lowe C (2017). Habitat preferences by individual humpback whale mothers in the Hawaiian breeding grounds vary with the age and size of their calves. *Animal Behaviour*, 133, 131-144.

Passey BH, Levin NE, Cerling TE, Brown FH, and Eiler JM (2010). High-temperature environments of human evolution in East Africa based on bond ordering in paleosol carbonates. *Proceedings of the National Academy of Sciences of the United States of America*, 107, 11245–11249.

Pilsbry HA (1916). The sessile barnacles (Cirripedia) contained in the collections of the U.S. National Museum; including a monograph of the American species. *United States National Museum Bulletin,* 93, 1–366.

Pilsbry HA and Olsson AA (1941). A Pliocene fauna from Western Ecuador. *Proceedings of the Academy of Natural Sciences of Philadelphia,* 93, 1–80.

Price TD, Burton JH, and Bentley RA (2002). The Characterization of Biologically Available Strontium Isotope Ratios for the Study of Prehistoric Migration. *Archaeometry*, 44(1): 117-135.

Pyenson ND and Lindberg DR (2011). What happened to gray whales during the Pleistocene? The ecological impact of sea-level change on benthic feeding areas in the North Pacific Ocean. *PLOS One,* 6(7): e21295. doi:10.1371/journal.pone.0021295

R Core Team (2020). R: A language and environment for statistical computing. R Foundation for Statistical Computing, Vienna, Austria. URL https://www.R-project.org/.Ramírez P (1988). The humpback whale *Megaptera novaeangliae* off the north coast of Peru. *Lima Bulletin*, 56, 91-96.

Rasmussen K, Palacios DM, Calambokidis J, Saborio MT, Dalla Rose L, Secchi ER, Steiger GH, Allen JM, and Stone GS (2007). Southern Hemisphere humpback whales wintering off Central America: Insights from water temperature into the longest mammalian migration. *Biology Letters*, 3, 302-305.

Ravelo AC, Dyke HA, Lyle M, Lyle AO, and Wara MW (2004). Regional climate shifts caused by gradual global cooling in the Pliocene epoch. *Nature,* 429, 263- 267.

Ridgeway SH, Lindner E, Mahoney KA, and Newman WA (1997). Gray whale barnacles Cryptolepas rhachianecti infest white whales, Delphinapterus leucas, housed in San Diego Bay. *Bulletin of Marine Science,* 61(2): 377-385.

Rodrigues ASL, Charpentier A, Bernal-Casasola D, Gardeisen A, Nores C, Millán JAP, McGrath K, and Speller CF (2018). Forgotten Mediterranean calving grounds of grey and North Atlantic right whales: evidence from Roman archaeological records. *Proceedings of the Royal Society B*, 285, 20180961.

Sadler J, Carre M, Azzoug M, Schauer AJ, Ledesma J, Cardenas F, Chase BM, Bentaleb I, Muller SD, Mandeng M, Rohling EJ, and Sachs JP (2012). Reconstructing past upwelling intensity and the seasonal dynamics of primary productivity along the Peruvian coastline from mollusk shell stable isotopes. *Geochemistry, Geophysics, Geosystems*, 13(1): DOI: 10.1029/2011GC003595.

Sancetta C & Silvestri S (1986). Pliocene-Pleistocene evolution of the North Pacific ocean-atmosphere system, interpreted from fossil diatoms. *Paleoceanography*, 1(2): 163- 180.

Savoyat E (1971). Leyenda explicativa de la hoja de Montecristi, 1/100.000: Quito, Ecuador, Departamento de Investigacion Geologica, Ministero de Recursos Naturales y Turismo, Direccion General de Geologia y Minas, 6 p.

Schmidt GA, Bigg GR, and Rohling EJ (1999). "Global Seawater Oxygen-18 Database - v1.22" https://data.giss.nasa.gov/o18data/.

Seilacher A (2005). Whale barnacles: Exaptational access to a forbidden paradise. *Paleobiology*, 31(2): 27- 35.

Seland O, Bentsen M, Graff LS, Olivie D, Toniazzo T, Gjermundsen A, Debernard JB, Gupta AK, He Y, Kirkevag A, Schwinger J, Tjiputra J, Aas KK, Bethke I, Fan Y, Griesfeller J, Grini A, Guo C, Ilicak M, Karset IHH, Landgren O, Liakka J, Moseid KO, Nummelin A, Spensberger C, Tang H, Zhang Z, Heinse C, Iverson T, and Schulz M (2020). The Norweigan Earth System Model, NorESM2 – Evaluation of the CMIP6 DECK and historical simulations. *Geoscientific Model Development*, doi.org/10.5194/gmd-2019-378.

Sheidat M, Castro C, Denkinger J, Gonzalez J, and Adelung D (2000). A breeding area for humpback whales (*Megaptera novaeangliae*) off Ecuador. *Journal of Cetacean Research,* 2(3): 165-171.

Sheppard, G., 1930. The geology of South Western Ecuador. *American Association of Petroleum Geologists Bulletin*, 14, 263–309.

Slater GJ, Goldbogen JA, and Pyenson ND (2017). Independent evolution of baleen whale gigantism linked to Plio-Pleistocene ocean dynamics. *Proceedings of the Royal Society B: Biological Sciences*, 284: 20170546.

Spencer C and Kim ST (2015). Carbonate clumped isotope paleothermometry: a review of recent advances in CO2 gas evolution, purification, measurement and standardization techniques. *Geosciences Journal*, 19(2): 357-374.

Swart PK, Burns SJ, and Leder JJ (1991). Fractionation of the stable isotopes of oxygen and carbon in carbon dioxide during the reaction of calcite with phosphoric acid as a function of temperature and technique. *Chemical Geology: Isotope Geoscience*, 86(2): 89-96.

Swartz SL, Taylor BL, and Rugh DJ (2006). Gray whale *Eschrichtius robustus* population and stock identity. *Mammal Review*, 36(1): 66-84.

Toro F, Vilina YA, Capella JJ, and Gibbons J (2016). Novel coastal feeding area for eastern South Pacific fin whales (*Balaenoptera physalus*) in mid-latitude Humboldt Current waters off Chile. *Aquatic Mammals*, 42(1): 47-55.

Triantaphyllou MV (2015). Calcareous nannoplankton dating of the Lte Quternary depositis in Greece and the eastern Mediterranean: Case studies from terrestrial and marine sites. *Journal of Palaeogography*, 4(4): 349-357.

Tsuchi R, Shuto T, Takayama T, Fujiyoshi A, Koizumi I, Ibaraki M, and Tirado GR (1988). Fundamental data on Cenozoic biostratigraphy of the Pacific coast of Ecuador, in Tsuchi, R., ed., Trans-Pacific correlation of Cenozoic geohistory: Shizuoka, Japan, Reports of Andean Studies, Shizuoka University Special Volume 2, p. 23–43.

Tucker ME and Wright VP (2008). Carbonate sedimentology. Oxford: Blackwell Science.

Voldoire A, Saint-Martin D, Senesi S, Decharme B, Alias A, Chevallier M, Colin J, Gueremy J-F, Michou M, Moine M-P, Nabat P, Roehrig R, Salas y Melia D, Seferian R, Valcke S, Beau I, Belamari S, Berthet S, Cassou C, Cattiaux J, Deshayes J, Douville H, Ethee C, Franchisteguy L, Geoffrey O, Levy C, Madec G, Meurdesoif Y, Msadek R, Ribes A, Sanchez-Gomez E, Terray L, and Waldman R (2019). Evaluation of CMIP6 DECK experiments with CNRM-CM6-1, *Journal of Advances in Modeling Earth Systems*, https://doi.org/10.1029/2019MS001683.

Wang Z, Schauble EA, and Eiler JM (2004). Equilibrium thermodynamics of multiply substituted isotopologues of molecular gases. *Geochimica et Cosmochimica Acta*, 68, 4779–4797.

Wehmiller JF, Lajoie KR, Kvenvoldern KA, Peterson E, Belknap DF, Kennedy GL, Addicott WO, Vedder JG and Wright RW (1977). Correlation and chronology of Pacific Coast marine terrace deposits of continental United States by fossil amino acid stereochemistry technique evaluation relative ages kinetic model ages and geologic implications. *U. S. Geological Survey Open File Report*, 77-680.

Whittaker JE (1988). Benthic Cenozoic foraminifera from Ecuador: Taxonomy and distribution of smaller benthic foraminifera from coastal Ecuador (Late Oligocene–Late Pliocene): London, British Museum (Natural History), 194 p.

Williams TM (1999). The evolution of cost efficient swimming in marine mammals: limits to energetic optimization. *Philosophical Transactions of The Royal Society B Biological Sciences,* 354, 193–201.

Zullo VA (1961). A new whale barnacle from Late Pleistocene deposits at San Quintín bay, Baja California. *The Veliger,* 4, 13–14.

Zullo VA (1969). Thoracic Cirripedia of the San Diego Formation, San Diego County, California. *Contributions in Sciences*, 159, 1- 25.

Appendix I: Bulk isotope data

$\delta^{18}O$ and $\delta^{13}C$ data are organized by specimen number (following pages). All samples were analyzed by the Center for Stable Isotope Biogeochemistry (CSIB) at UC Berkeley. Blank cells are samples that did not run. $\delta^{13}C$ and $\delta^{18}O$ values of carbonates are measured using a MultiCarb system in line with a GV IsoPrime mass spectrometer in Dual Inlet. Several replicates of the international standard NBS19, and two lab standards (CaCO3 I & II) are analyzed along with the samples for each run. Long term external precisions for ^{13}C and ^{18}O are ±0.05‰ and ±0.07‰, respectively.

UCMP 221031 (plate 1)		UCMP 221031 (plate 2)		CAS MAM 21691		UCMP 221032		UCMP 221033		UCMP 221034		CAS MAM 21149	
$\delta^{18}O$	$\delta^{13}C$	$\delta^{18}O$	$\delta^{13}C$	$\delta^{18}O$	$\delta^{13}C$	$\delta^{18}O$	$\delta^{13}C$	$\delta^{18}O$	$\delta^{13}C$	$\delta^{18}O$	$\delta^{13}C$	$\delta^{18}O$	$\delta^{13}C$
		0.49	0.7	-0.45	-0.48	0.30	-0.01	-0.94	-1.52	-0.81	0.00	3.47	-0.98
		0.74	0.37	-0.56	0.68			-0.76	-1.49			2.92	-1.04
0.45	-0.04	1.21	0.09	-0.19	0.64	-0.66	-0.59	-1.01	-1.65	-0.95	-0.06	2.24	0.85
0.40	-1.85	-0.32	-0.58	0.16	0.84			-1.11	-1.16			2.24	0.85
1.46	0.00	0.72	-0.16	-0.22	1.07	-1.07	-0.79	-1.24	-1.26	-0.62	0.05	1.66	0.1
1.23	-0.26	1.05	-0.02			-1.18	-0.79	0.14	-1.61			1.48	-0.15
1.06	0.09	1.54	0.00	1.47	-0.88			-0.85	-0.85	0.25	-0.29	0.78	-0.13
0.76	-0.05	1.03	0.02	1.32	-0.99	-0.51	-0.22	-0.19	-0.73			0.93	-0.53
0.76	0.20	1.16	0.01	1.14	-1.13	-0.34	-0.03	-0.93	-1.32	0.53	-1.03	2.08	-0.06
1.06	0.21	0.86	0.09	1.32	-1.21			-0.82	-1.20			0.66	0.03
0.66	-0.02	1.06	0.18	0.79	-1.35	-0.27	-0.20	-0.06	-0.93			0.54	-0.25
1.11	-0.44	0.73	0.08	0.42	-1.49	-0.50	-0.39	-0.09	-1.23			0.34	-0.64
1.09	-0.17	0.44	0.23	0.51	-1.25	-0.35	-0.77	-0.71	-0.83			0.28	-1.04
0.71	0.14	0.33	0.14	0.45	-1.11	-1.04	-0.85	-0.52	-0.46			0.19	-0.98
0.87	0.01	0.39	-0.19	0.07	-1.21	-0.94	-0.77	-0.17	-0.73				
0.69	0.45	0.26	0.51	0.19	-1.16	-0.66	-0.62	0.08	-0.62				
0.56	0.56	0.33	0.56	0.09	-0.92	-0.12	-0.51	0.19	-0.56				
0.74	-0.06	0.25	0.92	-0.2	-0.87	0.15	-0.45	0.51	-0.78				
0.25	0.83	0.08	0.92	0.17	-0.08	0.02	-0.60						
-0.05	0.79	0.29	1.02	-0.33	-0.50	0.40	-0.43						
-0.07	0.80	0.01	1.08	-0.44	-0.43								
-0.35	0.76	0.13	0.9	-0.46	-0.23								
-0.49	0.84	-0.52	0.81	-0.25	0.63								
-0.18	1.05	-0.01	1.02	-0.24	0.86								
-0.25	0.92	0.01	1.13	0.10	1.25								
-0.32	0.99	-0.18	1.01	-0.33	1.39								
-0.07	1.05	-0.39	0.99	-0.65	1.21								
-0.36	0.88	0.01	1.17	-0.67	1.45								
0.01	1.11	0.28	1.38	-0.24	1.54								
0.01	1.01	0.11	1.32	-0.29	1.16								
0.16	1.13	0.29	1.18	-0.21	0.74								
		0.42	1.11	0.02	0.19								
		1.15	1.27	0.27	0.15								
				0.24	-0.08								
				-0.11	-0.38								
				0.04	-0.18								
				-0.18	-0.52								
				-0.72	0.6								
				0.71	-0.26								
				0.62	-0.22								
				0.55	-0.17								
				0.74	0.37								
				0.25	0.83								
				0.81	-0.19								
				0.01	0.44								

SDSNH 50195		SDSNH 102564		SDSNH 30462		SDSNH 111656		SDSNH 134747		SDSNH 114317		CASG 78449	
$\delta^{18}O$	$\delta^{13}C$	$\delta^{18}O$	$\delta^{13}C$	$\delta^{18}O$	$\delta^{13}C$	$\delta^{18}O$	$\delta^{13}C$	$\delta^{18}O$	$\delta^{13}C$	$\delta^{18}O$	$\delta^{13}C$	$\delta^{18}O$	$\delta^{13}C$
1.97	-0.40	1.25	-1.20	2.00	-2.05	-0.15	-3.05	-0.95	-2.35	-0.29	-1.69	-2.00	-0.17
2.32	-0.47	1.16	-1.91	1.66	-1.72	1.41	-2.10	-1.49	-2.18	1.04	-0.85	-0.76	-0.15
2.59	-0.41	2.37	-1.97	1.69	-2.20	1.80	-2.36	-0.13	-1.99	1.93	-1.12	-2.53	-0.29
2.42	-0.28	2.85	-1.79	1.55	-2.07	1.64	-2.19	0.66	-1.23	1.16	-1.73	-1.44	-0.27
2.70	-0.32	2.33	-0.85	0.31	-1.62	2.10	-2.28	1.99	-2.29	0.74	-2.76	-4.20	-0.69
2.18	0.22	0.66	-1.27	1.26	-1.63	1.75	-1.93	0.90	-2.61	1.52	-1.78	-2.08	-0.02
2.67	-1.05	0.59	-1.51	0.35	-0.94	2.36	-2.33	1.95	-3.38	1.42	-0.96	-3.88	-1.48
1.88	-0.78	0.62	-1.08							1.41	-1.03	-3.11	-1.14
2.37	-0.77	1.41	-1.71							0.91	-1.91	-2.90	-0.77
0.91	-0.92									0.69	-1.62	-1.67	0.39
1.61	-1.24											-2.58	0.10
												-1.27	0.29
												-1.67	-0.24
												-1.59	-0.77
												-0.70	-0.52
												-0.35	-0.07
												-0.60	0.26
												-1.73	-0.17
												-1.98	-0.21
												-1.68	0.01
												-1.36	0.56
												-0.95	0.70
												-1.73	0.61
												-1.33	0.95
												-2.14	-0.03
												-2.29	-0.66
												-0.80	0.08
												-0.23	0.50
												0.65	-0.24
												-0.43	-0.55
												-0.33	-0.15
												-1.92	-0.38
												-2.52	-0.56
												-3.62	-0.62
												-0.92	0.11
												-2.15	-0.58

UCMP 221029		UCMP 221028		UCMP 221022		UCMP 221030		Bivalve #1 associated with UCMP 221028		Bivalve #2 associated with UCMP 221028	
$\delta^{18}O$	$\delta^{13}C$	$\delta^{18}O$	$\delta^{13}C$	$\delta^{18}O$	$\delta^{13}C$	$\delta^{18}O$	$\delta^{13}C$	$\delta^{18}O$	$\delta^{13}C$	$\delta^{18}O$	$\delta^{13}C$
0.01	0.06	2.17	0.82	-0.79	0.94	1.37	-0.76	-0.29	1.59	-0.02	1.43
-0.62	0.18	1.87	0.34	-0.12	0.75	1.32	-0.73	0.00	2.05	0.18	1.37
-0.31	0.54	3.43	1.02	-0.02	0.81	1.46	-0.68	-0.23	2.24	0.35	1.59
-0.42	0.59	2.62	1.03	1.75	0.23	1.19	-0.56	0.21	2.15	-0.23	2.03
-0.37	0.74	3.77	1.27	0.87	0.43	1.22	-0.51	-0.01	1.96		
-0.62	0.61	2.57	0.99	2.68	0.06	0.96	-0.58	0.26	2.24		
-0.45	0.73	3.36	0.88	2.15	-0.60	1.15	-0.34				
-0.53	0.74	1.59	0.46			1.15	-0.45				
-0.46	0.78	2.44	0.44	3.00	-0.58	1.29	-0.37				
-0.82	0.68	1.50	0.87	1.53	0.23	1.06	-0.36				
-0.88	0.26	1.07	0.65	1.66	-0.85	1.37	-0.19				
-0.47	0.42	0.76	0.68	1.39	0.40	1.13	-0.41				
0.26	-0.36	1.76	0.66	2.10	-0.47	1.00	-0.24				
1.20	-1.22	0.75	0.77			1.04	-0.06				
0.71	-0.97	1.44	0.49	2.29	-0.26	0.59	-0.10				
0.98	-1.08	-0.02	-1.48	1.02	-0.69	0.90	0.28				
1.44	-0.86	1.05	0.58	1.72	-0.36	0.45	0.38				
1.32	-0.96	0.14	0.79	2.07	-1.18	0.61	0.81				
0.65	-1.09	2.28	1.07	1.59	-0.28	0.83	0.58				
1.09	-0.38	2.67	1.36			0.79	0.21				
0.83	-0.42	1.31	1.03	0.70	-0.32	1.30	0.02				
0.91	0.49	1.01	1.24	1.38	1.06	1.08	-0.49				
1.10	0.87	0.97	0.69	1.15	0.00	1.82	-0.15				
		0.54	0.70			1.42	0.32				
		0.40	0.19	1.71	-0.37						
		0.99	0.50	2.71	-1.52						
		0.84	0.44	2.80	-0.18						
		0.50	0.52	1.52	-0.14						
		0.34	0.47	1.92	-0.03						
		0.68	0.51								
		0.52	0.45								

UCMP 116144		UCMP 116140		UCMP 116153		UCMP 116138		UCMP 116156		UCMP 116165		UCMP 116137	
$\delta^{18}O$	$\delta^{13}C$	$\delta^{18}O$	$\delta^{13}C$	$\delta^{18}O$	$\delta^{13}C$	$\delta^{18}O$	$\delta^{13}C$	$\delta^{18}O$	$\delta^{13}C$	$\delta^{18}O$	$\delta^{13}C$	$\delta^{18}O$	$\delta^{13}C$
1.37	0.44	-0.09	0.46	1.61	-0.09	0.88	0.48	-0.45	-0.40	-0.22	-2.32	0.12	-0.33
1.67	0.08	-0.33	0.36	2.00	0.22	1.61	0.10	-0.12	-0.55	0.19	-2.15	0.30	-0.50
1.01	0.48	-1.46	0.36	1.78	0.13	1.98	0.35	-0.25	-0.43	0.58	-1.99	0.81	-0.63
1.02	0.44	-0.50	0.81	1.75	0.52	2.21	0.63	-0.13	-0.32	0.65	-2.05	0.68	-0.48
0.70	-0.12	-0.20	-0.77	0.09	0.42	1.14	0.47	0.16	-0.22	1.04	-1.75	1.35	-0.99
0.67	-0.47	0.73	-1.75	0.48	0.32	1.03	0.53	0.18	-0.25	1.04	-1.98	0.57	0.21
1.09	-0.59	1.41	-1.69	0.05	-0.08	0.59	0.51	-0.18	-0.55	0.69	-2.04	0.63	0.22
1.46	-0.74	1.04	-1.92	0.15	0.33	0.14	0.59	0.19	-0.19	1.23	-2.04	0.84	0.19
2.10	-0.53	1.74	-1.42	1.16	-0.18	1.56	1.16	0.12	-0.13	0.96	-2.10	1.03	0.08
1.13	-0.61	1.87	-1.53	1.07	-0.16	0.91	1.11	-0.20	-0.16	0.99	-2.03	0.40	0.01
0.70	0.60	2.19	-1.74	0.54	0.04	1.20	0.64	-0.90	-0.23	1.01	-1.88	0.90	0.26
0.72	-0.24	2.09	-1.78	0.31	0.22	1.27	0.70	-0.55	-0.17	1.00	-1.36	1.21	0.10
0.69	-0.18	0.35	-0.62	0.35	0.60	1.94	0.38	-1.32	-0.59	1.13	-0.89	0.59	0.09
0.56	0.27	0.25	-0.83	0.48	0.11	2.77	0.24	-0.19	-0.22	1.34	-1.00	1.30	-0.18
0.57	-0.26	0.05	0.33	1.21	-0.71	1.69	0.16	0.02	-0.14	0.75	-1.10	1.44	0.26
1.10	-0.45	0.12	-1.11	0.92	-0.65	1.57	0.08	-0.45	-0.24	0.96	-1.53	2.09	0.16
1.04	0.52	-0.06	0.11	0.98	-0.80	1.56	0.37	0.30	0.00	1.54	-0.97	1.08	0.39
1.01	0.68	0.04	-0.22	0.99	-0.74	1.26	0.17	0.18	-0.08	0.72	-0.66	1.06	0.50
0.92	0.39	0.42	-0.30	1.00	-0.58	1.37	0.33	0.12	-0.07	1.45	-0.02	1.56	0.20
0.71	0.52	0.25	-0.07	0.65	-0.54	1.03	0.37	0.35	0.08	1.68	-0.65	0.79	0.70
0.75	1.00			0.56	-0.60	1.35	0.55	0.28	-0.02	1.59	-1.32	0.73	0.78
0.59	0.68			0.37	-0.77	0.83	0.02	0.05	-0.39	0.26	-1.44	0.58	0.74
0.65	0.61			0.95	-0.74	0.76	0.22	0.10	-0.98	0.36	-1.66	0.91	0.41
0.53	0.35			1.10	-0.20	1.24	0.90	-0.77	-1.11	0.20	-1.93	0.35	0.44
0.93	0.79			0.49	-0.60	0.98	0.50					0.58	0.24
0.73	0.82			0.84	-0.72	0.28	-0.41					0.71	0.29
0.88	0.30			1.08	-0.97	1.26	0.26					0.98	-0.09
0.84	-0.37			0.82	-0.90	-0.63	-1.01						
0.78	-0.30			0.91	-0.82								
0.86	-0.33			0.63	-0.27								
0.88	0.05			1.91	-0.86								
0.86	0.27												
0.74	0.75												
-0.03	1.59												
-0.60	0.52												

UCMP 116171		UCMP 116166		UCMP 116139		UCMP 116178		UCMP 116161		UCMP 116143		UCMP 116141	
$\delta^{18}O$	$\delta^{13}C$	$\delta^{18}O$	$\delta^{13}C$	$\delta^{18}O$	$\delta^{13}C$	$\delta^{18}O$	$\delta^{13}C$	$\delta^{18}O$	$\delta^{13}C$	$\delta^{18}O$	$\delta^{13}C$	$\delta^{18}O$	$\delta^{13}C$
1.95	0.37	0.22	0.78	-0.42	0.26	-0.49	-0.09	-0.08	-0.63	3.22	-1.17	-0.12	-1.21
2.12	0.45	-1.07	0.77	0.19	0.36	-0.21	0.14	0.60	-0.31	1.70	0.31	-0.15	-0.91
1.51	0.36	-0.54	0.75	0.02	0.14	-0.18	0.35	-0.21	0.32			-0.18	-0.62
1.40	0.35	-1.28	1.43	0.96	0.16	-0.25	0.69	0.23	0.33	1.96	0.22	0.44	-0.37
0.38	0.53	-1.37	1.13	0.31	0.33	-0.38	1.06	-0.65	0.97	2.54	0.64	-0.30	-0.07
0.65	0.90	-1.03	1.10	0.29	0.20	-0.76	0.95	-0.44	-1.81			0.82	0.64
1.13	0.38	-1.31	0.95	0.93	0.22	0.07	0.85	-0.20	0.30	2.79	0.46	-0.04	-0.26
0.60	0.33	-1.35	0.96	0.67	0.21	0.07	0.76	-0.34	0.31	2.54	0.21	-0.62	-0.39
-0.05	0.53	-0.17	1.21	0.71	0.20	-0.30	0.82	0.18	0.75	2.76	-0.15	-1.52	-0.86
0.76	0.20	-0.68	0.86	0.38	0.05	-0.09	0.55	-0.71	1.03	1.95	0.42	-1.27	-0.69
1.15	0.30	-0.66	0.69	-0.13	0.00	-0.05	0.09	-0.38	1.37	0.77	-0.11	-1.64	-0.64
0.85	0.34	-1.05	0.45	1.05	-0.56	0.20	0.18	0.34	1.01			-1.23	-0.28
0.82	0.34	-0.72	0.95	0.97	-0.87	0.22	-0.09	-0.24	1.21	1.45	0.61	-1.33	-0.29
0.47	0.26	-0.38	0.63	0.36	-0.24	0.56	-0.87	0.69	-0.23	2.32	0.24	-0.26	0.11
1.09	0.18	-0.19	0.05	1.39	-0.70	0.21	0.20	0.70	-0.94	1.33	0.48	-0.38	0.26
0.97	0.06	0.07	-0.06	2.08	-1.19	0.08	0.82	1.01	-1.69			0.14	0.25
1.19	0.46	0.28	0.04	2.49	-1.64	0.05	0.45	1.58	-2.46	1.11	0.62	-0.07	-0.36
0.98	1.01	0.31	0.13	1.96	-1.57	-0.13	0.50	1.60	-1.81	1.07	0.45	0.05	0.13
0.97	0.99	-0.10	-0.17	1.27	-0.68	0.27	0.22	0.50	0.36	1.28	0.34	1.20	0.26
1.02	0.91	1.13	1.00	1.16	-0.47	0.28	-0.02	0.32	0.24	-0.06	0.09	0.42	0.01
0.63	1.00	0.36	0.70	0.33	-1.06	0.51	0.12	0.21	0.22	0.73	0.51	0.16	0.02
0.35	1.02	0.71	0.67	0.79	-0.66	-0.07	-0.39	0.07	0.24			-0.20	0.58
0.35	0.62	0.82	1.01	0.28	-0.51	0.31	-0.11	-0.17	1.04	0.46	0.32	0.24	0.47
0.49	0.74	0.95	1.07	0.48	-1.38	0.46	-0.07	-0.58	-1.40	0.34	0.58	-0.31	0.26
0.43	0.69	2.35	1.37	1.43	-0.38	0.70	-0.61			0.12	1.03	0.13	0.55
0.59	0.13	0.28	0.46	0.39	-0.63	0.02	-0.37			0.81	0.12	-0.76	0.08
0.38	0.55			0.90	-0.18	-0.14	-0.51			-0.55	-1.21		
				0.16	-0.17	1.12	-0.06			-0.08	-0.95		
				0.21	0.15	-1.27	-1.87						
				0.26	-0.53	0.13	-1.10						
				-0.46	-0.38								

UCMP 116157		UCMP 116168		UCMP 116135	
$\delta^{18}O$	$\delta^{13}C$	$\delta^{18}O$	$\delta^{13}C$	$\delta^{18}O$	$\delta^{13}C$
-1.12	-0.61	0.63	0.77	2.34	-0.22
-0.87	-0.35	1.04	0.40	1.53	0.32
-0.99	-1.00	0.75	0.26	0.86	0.21
-0.27	-0.02	1.01	0.40	0.66	0.00
0.60	0.23	1.18	0.07	0.93	-0.04
-0.09	0.18	0.82	-0.05	1.42	-0.53
-0.53	-0.29	0.67	0.56	1.63	-0.25
-0.31	0.13	0.60	0.57	1.40	-0.63
-0.52	0.20	0.92	0.77	1.62	-0.62
0.45	0.49	1.06	0.61	1.34	-0.62
0.08	0.68	1.50	0.69	1.32	-0.58
0.84	0.74	1.46	0.44	2.14	-0.64
0.86	0.31	1.20	0.68	1.41	-0.78
0.85	0.88	0.82	1.19	1.79	-0.62
1.09	0.91	0.85	1.36	4.33	-0.04
0.40	0.83	0.47	1.38	2.76	-0.30
0.24	1.23	0.34	0.50	1.87	-0.29
0.39	1.39	1.45	0.89	2.47	-0.18
0.08	1.34	1.73	0.55	1.53	-0.36
-0.23	1.36	1.89	0.66	0.33	-0.33
-0.20	1.51	1.39	0.44	1.13	-0.65
-0.29	1.55	1.51	0.84	1.90	-0.94
-1.11	0.46	0.84	0.94	0.63	-0.38
-0.13	1.10	0.63	1.04	-1.46	-1.60
-0.38	1.19	1.13	0.75	0.02	-0.92
-0.35	1.02	1.09	0.95	1.30	-0.52
-0.28	1.09	0.84	1.12	1.07	-0.45
-0.56	1.00	0.78	0.62	1.38	-0.71
-0.37	1.34	1.28	0.57	1.65	-0.73
-0.39	0.72	0.81	0.48	1.55	-0.63
-0.26	1.32	1.18	0.63	0.72	-0.76
-0.50	1.22	1.07	0.42	0.90	-0.42
-0.75	0.89	1.63	0.71	1.71	-0.29
-0.21	1.32	2.49	0.74	1.42	-0.78
-0.77	1.27	1.25	0.59	3.18	-0.84
-1.22	1.22	1.00	0.57	1.54	-0.67
-0.91	0.89	1.44	0.65	0.29	-1.37
-0.72	1.05	0.95	0.50	0.74	-0.81
-0.61	1.06	0.89	0.91	0.79	-0.56
-0.01	0.77	0.65	0.78	-0.27	-0.89
-0.48	1.01	0.92	0.45	-0.15	-1.09
-0.45	1.18	1.21	0.25	3.48	0.06
-0.35	0.97	1.54	0.09	1.53	-1.50
0.03	0.63	0.54	0.16	1.43	-1.31
1.88	1.29	0.58	0.39	0.84	-1.11
1.13	1.10	0.94	0.30	1.36	-1.10
1.62	1.33	0.98	0.18	0.67	-1.01
1.49	1.11	1.02	0.25	0.04	-1.52

continued on next page

continued from previous page					
UCMP 116157		UCMP 116168		UCMP 116135	
$\delta^{18}O$	$\delta^{13}C$	$\delta^{18}O$	$\delta^{13}C$	$\delta^{18}O$	$\delta^{13}C$
2.11	1.04	1.65	0.10	0.09	-1.32
0.91	1.39	0.72	0.03	0.62	-1.18
1.68	0.57			0.71	-0.91
0.66	0.98			0.64	-1.28
-0.14	0.96			2.06	-1.55
-0.09	0.34			0.76	-0.71
0.19	-0.16			0.21	-0.05
-0.82	-0.67			0.66	-0.78
				1.70	-0.16
				-0.01	-0.55
				0.34	-0.76
				0.24	-0.20
				0.45	-0.62
				1.57	-0.42
				1.73	-1.13
				3.83	0.55
				0.60	0.85
				1.07	-0.94
				-0.40	-1.83

Appendix II: Clumped isotope data

Clumped isotope data are listed with museum specimen numbers and with Stolper Lab (UC Berkeley) sample identifiers (following pages). The first page of data tables includes the sample site from the CSIB-generated $\delta^{18}O$ profile on which clumped samples were centered. On all data tables, data below the light gray bar are those at sample sites that either did not produce enough calcite for the desired minimum of three replicates, or are of calcite collected from the same region of a barnacle but which are not true replicates of the same tube of powder. These data are therefore less reliable but included for usefulness to future researchers. All samples above the gray line are true replicates of the exact same sample sites, with each coming from the same original tube of collected shell powder. All measurements and corrections are included, with final, corrected values and calculated temperature on the last page (page 106).

Measurements were made on a Thermo 253 Plus IRMS purified. CO_2 was extracted and purified using an automated gas purification system identical to that described in Passey et al. (2010). The He stream used for purification is also Grade 5.0 (99.999%). Isotopic measurements are made at masses 44-49 amu as well as a half mass cup at 47.5 amu. Measurements are made in blocks of 10 cycles and each block is replicated 9 times yielding internal measurement precisions for Δ_{47} of ~0.012‰ typically.

All original measurements and corrections are included, as follows. Subtle re-equilibration in the source can increase Δ_{47} values by up to 0.035‰ over the course of the measurement, which is corrected for by noting the trend of measured Δ_{47} values vs. time and projecting all values to the starting acquisition time. The dependence of Δ_{47} values on bulk compositions (δ^{47} values) is first corrected for using a pressure base line correction derived from measured intensities at the mass 47.5 cup. A residual dependence of Δ_{47} on measured δ^{47} values (typical slope of 0.0005 ‰/‰) is corrected for by measuring CO_2 samples with a variation in δ^{47} values of ~ -3 to 42‰ (relative to the working gas) heated to 1000°C. Following this, Δ_{47} values are corrected to the so-called Absolute Reference Frame (ARF) based on measured differences in samples equilibrated at 25°C or heated to 1000°C vs. that expected based on theory. An acid digestion correction of 0.082‰ is then added to all samples to place them into a 25°C acid-digestion reference frame. Finally, samples are corrected based on measured vs. expected values of the ETH 1-4 standards using the values given in Bernasconi et al. (2018). At least four replicates of all four ETH standards measured over 1 month are used for the secondary ETH correction following transfer of the raw measurements to the ARF.

Measured $\delta^{18}O$ and $\delta^{13}C$ values are first calculated based on the Brand parameters. Measured $\delta^{18}O$ and $\delta^{13}C$ of samples are corrected based on differences in measured values of the ETH standards vs. values given in Bernasconi et al. (2018). Finally, $\delta^{18}O$ values were corrected using an acid fractionation factor for $\delta^{18}O$ ($^{18}R_{CaCO3}/^{18}R_{CO2} = 1.00821$ at 90 ºC). We measured three secondary standards to assess the accuracy and long-term precision of measured $\delta^{18}O$, $\delta^{13}C$ and Δ_{47} measurements. We measured an in-house marble (CAR1), in-house travertine (TRV1) and the international IAEA-603 standard. Carbonate samples were measured three to five times across at least three analytical weeks. All samples were replicated across multiple calibration sessions.

Specimen #	Lab Sample ID	Sample sites on 18O profile	Reaction temp.	k-factor	d13C VPDB	d13C stdev	d18O gas VSMOW	d18O mineral VPDB	d18O stdev
UCMP116161	1.12A	17 – 18	90.000	0.712	-1.216	0.003	40.937	1.494	0.007
UCMP116161	1.12B_D2	17 – 18	90.000	0.691	-1.166	0.002	40.694	1.260	0.006
UCMP116161	1.12C_D3	17 – 18	90.000	0.691	-1.547	0.002	40.861	1.421	0.003
UCMP116161	1.12D_D4	17 – 18	90.000	0.698	-1.437	0.003	40.879	1.439	0.005
UCMP116161	1.12E_D5	23 – 24	90.000	0.691	-2.081	0.005	38.871	-0.493	0.008
UCMP116161	1.12G_D7	23 – 24	90.000	0.692	-2.082	0.003	38.889	-0.476	0.007
UCMP116161	1.12F_D6	23 – 24	90.000	0.690	-2.111	0.003	38.722	-0.637	0.006
UCMP116157	3.8E	46 – 50	90.000	0.712	1.368	0.003	39.579	0.188	0.005
UCMP116157	3.8H_F4	46 – 50	90.000	0.702	1.140	0.003	39.354	-0.029	0.006
UCMP116157	3.8G_F3	46 – 50	90.000	0.703	1.232	0.003	39.354	-0.029	0.004
UCMP116157	3.8I_F5	46 – 50	90.000	0.699	1.205	0.002	39.362	-0.021	0.004
UCMP116157	3.8F_F2	46 – 50	90.000	0.693	1.267	0.003	39.463	0.076	0.004
UCMP116157	3.8J_F6	35 – 37	90.000	0.691	1.561	0.003	38.552	-0.800	0.006
UCMP116157	3.8K_F7	35 – 37	90.000	0.702	1.433	0.004	38.541	-0.811	0.007
UCMP116157	3.8L_F8	35 – 37	90.000	0.702	1.501	0.003	38.590	-0.764	0.004
UCMP116157	3.8M_F9	35 – 37	90.000	0.703	1.488	0.003	38.504	-0.847	0.006
UCMP116157	3.8S_E1	55 – 56	90.000	0.693	-1.107	0.003	38.548	-0.804	0.005
UCMP116157	3.8T_E2	55 – 56	90.000	0.700	-0.975	0.002	38.546	-0.806	0.005
UCMP116157	3.8U_E3	55 – 56	90.000	0.696	-0.915	0.003	38.415	-0.932	0.006
UCMP116157	3.8V_E4	55 – 56	90.000	0.703	-1.197	0.004	38.348	-0.997	0.006
UCMP116135	1.7A_A9	14 – 16	90.000	0.693	-0.179	0.003	40.827	1.389	0.008
UCMP116135	1.7C_G3	14 – 16	90.000	0.693	-0.325	0.003	40.656	1.224	0.005
UCMP116135	1.7D_G4	14 – 16	90.000	0.700	-0.234	0.003	40.641	1.210	0.006
UCMP116135	1.7E_G5	14 – 16	90.000	0.695	-0.255	0.004	40.713	1.279	0.007
UCMP116135	1.7B_A10	23 – 25	90.000	0.698	-0.371	0.003	39.532	0.142	0.009
UCMP116135	1.7F_G7	23 – 25	90.000	0.696	-0.437	0.004	39.393	0.009	0.007
UCMP116135	1.7G_G8	23 – 25	90.000	0.702	-0.352	0.003	39.464	0.077	0.006
UCMP116135	1.7H_G9	23 – 25	90.000	0.701	-0.423	0.010	39.551	0.161	0.009
UCMP116140	222-A_C1	3 – 6	90.000	0.763	0.990	0.002	39.238	-0.140	0.002
UCMP116140	222-B	3 – 6	90.000	0.771	-0.437	0.002	42.557	3.052	0.003
UCMP116140	2.22E	2 – 5	90.000	0.714	-0.296	0.003	41.562	2.095	0.004
UCMP116140	2.22F_H2	2 – 5	90.000	0.692	0.222	0.004	41.106	1.657	0.006
UCMP116140	222.C	11 – 12	90.000	0.773	-1.828	0.002	41.563	2.097	0.004
UCMP116140	222-D	11 – 12	90.000	0.771	-0.005	0.002	41.474	2.011	0.002
UCMP116140	2.22I	10 – 13	90.000	0.712	0.586	0.004	41.017	1.571	0.006
UCMP116140	2.22J_H6	10 – 13	90.000	0.699	0.598	0.004	40.857	1.417	0.007
UCMP116138	1.9b_H_A1	2 – 4	90.000	0.755	0.083	0.002	40.311	0.892	0.004
UCMP116138	1.9b-H_A1	2 – 4	90.000	0.728	0.040	0.001	39.840	0.439	0.004
UCMP116138	1.9b_L_A2	7 – 8	90.000	0.755	-1.345	0.002	39.299	-0.082	0.004
UCMP116153	3.4_H_A3	2 – 4	90.000	0.755	0.246	0.002	41.728	2.255	0.004
UCMP116153	3.4-H_A7	2 – 4	90.000	0.726	0.265	0.002	41.248	1.794	0.005
UCMP116153	3.4_L_A4	27 –28	90.000	0.755	-0.228	0.001	40.562	1.134	0.002
UCMP116157	3.8N_C1	10 – 12	90.000	0.691	1.247	0.003	38.988	-0.380	0.004
UCMP116157	3.8O_C2	12 – 14	90.000	0.695	1.136	0.003	38.918	-0.449	0.006
UCMP116157	3.8-A_A11	45 – 48	90.000	0.755	1.290	0.002	39.735	0.338	0.004
UCMP116157	3.8-D_D4	45 – 48	90.000	0.749	0.896	0.002	39.600	0.208	0.003
UCMP116157	3.8-B_C3	47 – 50	90.000	0.754	1.118	0.002	39.481	0.094	0.002
UCMP116157	3.8-C_A12	35 – 36	90.000	0.757	1.360	0.001	38.987	-0.382	0.003

Specimen #	Lab Sample ID	d47	d47 stdev	D47 (v. Oz)	D47 PBL	D47 st.dev.	D47 st.err.	d48	d48 st.dev.
UCMP116161	1.12A	18.089	0.021	-0.205	-0.285	0.021	0.007	33.649	0.164
UCMP116161	1.12B_D2	17.906	0.024	-0.195	-0.270	0.023	0.008	33.155	0.113
UCMP116161	1.12C_D3	17.686	0.024	-0.206	-0.276	0.023	0.008	33.398	0.100
UCMP116161	1.12D_D4	17.815	0.027	-0.203	-0.279	0.026	0.009	33.625	0.165
UCMP116161	1.12E_D5	15.163	0.032	-0.224	-0.293	0.026	0.009	29.362	0.183
UCMP116161	1.12G_D7	15.179	0.022	-0.224	-0.289	0.016	0.005	29.327	0.133
UCMP116161	1.12F_D6	14.993	0.027	-0.216	-0.278	0.025	0.008	28.960	0.197
UCMP116157	3.8E	19.290	0.019	-0.194	-0.277	0.017	0.006	30.819	0.097
UCMP116157	3.8H_F4	18.838	0.021	-0.197	-0.277	0.017	0.006	30.309	0.145
UCMP116157	3.8G_F3	18.922	0.017	-0.203	-0.283	0.014	0.005	30.275	0.159
UCMP116157	3.8I_F5	18.922	0.024	-0.183	-0.262	0.022	0.007	30.318	0.108
UCMP116157	3.8F_F2	19.083	0.020	-0.185	-0.269	0.017	0.006	30.630	0.121
UCMP116157	3.8J_F6	18.439	0.021	-0.209	-0.284	0.013	0.004	28.649	0.171
UCMP116157	3.8K_F7	18.303	0.015	-0.208	-0.284	0.016	0.005	28.604	0.148
UCMP116157	3.8L_F8	18.436	0.029	-0.191	-0.273	0.025	0.008	28.814	0.120
UCMP116157	3.8M_F9	18.314	0.026	-0.213	-0.288	0.023	0.008	28.428	0.147
UCMP116157	3.8S_E1	15.802	0.029	-0.221	-0.290	0.024	0.008	28.641	0.156
UCMP116157	3.8T_E2	15.931	0.024	-0.220	-0.288	0.023	0.008	28.621	0.096
UCMP116157	3.8U_E3	15.850	0.028	-0.229	-0.295	0.021	0.007	28.250	0.114
UCMP116157	3.8V_E4	15.501	0.021	-0.233	-0.300	0.018	0.006	28.217	0.144
UCMP116135	1.7A_A9	19.010	0.024	-0.196	-0.277	0.021	0.007	33.500	0.109
UCMP116135	1.7C_G3	18.683	0.028	-0.208	-0.287	0.024	0.008	33.047	0.140
UCMP116135	1.7D_G4	18.780	0.023	-0.187	-0.267	0.018	0.006	33.062	0.122
UCMP116135	1.7E_G5	18.822	0.032	-0.196	-0.272	0.026	0.009	33.157	0.201
UCMP116135	1.7B_A10	17.506	0.025	-0.220	-0.299	0.023	0.008	30.907	0.143
UCMP116135	1.7F_G7	17.316	0.029	-0.206	-0.283	0.032	0.011	30.459	0.167
UCMP116135	1.7G_G8	17.464	0.018	-0.213	-0.289	0.016	0.005	30.519	0.139
UCMP116135	1.7H_G9	16.867	1.901	-0.816	-0.446	1.850	0.617	24.356	19.096
UCMP116140	222-A_C1	18.562	0.021	-0.210	-0.285	0.021	0.007	29.614	0.127
UCMP116140	222-B	20.483	0.022	-0.192	-0.277	0.021	0.007	36.573	0.074
UCMP116140	2.22E	19.637	0.030	-0.186	-0.272	0.025	0.008	35.000	0.134
UCMP116140	2.22F_H2	19.705	0.029	-0.174	-0.259	0.021	0.007	34.095	0.181
UCMP116140	222.C	18.114	0.026	-0.200	-0.274	0.025	0.008	34.423	0.113
UCMP116140	222-D	19.830	0.024	-0.191	-0.275	0.024	0.008	34.312	0.113
UCMP116140	2.22I	19.964	0.023	-0.185	-0.273	0.022	0.007	33.897	0.141
UCMP116140	2.22J_H6	19.810	0.029	-0.191	-0.273	0.022	0.007	33.502	0.179
UCMP116138	1.9b_H_A1	18.802	0.016	-0.149	-0.278	0.016	0.005	33.012	0.110
UCMP116138	1.9b-H_A1	18.227	0.019	-0.210	-0.281	0.020	0.007	30.871	0.073
UCMP116138	1.9b_L_A2	16.378	0.022	-0.159	-0.270	0.021	0.007	30.863	0.117
UCMP116153	3.4_H_A3	20.411	0.032	-0.113	-0.252	0.032	0.011	36.263	0.143
UCMP116153	3.4-H_A7	19.843	0.029	-0.220	-0.297	0.025	0.008	33.859	0.092
UCMP116153	3.4_L_A4	18.777	0.036	-0.118	-0.246	0.036	0.013	33.735	0.074
UCMP116157	3.8N_C1	18.566	0.016	-0.208	-0.287	0.012	0.004	29.557	0.117
UCMP116157	3.8O_C2	18.393	0.016	-0.202	-0.284	0.012	0.004	29.490	0.120
UCMP116157	3.8-A_A11	19.342	0.021	-0.219	-0.296	0.021	0.007	30.656	0.098
UCMP116157	3.8-D_D4	18.819	0.021	-0.220	-0.295	0.018	0.006	30.326	0.102
UCMP116157	3.8-B_C3	18.925	0.019	-0.214	-0.290	0.018	0.006	30.152	0.121
UCMP116157	3.8-C_A12	18.684	0.015	-0.200	-0.274	0.015	0.005	29.039	0.075

Specimen #	Lab Sample ID	D48	D48 st.dev.	d49	d49 st.dev.	D49	D49 st.dev.
UCMP116161	1.12A	2.066	0.150	-7.137	1.892	-39.811	1.843
UCMP116161	1.12B_D2	2.055	0.103	-7.422	1.762	-39.685	1.715
UCMP116161	1.12C_D3	1.970	0.096	-6.171	1.080	-38.417	1.050
UCMP116161	1.12D_D4	2.154	0.154	-7.769	1.815	-40.103	1.765
UCMP116161	1.12E_D5	1.882	0.167	-8.522	2.536	-36.498	2.483
UCMP116161	1.12G_D7	1.813	0.121	-6.843	1.819	-34.899	1.778
UCMP116161	1.12F_D6	1.778	0.182	-6.745	2.224	-34.466	2.174
UCMP116157	3.8E	1.921	0.090	-7.078	1.898	-39.728	1.847
UCMP116157	3.8H_F4	1.860	0.132	-8.215	1.962	-40.193	1.913
UCMP116157	3.8G_F3	1.826	0.150	-6.866	1.458	-38.977	1.419
UCMP116157	3.8I_F5	1.853	0.101	-6.750	1.403	-38.852	1.365
UCMP116157	3.8F_F2	1.960	0.112	-9.882	1.310	-42.129	1.273
UCMP116157	3.8J_F6	1.786	0.159	-6.566	1.733	-37.518	1.691
UCMP116157	3.8K_F7	1.766	0.134	-6.771	1.766	-37.572	1.725
UCMP116157	3.8L_F8	1.875	0.113	-9.317	1.596	-40.195	1.555
UCMP116157	3.8M_F9	1.666	0.136	-5.919	1.612	-36.730	1.574
UCMP116157	3.8S_E1	1.798	0.145	-8.020	1.528	-36.352	1.496
UCMP116157	3.8T_E2	1.782	0.095	-7.051	1.172	-35.534	1.146
UCMP116157	3.8U_E3	1.674	0.102	-6.708	2.509	-35.015	2.450
UCMP116157	3.8V_E4	1.772	0.130	-7.668	2.222	-35.550	2.173
UCMP116135	1.7A_A9	2.128	0.097	-8.127	2.024	-41.561	1.971
UCMP116135	1.7C_G3	2.019	0.133	-7.769	1.851	-40.759	1.800
UCMP116135	1.7D_G4	2.061	0.111	-7.761	1.854	-40.812	1.803
UCMP116135	1.7E_G5	2.015	0.183	-7.001	2.201	-40.190	2.143
UCMP116135	1.7B_A10	2.105	0.132	-9.025	1.915	-39.856	1.874
UCMP116135	1.7F_G7	1.938	0.151	-8.448	2.106	-38.977	2.057
UCMP116135	1.7G_G8	1.858	0.126	-8.102	2.088	-38.854	2.036
UCMP116135	1.7H_G9	-4.300	18.546	-33.208	78.488	-63.274	76.027
UCMP116140	222-A_C1	1.408	0.126	-9.248	1.750	-40.836	1.692
UCMP116140	222-B	1.780	0.072	-11.397	1.140	-47.642	1.096
UCMP116140	2.22E	2.169	0.125	-7.337	1.961	-42.038	1.900
UCMP116140	2.22F_H2	2.166	0.167	-8.751	1.807	-43.061	1.758
UCMP116140	222.C	1.614	0.110	-9.278	1.553	-42.446	1.498
UCMP116140	222-D	1.671	0.111	-10.582	1.107	-45.286	1.066
UCMP116140	2.22I	2.145	0.126	-8.038	2.234	-42.556	2.171
UCMP116140	2.22J_H6	2.069	0.163	-7.677	2.737	-41.926	2.658
UCMP116138	1.9b_H_A1	2.647	0.112	-10.478	0.685	-43.134	0.657
UCMP116138	1.9b-H_A1	1.475	0.070	-9.461	1.295	-41.242	1.249
UCMP116138	1.9b_L_A2	2.515	0.117	-10.722	0.748	-40.136	0.725
UCMP116153	3.4_H_A3	3.070	0.145	-14.268	0.931	-49.545	0.892
UCMP116153	3.4-H_A7	1.664	0.098	-9.883	1.602	-44.456	1.537
UCMP116153	3.4_L_A4	2.866	0.073	-14.002	0.379	-46.706	0.364
UCMP116157	3.8N_C1	1.832	0.111	-7.758	1.619	-39.178	1.574
UCMP116157	3.8O_C2	1.904	0.108	-8.580	2.089	-39.737	2.036
UCMP116157	3.8-A_A11	1.463	0.099	-9.573	1.536	-42.353	1.479
UCMP116157	3.8-D_D4	1.403	0.100	-8.425	1.542	-40.617	1.489
UCMP116157	3.8-B_C3	1.462	0.120	-9.200	2.163	-41.360	2.089
UCMP116157	3.8-C_A12	1.330	0.073	-8.912	1.746	-40.401	1.689

Specimen #	Lab Sample ID	d47 int.	D47 int.	d48 int.	D48 int.	D47 proj. to 0	D47 abs. ref.	Acid dig. D47	Corrected to ETH
UCMP116161	1.12A	18.007	-0.285	33.649	2.066	-0.306	0.588	0.670	0.689
UCMP116161	1.12B_D2	17.830	-0.270	33.155	2.055	-0.290	0.604	0.686	0.707
UCMP116161	1.12C_D3	17.615	-0.276	33.398	1.970	-0.296	0.597	0.679	0.700
UCMP116161	1.12D_D4	17.738	-0.279	33.625	2.154	-0.300	0.594	0.676	0.696
UCMP116161	1.12E_D5	15.093	-0.293	29.362	1.882	-0.310	0.583	0.665	0.683
UCMP116161	1.12G_D7	15.107	-0.289	29.257	1.756	-0.307	0.587	0.669	0.687
UCMP116161	1.12F_D6	14.909	-0.299	28.947	1.763	-0.315	0.575	0.657	0.676
UCMP116157	3.8E	19.205	-0.277	30.819	1.921	-0.299	0.595	0.677	0.697
UCMP116157	3.8H_F4	18.755	-0.277	30.309	1.860	-0.299	0.593	0.675	0.696
UCMP116157	3.8G_F3	18.841	-0.283	30.275	1.826	-0.304	0.587	0.669	0.689
UCMP116157	3.8I_F5	18.842	-0.262	30.318	1.853	-0.284	0.610	0.692	0.714
UCMP116157	3.8F_F2	18.997	-0.269	30.630	1.960	-0.291	0.603	0.685	0.706
UCMP116157	3.8J_F6	18.350	-0.291	28.649	1.786	-0.312	0.581	0.663	0.681
UCMP116157	3.8K_F7	18.225	-0.284	28.604	1.766	-0.305	0.588	0.670	0.689
UCMP116157	3.8L_F8	18.352	-0.273	28.814	1.875	-0.294	0.599	0.681	0.702
UCMP116157	3.8M_F9	18.238	-0.288	28.428	1.666	-0.308	0.583	0.665	0.684
UCMP116157	3.8S_E1	15.731	-0.290	28.641	1.798	-0.308	0.585	0.667	0.686
UCMP116157	3.8T_E2	15.843	-0.304	28.641	1.805	-0.322	0.570	0.652	0.669
UCMP116157	3.8U_E3	15.774	-0.302	28.241	1.670	-0.319	0.572	0.654	0.672
UCMP116157	3.8V_E4	15.433	-0.300	28.217	1.772	-0.318	0.573	0.655	0.673
UCMP116135	1.7A_A9	18.927	-0.277	33.500	2.128	-0.299	0.594	0.676	0.697
UCMP116135	1.7C_G3	18.603	-0.287	33.047	2.019	-0.308	0.585	0.667	0.686
UCMP116135	1.7D_G4	18.681	-0.282	33.104	2.104	-0.303	0.589	0.671	0.691
UCMP116135	1.7E_G5	18.744	-0.272	32.957	1.834	-0.293	0.599	0.681	0.702
UCMP116135	1.7B_A10	17.425	-0.299	30.907	2.105	-0.319	0.573	0.655	0.672
UCMP116135	1.7F_G7	17.238	-0.283	30.459	1.938	-0.302	0.591	0.673	0.693
UCMP116135	1.7G_G8	17.386	-0.289	30.519	1.858	-0.309	0.583	0.665	0.684
UCMP116135	1.7H_G9	17.409	-0.288	30.721	1.882	-0.308	0.584	0.666	0.685
UCMP116140	222-A_C1	18.478	-0.293	29.540	1.336	-0.301	0.605	0.687	0.694
UCMP116140	222-B	20.402	-0.271	36.531	1.745	-0.282	0.630	0.712	0.730
UCMP116140	2.22E	19.528	-0.289	34.867	2.047	-0.312	0.581	0.663	0.681
UCMP116140	2.22F_H2	19.603	-0.265	33.999	2.088	-0.288	0.607	0.689	0.710
UCMP116140	222.C	18.039	-0.274	34.303	1.499	-0.283	0.629	0.711	0.728
UCMP116140	222-D	19.723	-0.295	34.374	1.733	-0.306	0.605	0.687	0.702
UCMP116140	2.22I	19.855	-0.287	33.824	2.081	-0.310	0.583	0.665	0.684
UCMP116140	2.22J_H6	19.726	-0.273	33.502	2.069	-0.296	0.597	0.679	0.700
UCMP116138	1.9b_H_A1	18.665	-0.283			-0.308	0.596	0.678	0.673
UCMP116138	1.9b-H_A1	18.155	-0.281	30.799	1.408	-0.289	0.618	0.700	0.708
UCMP116138	1.9b_L_A2	16.258	-0.277			-0.299	0.605	0.687	0.683
UCMP116153	3.4_H_A3	20.284	-0.237			-0.264	0.642	0.724	0.722
UCMP116153	3.4-H_A7	19.764	-0.297	33.938	1.753	-0.306	0.600	0.682	0.689
UCMP116153	3.4_L_A4	18.672	-0.220			-0.245	0.662	0.744	0.743
UCMP116157	3.8N_C1	18.487	-0.287	29.557	1.832	-0.308	0.585	0.667	0.686
UCMP116157	3.8O_C2	18.302	-0.290	29.490	1.904	-0.310	0.581	0.663	0.682
UCMP116157	3.8-A_A11	19.248	-0.309	30.637	1.451	-0.318	0.588	0.670	0.675
UCMP116157	3.8-D_D4	18.743	-0.295	30.232	1.315	-0.304	0.602	0.684	0.691
UCMP116157	3.8-B_C3	18.847	-0.294	30.099	1.406	-0.302	0.604	0.686	0.693
UCMP116157	3.8-C_A12	18.609	-0.274	28.992	1.286	-0.283	0.625	0.707	0.716

Specimen #	Lab Sample ID	Temp.	d13C VPDB	d13C st.dev.	d18O mineral VPDB	d18O st.dev.	d18O mineral VSMOW	Barnacle Epsilon	Calc. 18Osw VSMOW
UCMP116161	1.12A	20.264	-1.437	0.003	1.794	0.007	32.760	30.794	1.441
UCMP116161	1.12B_D2	15.102	-1.387	0.002	1.559	0.006	32.517	32.024	-0.024
UCMP116161	1.12C_D3	17.095	-1.766	0.002	1.726	0.003	32.689	31.544	0.623
UCMP116161	1.12D_D4	18.260	-1.659	0.003	1.739	0.005	32.700	31.267	0.911
UCMP116161	1.12E_D5	21.767	-2.305	0.005	-0.205	0.008	30.699	30.445	-0.208
UCMP116161	1.12G_D7	20.575	-2.307	0.003	-0.188	0.007	30.717	30.722	-0.467
UCMP116161	1.12F_D6	23.924	-2.329	0.003	-0.340	0.006	30.559	29.949	0.153
UCMP116157	3.8E	17.939	1.156	0.003	0.480	0.005	31.405	31.343	-0.421
UCMP116157	3.8H_F4	18.207	0.936	0.003	0.272	0.006	31.190	31.279	-0.565
UCMP116157	3.8G_F3	20.039	1.028	0.003	0.272	0.004	31.190	30.847	-0.133
UCMP116157	3.8I_F5	13.250	0.992	0.002	0.271	0.004	31.189	32.476	-1.762
UCMP116157	3.8F_F2	15.520	1.055	0.003	0.368	0.004	31.290	31.923	-1.112
UCMP116157	3.8J_F6	22.520	1.350	0.003	-0.513	0.006	30.381	30.271	-0.342
UCMP116157	3.8K_F7	20.093	1.227	0.004	-0.520	0.007	30.374	30.834	-0.912
UCMP116157	3.8L_F8	16.580	1.298	0.003	-0.468	0.004	30.428	31.667	-1.692
UCMP116157	3.8M_F9	21.434	1.285	0.003	-0.552	0.006	30.341	30.522	-0.632
UCMP116157	3.8S_E1	21.095	-1.328	0.003	-0.517	0.005	30.377	30.601	-0.676
UCMP116157	3.8T_E2	25.942	-1.191	0.002	-0.515	0.005	30.379	29.491	0.436
UCMP116157	3.8U_E3	25.038	-1.131	0.003	-0.642	0.006	30.248	29.695	0.104
UCMP116157	3.8V_E4	24.644	-1.412	0.004	-0.703	0.006	30.186	29.785	-0.045
UCMP116135	1.7A_A9	18.060	-0.396	0.003	1.688	0.008	32.650	31.314	0.815
UCMP116135	1.7C_G3	20.986	-0.543	0.003	1.522	0.005	32.479	30.626	1.338
UCMP116135	1.7D_G4	19.617	-0.447	0.003	1.514	0.006	32.470	30.946	1.009
UCMP116135	1.7E_G5	16.454	-0.465	0.004	1.587	0.007	32.546	31.698	0.330
UCMP116135	1.7B_A10	24.930	-0.589	0.003	0.434	0.009	31.360	29.720	1.159
UCMP116135	1.7F_G7	19.129	-0.652	0.004	0.305	0.007	31.224	31.061	-0.315
UCMP116135	1.7G_G8	21.600	-0.562	0.003	0.378	0.006	31.300	30.483	0.336
UCMP116135	1.7H_G9	21.262	-0.634	0.010	0.462	0.009	31.386	30.562	0.342
UCMP116140	222-A_C1	18.666	0.917	0.002	0.259	0.002	31.177	31.170	-0.469
UCMP116140	222-B	9.317	-0.541	0.002	3.452	0.003	34.469	33.455	0.433
UCMP116140	2.22E	22.349	-0.514	0.003	2.399	0.004	33.384	30.310	2.532
UCMP116140	2.22F_H2	14.317	0.006	0.004	1.959	0.006	32.929	32.215	0.184
UCMP116140	222.C	9.678	-1.935	0.002	2.490	0.004	33.477	33.364	-0.435
UCMP116140	222-D	16.590	-0.108	0.002	2.404	0.002	33.388	31.665	1.179
UCMP116140	2.22I	21.627	0.372	0.004	1.872	0.006	32.839	30.477	1.836
UCMP116138	1.9b_H_A1	24.833	-0.007	0.002	1.312	0.004	32.263	29.742	2.014
UCMP116138	1.9b-H_A1	14.869	-0.035	0.001	0.841	0.004	31.778	32.080	-0.797
UCMP116138	1.9b_L_A2	21.935	-1.444	0.002	0.328	0.004	31.248	30.406	0.364
UCMP116153	3.4_H_A3	11.319	0.157	0.002	2.689	0.004	33.682	32.953	0.175
UCMP116153	3.4-H_A7	20.141	0.191	0.002	2.203	0.005	33.181	30.823	1.821
UCMP116153	3.4_L_A4	5.952	-0.320	0.001	1.556	0.002	32.514	34.315	-2.315
UCMP116157	3.8N_C1	20.975	1.035	0.003	-0.091	0.004	30.816	30.628	-0.278
UCMP116157	3.8O_C2	22.093	0.932	0.003	-0.151	0.006	30.754	30.369	-0.078
UCMP116157	3.8-A_A11	24.075	1.217	0.002	0.740	0.004	31.672	29.914	1.268
UCMP116157	3.8-D_D4	19.436	0.823	0.002	0.610	0.003	31.539	30.989	0.063
UCMP116157	3.8-B_C3	18.983	1.045	0.002	0.495	0.002	31.420	31.096	-0.159
UCMP116157	3.8-C_A12	12.863	1.288	0.001	0.017	0.003	30.927	32.571	-2.110

Appendix III: R code

#Mapping regions of plausibility using modern temperature and 18O data

#makes a map of predicted barnacle 18O using Killingley equation

#can then layer on top regions of plausibility according to set limits (18O ranges from barnacles)

#load in separate temperature files depending on time (month/ season) you want to map/ test

```
library(ncdf4)

library(ggplot2)

library(rgdal)

library(raster)

library(RColorBrewer)


#set working directory

setwd(dir="directory")


#bring in and process seawater 18O file

dat <- nc_open("calculated_d18O_v1_1.nc", write=FALSE, readunlim=TRUE,
verbose=FALSE, auto_GMT=TRUE, suppress_dimvals=FALSE )

lon <- ncvar_get(dat, "lon")

lat <- ncvar_get(dat, "lat")

d18O <- ncvar_get(dat, varid="d18o")

d18O.slice <- d18O[, , 1]

d18O.vec <- as.vector(d18O.slice)

lonlat <- expand.grid(lon, lat)

surf.d18O <- data.frame(lonlat,d18O.vec)

colnames(surf.d18O) <- c("lon","lat","d18Osw")
```

```
## plot and check

p <- ggplot(surf.d18O ,aes(lon,lat,fill=d18Osw))

p + geom_tile(colour=NA) + coord_equal() + scale_fill_gradientn(colours =
rev(rainbow(10)),name =expression(paste(delta^18,"O"[seawater],", V-SMOW")))


## bring in and process SST data

#add file for month of interest

## download site: http://www.esrl.noaa.gov/psd/data/gridded/data.noaa.oisst.v2.html

dat2 <- nc_open("januarynew.nc", write=FALSE, readunlim=TRUE, verbose=FALSE,
auto_GMT=TRUE, suppress_dimvals=FALSE )

lon <- ncvar_get(dat2, "lon")

###center long on prime meridian

lon <- c(seq(.5,179.5),seq(-179.5,-.5))

lat <- ncvar_get(dat2, "lat")

sst <- ncvar_get(dat2, varid="sst")

sst.vec <- as.vector(sst)

lonlat <- expand.grid(lon, lat)

sst.grid <- data.frame(lonlat,sst.vec)

colnames(sst.grid) <- c("lon","lat","sst")

## plot and check

p <- ggplot(sst.grid ,aes(lon,lat,fill=sst))

p + geom_tile(colour=NA) + coord_equal() + scale_fill_gradientn(colours = rev(rainbow(10)))


#combine datasets, cull

all.dat <- merge(sst.grid,surf.d18O,by=c("lat","lon"))


#make d81Ocarb estimate using Killingley equation

all.dat$d18Ocarb <-  all.dat$d18Osw + (1/14)* (437-((2800*all.dat$sst)+ 128997)^.5)
```

```
#make base map of predicted barnacle 18O

p <- ggplot(all.dat ,aes(lon,lat,fill= d18Ocarb))

p + geom_tile(colour=NA,alpha=.80) + coord_map(projection = "orthographic",orientation =
c(-35,-100,0))  + scale_fill_gradientn(colors = brewer.pal(11, "Spectral"),name
=expression(paste(delta^18,"O"[calcite],"VPDB ")))+ theme(panel.background
=element_blank())+ theme(legend.position="top")


#subset ocean region of interest

all.dat <- all.dat[(all.dat$lat < 15 & all.dat$lon > -150& all.dat$lon < -30),]


#below, add limits for one or multiple barnacles (barnacle 18O ranges you want to map)

#map will layer selected range on top of base map

# select threshold values for top layer #1

lower <- 1.62

upper <- 2.11

# make an additional dataset limited to tiles above the threshold

select.dat <- all.dat[(all.dat$d18Ocarb > lower & all.dat$d18Ocarb < upper),]

#make map with single layer

#may want to increase select.dat alpha for single layer

p <- ggplot(all.dat ,aes(lon,lat,fill= d18Ocarb))

p + geom_tile(colour=NA,alpha=.80) + coord_map(projection = "orthographic",orientation =
c(-35,-100,0))  + scale_fill_gradientn(colors = brewer.pal(11, "Spectral"),name
=expression(paste(delta^18,"O"[calcite],"VPDB ")))+ geom_tile(data=select.dat,aes(lon,lat),
fill="black",alpha=.25)+ theme(panel.background =element_blank())+
theme(legend.position="top")


#can add multiple regions (ranges from multiple barnacle) by creating additional “select.dats”
and plotting each as additional “+geom_tile(data=select.dat,aes(lon,lat),fill="color",alpha=.25)
+theme(panel.element_blank())
```

#Ensemble average paleoclimate map with layered regions of plausibility

#Map is average of ten paleoclimate models interpolated to same grid

#code will produce base map, then can layer on regions of plausibility (barnacle 18O ranges)

```
rm(list = ls())
library(ncdf4);library(ggplot2)
library(rgdal);library(raster)
library(RColorBrewer);library(chron)
library(lattice);library(akima)
library(maps);library(mapdata)
library(mapproj)

#set working directory
setwd(dir="directory")

#bring in models one at a time for season of interest
#DJF = December/ January/ February, JJA files = June/ July/ August; below code example is using DJF
# FGOALS-g3 ####
dat1 <- nc_open("FGOALS-g3_LIG_tos_DJF.nc", write=FALSE, readunlim=TRUE, verbose=FALSE,
auto_GMT=TRUE, suppress_dimvals=FALSE )
lon <- ncvar_get(dat1, "longitude"); lat <- ncvar_get(dat1, "latitude"); sst <- ncvar_get(dat1,
varid="LIG_tos")

# Make into vectors
lon = as.vector(lon); lat = as.vector(lat); sst.vec <- as.vector(sst)
grid.fgoals.djf<-cbind(lat,lon,sst.vec)

# remove land
lon.fil = lon[-which(is.na(sst.vec))]
lon.fil = ifelse(lon.fil<0, 360+lon.fil ,lon.fil)
lat.fil = lat[-which(is.na(sst.vec))]
sst.fil = sst.vec[-which(is.na(sst.vec))]
```

```
# Plot of DJF Temp

require(akima)

fld1 <- interp(lon.fil,lat.fil,sst.fil,xo=seq(0,360,0.5),yo=seq(-88,89.7,0.5),duplicate="mean")


# FGOALS-f3

dat2 <- nc_open("FGOALS-f3_LIG_tos_DJF.nc", write=FALSE, readunlim=TRUE, verbose=FALSE,
auto_GMT=TRUE, suppress_dimvals=FALSE )

lon <- ncvar_get(dat2, "longitude"); lat <- ncvar_get(dat2, "latitude"); sst <- ncvar_get(dat2,
varid="LIG_tos")


# Make into vectors

lon = as.vector(lon); lat = as.vector(lat); sst.vec <- as.vector(sst)

grid.fgoals3.djf<-cbind(lat,lon,sst.vec)


# remove land

lon.fil = lon[-which(is.na(sst.vec))]

lon.fil = ifelse(lon.fil<0, 360+lon.fil ,lon.fil)

lat.fil = lat[-which(is.na(sst.vec))]

sst.fil = sst.vec[-which(is.na(sst.vec))]


# Plot of DJF Temp

require(akima)

fld2 <- interp(lon.fil,lat.fil,sst.fil,xo=seq(0,360,0.5),yo=seq(-88,89.7,0.5),duplicate="mean")


# MIROC

dat3 <- nc_open("MIROC_LIG_tos_DJF.nc", write=FALSE, readunlim=TRUE, verbose=FALSE,
auto_GMT=TRUE, suppress_dimvals=FALSE )

lon <- ncvar_get(dat3, "longitude"); lat <- ncvar_get(dat3, "latitude"); sst <- ncvar_get(dat3,
varid="LIG_tos")
```

```
# Make into vectors
lon = as.vector(lon); lat = as.vector(lat); sst.vec <- as.vector(sst)
grid.miroc.djf<-cbind(lat,lon,sst.vec)

# remove land
lon.fil = lon[-which(is.na(sst.vec))]
lon.fil = ifelse(lon.fil<0, 360+lon.fil ,lon.fil)
lat.fil = lat[-which(is.na(sst.vec))]
sst.fil = sst.vec[-which(is.na(sst.vec))]

# Plot of DJF Temp
require(akima)
fld3 <- interp(lon.fil,lat.fil,sst.fil,xo=seq(0,360,0.5),yo=seq(-88,89.7,0.5),duplicate="mean")

# NESM3 ####
dat4 <- nc_open("NESM3_LIG_tos_DJF.nc", write=FALSE, readunlim=TRUE, verbose=FALSE,
auto_GMT=TRUE, suppress_dimvals=FALSE )
lon <- ncvar_get(dat4, "longitude"); lat <- ncvar_get(dat4, "latitude"); sst <- ncvar_get(dat4,
varid="LIG_tos")

# Make into vectors
lon = as.vector(lon); lat = as.vector(lat); sst.vec <- as.vector(sst)
grid.nesm3.djf<-cbind(lat,lon,sst.vec)

# remove land
lon.fil = lon[-which(is.na(sst.vec))]
lon.fil = ifelse(lon.fil<0, 360+lon.fil ,lon.fil)
lat.fil = lat[-which(is.na(sst.vec))]
sst.fil = sst.vec[-which(is.na(sst.vec))]
```

```
# Plot of DJF Temp

require(akima)

fld4 <- interp(lon.fil,lat.fil,sst.fil,xo=seq(0,360,0.5),yo=seq(-88,89.7,0.5),duplicate="mean")


# CNRM-CM6 ####

dat5 <- nc_open("CNRM-CM6_LIG_tos_DJF.nc", write=FALSE, readunlim=TRUE, verbose=FALSE,
auto_GMT=TRUE, suppress_dimvals=FALSE )

lon <- ncvar_get(dat5, "longitude"); lat <- ncvar_get(dat5, "latitude"); sst <- ncvar_get(dat5,
varid="LIG_tos")


# Make into vectors

lon = as.vector(lon); lat = as.vector(lat); sst.vec <- as.vector(sst)

grid.cnrmcm6.djf<-cbind(lat,lon,sst.vec)


# remove land

lon.fil = lon[-which(is.na(sst.vec))]

lon.fil = ifelse(lon.fil<0, 360+lon.fil ,lon.fil)

lat.fil = lat[-which(is.na(sst.vec))]

sst.fil = sst.vec[-which(is.na(sst.vec))]


# Plot of DJF Temp

require(akima)

fld5 <- interp(lon.fil,lat.fil,sst.fil,xo=seq(0,360,0.5),yo=seq(-88,89.7,0.5),duplicate="mean")


# IPSL ####

dat6 <- nc_open("IPSL_LIG_tos_DJF.nc", write=FALSE, readunlim=TRUE, verbose=FALSE,
auto_GMT=TRUE, suppress_dimvals=FALSE )

lon <- ncvar_get(dat6, "longitude"); lat <- ncvar_get(dat6, "latitude"); sst <- ncvar_get(dat6,
varid="LIG_tos")
```

```
# Make into vectors
lon = as.vector(lon); lat = as.vector(lat); sst.vec <- as.vector(sst)
grid.ipsl.djf<-cbind(lat,lon,sst.vec)

# remove land
lon.fil = lon[-which(is.na(sst.vec))]
lon.fil = ifelse(lon.fil<0, 360+lon.fil ,lon.fil)
lat.fil = lat[-which(is.na(sst.vec))]
sst.fil = sst.vec[-which(is.na(sst.vec))]

# Plot of DJF Temp
require(akima)
fld6 <- interp(lon.fil,lat.fil,sst.fil,xo=seq(0,360,0.5),yo=seq(-88,89.7,0.5),duplicate="mean")

# NorESM1 ####
dat7 <- nc_open("NorESM1_LIG_tos_DJF.nc", write=FALSE, readunlim=TRUE, verbose=FALSE,
auto_GMT=TRUE, suppress_dimvals=FALSE )
lon <- ncvar_get(dat7, "longitude"); lat <- ncvar_get(dat7, "latitude"); sst <- ncvar_get(dat7,
varid="LIG_tos")

# Make into vectors
lon = as.vector(lon); lat = as.vector(lat); sst.vec <- as.vector(sst)
grid.noresm1.djf<-cbind(lat,lon,sst.vec)

# remove land
lon.fil = lon[-which(is.na(sst.vec))]
lon.fil = ifelse(lon.fil<0, 360+lon.fil ,lon.fil)
lat.fil = lat[-which(is.na(sst.vec))]
sst.fil = sst.vec[-which(is.na(sst.vec))]
```

```
# Plot of DJF Temp

require(akima)

fld7 <- interp(lon.fil,lat.fil,sst.fil,xo=seq(0,360,0.5),yo=seq(-88,89.7,0.5),duplicate="mean")


# NorESM2 ####

dat8 <- nc_open("NorESM2_LIG_tos_DJF.nc", write=FALSE, readunlim=TRUE, verbose=FALSE,
auto_GMT=TRUE, suppress_dimvals=FALSE )

lon <- ncvar_get(dat8, "longitude"); lat <- ncvar_get(dat8, "latitude"); sst <- ncvar_get(dat8,
varid="LIG_tos")


# Make into vectors

lon = as.vector(lon); lat = as.vector(lat); sst.vec <- as.vector(sst)

grid.noresm2.djf<-cbind(lat,lon,sst.vec)


# remove land

lon.fil = lon[-which(is.na(sst.vec))]

lon.fil = ifelse(lon.fil<0, 360+lon.fil ,lon.fil)

lat.fil = lat[-which(is.na(sst.vec))]

sst.fil = sst.vec[-which(is.na(sst.vec))]


# Plot of DJF Temp

require(akima)

fld8 <- interp(lon.fil,lat.fil,sst.fil,xo=seq(0,360,0.5),yo=seq(-88,89.7,0.5),duplicate="mean")


# CESM2 ####

dat9 <- nc_open("CESM2_LIG_tos_DJF.nc", write=FALSE, readunlim=TRUE, verbose=FALSE,
auto_GMT=TRUE, suppress_dimvals=FALSE )

lon <- ncvar_get(dat9, "lon");range(lon,na.rm=T)

lat <- ncvar_get(dat9, "lat");sst <- ncvar_get(dat9, varid="LIG_tos")
```

```
# # Make into vectors
lon = as.vector(lon)
lon.grid = matrix(rep(lon,dim(sst)[2]),nrow=dim(sst)[1],ncol=dim(sst)[2])
lat.grid = matrix(rep(lat,dim(sst)[1]),nrow=dim(sst)[1],ncol=dim(sst)[2],byrow=TRUE)
sst.vec <- as.vector(sst)
grid.cesm2.djf<-cbind(lat,lon,sst.vec)

# # remove land
lon.fil = lon.grid[-which(is.na(sst.vec))]
lon.fil = ifelse(lon.fil<0, 360+lon.fil ,lon.fil)
lat.fil = lat.grid[-which(is.na(sst.vec))]
sst.fil = sst.vec[-which(is.na(sst.vec))]

# Plot of DJF Temp
require(akima)
fld9 <- interp(lon.fil,lat.fil,sst.fil,xo=seq(0,360,0.5),yo=seq(-88,89.7,0.5),duplicate="mean")

# GISS ####
dat10 <- nc_open("GISS_LIG_tos_DJF.nc", write=FALSE, readunlim=TRUE, verbose=FALSE,
auto_GMT=TRUE, suppress_dimvals=FALSE )
lon <- ncvar_get(dat10, "lon");range(lon,na.rm=T)
lat <- ncvar_get(dat10, "lat");sst <- ncvar_get(dat10, varid="LIG_tos")

# # Make into vectors
lon = as.vector(lon)
lon.grid = matrix(rep(lon,dim(sst)[2]),nrow=dim(sst)[1],ncol=dim(sst)[2])
lat.grid = matrix(rep(lat,dim(sst)[1]),nrow=dim(sst)[1],ncol=dim(sst)[2],byrow=TRUE)
sst.vec <- as.vector(sst)
grid.giss.djf<-cbind(lat,lon,sst.vec)
```

```
# # remove land
lon.fil = lon.grid[-which(is.na(sst.vec))]
lon.fil = ifelse(lon.fil<0, 360+lon.fil ,lon.fil)
lat.fil = lat.grid[-which(is.na(sst.vec))]
sst.fil = sst.vec[-which(is.na(sst.vec))]

# Plot of DJF Temp
require(akima)
fld10 <- interp(lon.fil,lat.fil,sst.fil,xo=seq(0,360,0.5),yo=seq(-88,89.7,0.5),duplicate="mean")



range(fld10$z,na.rm=T)
fld.avg = fld.sd = fld1

for(i in 1:dim(fld.avg$z)[1]){for(j in 1:dim(fld1$z)[2]){
  fld.avg$z[i,j] = mean(c(fld1$z[i,j],fld2$z[i,j],fld3$z[i,j],fld4$z[i,j],fld5$z[i,j],
                      fld6$z[i,j],fld7$z[i,j],fld8$z[i,j],fld9$z[i,j],fld10$z[i,j]),na.rm=T)
  fld.sd$z[i,j] = sd(c(fld1$z[i,j],fld2$z[i,j],fld3$z[i,j],fld4$z[i,j],fld5$z[i,j],
                    fld6$z[i,j],fld7$z[i,j],fld8$z[i,j],fld9$z[i,j],fld10$z[i,j]),na.rm=T)
}}

# Make ensemble map as is (no barnacle data yet)
pdf("ENSEMBLE_Avg_DJF.pdf",width=7,height=5)
filled.contour(fld.avg,
             xlim=c(100,300),level=seq(-2,38,4),col=rev(brewer.pal(11,'RdYlBu')),
             plot.axes={axis(1);axis(2);
               map('world2',fill = TRUE, col = 1,add=T,xlim=c(100, 300))},main="DJF LIG Temp")
dev.off()
```

```
#map of standard deviation
pdf("ENSEMBLE_SD_DJF.pdf",width=7,height=5)
filled.contour(fld.sd,
        xlim=c(100,300),level=seq(0,4.5,0.5),col=brewer.pal(9,'YlOrRd'),
        plot.axes={axis(1);axis(2);
          map('world2',fill = TRUE, col = 1,add=T,xlim=c(100, 300))},main="DJF LIG Temp SD")
dev.off()

#now bring in other data to do barnacle calcite 18O plausibility calculations
#bring in paleo seawater 18O data
dat11 <- nc_open("JAN2900-2999.toijlE2p1_anl_127kGorb.nc", write=FALSE, readunlim=TRUE,
verbose=FALSE, auto_GMT=TRUE, suppress_dimvals=FALSE )
lon <- ncvar_get(dat11, "lono"); lat <- ncvar_get(dat11, "lato"); d18Ow <- ncvar_get(dat11,
varid="H2O18")
d18Ow <- d18Ow[,,1]

# Make into vectors
lon = as.vector(lon); lat = as.vector(lat); d18Ow.vec <- as.vector(d18Ow)
grid <- merge(lon,lat)
colnames(grid) <- c("x","y")

grid$d18Ow <- d18Ow.vec
grid <- na.omit(grid)
grid$x <- ifelse(grid$x<0, 360+grid$x ,grid$x)
#View(grid)
# Interpolate LIG d18Owater
require(akima)
fld11 <- interp(grid$x,grid$y,grid$d18Ow,xo=seq(0,360,0.5),yo=seq(-88,89.7,0.5),duplicate="mean")
```

```
# make into data frame and plot to check it

grid22 <- merge(fld11$x,fld11$y)

colnames(grid22) <- c("x","y")

grid22$d18Ow <- as.vector(fld11$z)

grid22$sst <- as.vector(fld.avg$z)


#make d81Ocarb estimate using Killingsley equation

grid22$d18Ocarb <-  grid22$d18Ow + (1/14)* (437-((2800*grid22$sst)+ 128997)^.5)


#make base map – predicted barnacle 18O based on average of ten models

p <- ggplot(grid22 ,aes(x,y,fill= d18Ocarb))

p + geom_tile(colour=NA,alpha=.80) + coord_map(projection = "orthographic",orientation = c(-
35,260,0))  + scale_fill_gradientn(colors = brewer.pal(11, "Spectral"),name
=expression(paste(delta^18,"O"[calcite],"VPDB ")))+ theme(panel.background
=element_blank())+theme(legend.position="top")


#subset only southeast Pacific/ other area of interest

grid22 <- grid22[(grid22$y < 15 &grid22$x > 210&grid22$x < 330),]


#select thresholds/ 18O range of interest for each barnacle

#this example is using range for barnacle O18 peak (three most enriched 18O values from profile)

# select threshold values

lower <- 1.62

upper <- 2.11


# make an additional dataset limited to tiles above the threshold

select.dat <- grid22[(grid22$d18Ocarb > lower & grid22$d18Ocarb < upper),]
```

```
#make map with region of plausibility layered on top of base map

p <- ggplot(grid22 ,aes(x,y,fill= d18Ocarb))

p + geom_tile(colour=NA,alpha=.80) + coord_map(projection = "orthographic",orientation = c(-
35,260,0))  + scale_fill_gradientn(colors = brewer.pal(11, "Spectral"),
name=expression(paste(delta^18,"O"[calcite],"VPDB "))) + geom_tile(data=select.dat,aes(x,y),
fill="gray26",alpha=.25)+ theme(panel.background =element_blank())+theme(legend.position="top")


#can add additional layers for other barnacles by adding “select.dat” arguments and then adding
“geom_tile” arguments to the above
```